NASA
Technical
Paper
2822

June 1988

# Flight Control Systems Development and Flight Test Experience With the HiMAT Research Vehicles

Robert W. Kempel
and Michael R. Earls

NASA

NASA
Technical
Paper
2822

1988

# Flight Control Systems Development and Flight Test Experience With the HiMAT Research Vehicles

Robert W. Kempel
and Michael R. Earls
*Ames Research Center*
*Dryden Flight Research Facility*
*Edwards, California*

National Aeronautics
and Space Administration

Scientific and Technical
Information Division

# CONTENTS

SUMMARY 1

INTRODUCTION 1

NOMENCLATURE 1
Letter and Mathematical Symbols . . . 1
Abbreviations . . . 2

HiMAT VEHICLE DESCRIPTION AND OPERATIONAL PROCEDURE 2

HiMAT SYSTEMS DESCRIPTIONS 3
Systems Overview . . . 3
Ground Systems . . . 4
Downlink Receiving Station . . . 4
V-77 Computer . . . 4
Pilot's and Flight Test Engineer's Station . . . 4
Control Law, Maneuver, and Navigation Computers . . . 4
Uplink Encoder . . . 5
Airborne Systems . . . 5
Uplink Receivers–Diversity Combiner–Decoders . . . 5
Airborne Computers . . . 6
Flight Control Sensors . . . 6
Servoactuator Electronics Box . . . 6
Flight Test Instrumentation System . . . 6

CONTROL SYSTEMS DESCRIPTIONS 7
Systems Overview . . . 7
Stable Control Systems . . . 7
Stable Primary Control System . . . 7
Stable Backup Control System . . . 8
Degraded Primary Mode . . . 8
Integrated Propulsion Control System . . . 8
Relaxed Static Stability Control Systems . . . 9
Longitudinal RSS PCS . . . 9
Lateral–Directional RSS PCS . . . 10
Backup Flight Control System Modes . . . 10
Recovery Mode . . . 11
Orbit Mode . . . 11
Climb–Dive Mode . . . 11
Turn Mode . . . 11
Landing Mode . . . 11
Engine-Out Mode . . . 11
Backup Flight Control System Loop Structure . . . 12
Longitudinal RSS BCS Control Law Loop Structure . . . 12
Lateral-Directional RSS BCS Control Law Loop Structure . . . 12
BCS Throttle Control Law . . . 12

FLIGHT SYSTEMS FAILURE MANAGEMENT 13
Ground Failure Management . . . 13
Downlink Integrity . . . 13
Uplink Integrity . . . 13
Real-Time Loop Integrity . . . 13
Computer Watch-Dog Timer . . . 14
Stick Input Checks . . . 14
DAC/ADC Wrap Tests . . . 14
Air-Data Miscompares . . . 14
Angle-of-Attack Miscompares . . . 14
Airborne Failure Management . . . 14
Hydraulic Systems . . . 14
Electrical Systems . . . 14
Duplex Actuators . . . 14
Simplex Actuators . . . 14
Triplex Sensors . . . 15
Duplex Sensors . . . 15
Downlink System . . . 15
Uplink System . . . 15
Computer Self-Test Diagnostics . . . 15
Systems Flight Qualification . . . 15
Qualification Tests . . . 15
Simulation Systems . . . 16
Software Qualification . . . 17
Ground Test Requirements . . . 17
Configuration Control . . . 18

PRIMARY CONTROL SYSTEM FLIGHT TEST RESULTS 18
Verification of Vehicle Aerodynamics . . . 18
Control Surface Pulse Command Inputs . . . 18
Aileron Active and Inactive . . . 19
Aileron-to-Rudder Interconnect . . . 19
Relaxed Static Stability Configuration . . . 19
Lateral Acceleration Aliasing . . . 19
Angle-of-Attack Limiter . . . 20
Surface Angular Rate Probability Distribution . . . 20
Flight Test Maneuver Autopilot . . . 21

BACKUP CONTROL SYSTEM FLIGHT TEST RESULTS 21
Stable Configuration . . . 21
Transfer to BCS Recovery Mode . . . 21
Orbit Mode . . . 21
Dive Mode . . . 22
Turn Mode . . . 22
Transfer From BCS to PCS . . . 22
Powered-Landing Mode . . . 22
Pilot Comments . . . 22
Relaxed Static Stability Configuration . . . 22
Aeroservoelastic Instability . . . 22

Transfer to BCS Recovery Mode at Supersonic Speed . . . . . 23

CONCLUDING REMARKS 24

REFERENCES 25

# SUMMARY

Two highly maneuverable aircraft technology (HiMAT) remotely piloted vehicles were flown a total of 26 flights. These subscale vehicles were of advanced aerodynamic configuration with advanced technology concepts such as composite and metallic structures, digital integrated propulsion control, and ground (primary) and airborne (backup) relaxed static stability digital fly-by-wire control systems. Extensive systems development, checkout, and flight qualification were required to conduct the flight test program.

The design maneuver goal was to achieve a sustained 8-g turn at Mach 0.9 at an altitude of 25,000 ft. This goal was achieved, along with the acquisition of high-quality flight data at subsonic and supersonic Mach numbers. Control systems were modified in a variety of ways using the flight-determined aerodynamic characteristics. The HiMAT program was successfully completed with approximately 11 hr of total flight time.

# INTRODUCTION

The National Aeronautics and Space Administration (NASA) has demonstrated advanced technology concepts through flight testing of two highly maneuverable aircraft technology (HiMAT) vehicles. These subscale remotely piloted research vehicles (RPRVs) were flown at the NASA Ames Research Center, Dryden Flight Research Facility (Ames-Dryden), at Edwards, California. The HiMAT vehicles included an advanced aerodynamic configuration and advanced technology concepts such as composite and metallic structures, a digital integrated propulsion control system (IPCS), and ground and airborne digital fly-by-wire control systems.

One of the primary features of the HiMAT vehicle was its construction from advanced materials. In particular, the wing and canard were constructed from graphite–epoxy using a nonstandard ply layup technique. This technique provided aerodynamically beneficial spanwise twist by aeroelastic tailoring designed to reduce aircraft drag. In addition, the vehicles were designed to fly in a relaxed static stability (RSS) configuration to reduce trim drag. The design maneuverability goal was to achieve a sustained 8-g turn at Mach 0.9 at an altitude of 25,000 ft. With a ground-changeable wing leading edge (less camber), the vehicle could also achieve sustained supersonic flight.

The RPRV concept, combined with the requirements that no single failure result in loss of the vehicle and that the vehicle fly statically unstable, dictated a complex approach to the development of flight control systems, vehicle systems, fault detection and failure management, and systems flight qualification. Virtually all HiMAT systems were divided into two categories: primary and backup. Dual onboard microprocessor computers provided the key interfaces with the ground and various vehicle subsystems, and each was designed to provide for the safe return of the vehicle should the other fail. There were dual electrical and hydraulic systems, and dual flight control systems as well as redundant flight sensors.

The HiMAT program was completed after a total of 26 flights were flown with approximately 11 hr of flight time. The initial portion of the flight test program consisted of a series of flights in which both vehicles were ballasted in a stable or forward center-of-gravity configuration. The final 14 flights of the test program were flown in the relaxed static stability configuration.

This paper presents the design features, flight qualification, and flight testing of the HiMAT digital primary and backup flight control systems for both the stable and relaxed static stability portions of the program. Included in the discussion are the fault detection and redundancy management methods developed and simulation techniques required for final flight qualification of the control systems. Extensive flight test data are presented that illustrate particular problems and the quality of the flight data.

# NOMENCLATURE

## Letter and Mathematical Symbols

Where appropriate, parameters are referenced to a fuselage body axis system according to a right-hand sign convention.

| | |
|---|---|
| $a_n$ | normal acceleration, g |
| $\bar{c}$ | mean aerodynamic chord, 4.347 ft |
| DAP | pilot's lateral stick displacement, in |
| DEP | pilot's longitudinal stick displacement, in |
| DRP | pilot's rudder pedal displacement, in |
| $g$ | acceleration due to gravity, 32.174 ft/sec$^2$ |
| $h$ | altitude, ft |
| $K$ | system gains (units as required) |
| $M$ | Mach number |
| $p$ | roll angular rate, deg/sec |
| $q$ | pitch angular rate, deg/sec |
| $\bar{q}$ | dynamic pressure, lb/ft$^2$ |
| $r$ | yaw angular rate, deg/sec |
| $s$ | Laplace transform operator, rad/sec |
| $V_c$ | calibrated airspeed, knots |
| $\alpha$ | angle of attack, deg |
| $\beta$ | angle of sideslip, deg |
| $\delta_a$ | aileron deflection, deg; $\delta_a = (\delta_{aL} - \delta_{aR})$ |
| $\delta_c$ | canard deflection, deg; $\delta_c = (\delta_{cL} + \delta_{cR})/2$ |
| $\delta_e$ | elevator deflection, deg; $\delta_e = (\delta_{eL} + \delta_{eR})/2$ |
| $\delta_r$ | rudder deflection, deg; $\delta_r = (\delta_{rL} + \delta_{rR})/2$ |
| $\delta_v$ | elevon deflection, deg; $\delta_v = (\delta_{vL} + \delta_{vR})/2$ |
| $\delta_{va}$ | differential elevon, deg; $\delta_{va} = (\delta_{vL} - \delta_{vR})$ |
| $\delta_{aL}$ | left aileron deflection, deg |
| $\delta_{aR}$ | right aileron deflection, deg |
| $\delta_{cL}$ | left canard deflection, deg |
| $\delta_{cR}$ | right canard deflection, deg |
| $\delta_{eL}$ | left elevator deflection, deg |
| $\delta_{eR}$ | right elevator deflection, deg |
| $\delta_{rL}$ | left rudder deflection, deg |
| $\delta_{rR}$ | right rudder deflection, deg |
| $\delta_{vL}$ | left elevon deflection, deg |
| $\delta_{vR}$ | right elevon deflection, deg |

### Abbreviations

| | |
|---|---|
| ADC | analog-to-digital converter |
| ADI | attitude direction indicator |
| AGL | above ground level |
| AIDS | aircraft interrogation and display system |
| ARI | aileron-to-rudder interconnect |
| ASE | aeroservoelastic |
| BCS | backup control system |
| CASH | computation and simulation of HiMAT |
| CRT | cathode ray tube |
| CSMC | computer select mode control |
| DAC | digital-to-analog converter |
| DPM | degraded primary mode |
| EGT | exhaust gas temperature |
| EPROM | erasable programmable read only memory |
| FTE | flight test engineer |
| FTIS | flight test instrumentation system |
| FTMAP | flight test maneuver autopilot |
| HiMAT | highly maneuverable aircraft technology |
| ILS | instrument landing system |
| IO | input-output |
| IPCS | integrated propulsion control system |
| KARI | aileron-to-rudder interconnect gain |
| KBQ | onboard fixed rate gain |
| MAC | mean aerodynamic chord |
| MCWP | master caution and warning panel |
| MDS | microprocessor development system |
| PCM | pulse code modulation |
| PCS | primary control system |
| RAM | random access memory |
| RPRV | remotely piloted research vehicle |
| RSS | relaxed static stability |
| SAE | servoactuator electronics |
| TM | telemetered |

## HiMAT VEHICLE DESCRIPTION AND OPERATIONAL PROCEDURE

The HiMAT vehicles were remotely piloted, 0.44-scale versions of an envisioned full-scale aircraft. The overall vehicle configuration (fig. 1) was characterized by a swept wing with a close coupled canard. Overall vehicle dimensions are shown in figure 1. The five pairs of aerodynamic control surfaces are shown in figure 2. Table 1 presents the average angular surface rate capability, full surface travel positions, and control mode function. The surfaces include the twin all-movable boom-mounted rudders which deflected symmetrically for yaw control and asymmetrically (toe-in) for speed-brake con-

trol. The elevator was used for pitch control, the elevons for pitch and roll control, and the ailerons for roll control. Later in the program, the ailerons were mechanically locked and only elevons were used for roll control. The canard flaps had the capability of providing pitch and sideforce control; however, no attempt was made to mechanize them in this fashion.

The vehicle gross weight was approximately 3501 lb with 659 lb of fuel. Each vehicle was powered by a J85-21 turbojet engine rated at 5004 lb sea level static thrust. The engine was equipped with a nine-stage, variable-geometry axial compressor, a two-stage turbine, afterburner, and variable-area exhaust nozzle. Engine control was provided through an IPCS resident in the backup onboard computer. For additional details, see Bayati (1976) and Baer-Riedhart (1981).

In keeping with the ground rule that no single failure should cause loss of the vehicle, dual electrical and hydraulic systems were implemented. These dual systems were designated primary and backup.

The HiMAT vehicle primary electrical power was supplied by an engine-driven dc generator. In the event of a primary electrical system failure (engine, generator) backup power was supplied by a 35-V silver–zinc battery. A 32-V transition battery provided electrical power to the computers during the transition from generator to backup power.

Primary hydraulic power was supplied by an engine-driven pump. In the event of a primary hydraulic system failure, an electrically driven pump supplied power to the backup hydraulic system. The electrically driven pump operated continuously in a no-load condition until a primary hydraulic failure was detected, in which case the backup hydraulic system was engaged.

There were no single points of contact between the primary and backup hydraulic systems other than the dual tandem actuators used for the elevons and rudders. In these actuators, the systems were separated by dual seals. If a primary hydraulic failure was detected, airborne logic switched out the simplex canard, aileron, and elevator servoactuators, and they were commanded to a predetermined locked position (table 1). When a transfer to backup control occurred, the dual elevon and rudder servoactuators switched to the backup hydraulic system.

Operationally, the HiMAT vehicles were carried aloft under the right wing of a specially modified B-52 aircraft and were launched at approximately 45,000 ft at Mach 0.68. Typical missions were approximately 30 min. The pilot, in a fully instrumented fixed-base ground cockpit, flew the vehicles through various research maneuvers using conventional fighter aircraft controls. Control of the vehicle was maintained through the ground computers and uplink system. Aircraft response parameters were downlinked to the ground station and displayed to the pilot. A flight engineer, next to the cockpit, assisted the pilot in the overall conduct of research maneuvers and navigation tasks throughout each flight. NASA ground radar tracked the vehicles and supplied the ground station with ground track, backup airspeed, and altitude information. In the event of certain ground or airborne failures, a backup flight control system could be engaged and flown from either the ground or the back seat of an airborne chase plane, and the aircraft could be guided to an emergency landing. The vehicles were equipped with landing skids for horizontal landing on Rogers dry lakebed. The landing runways were about 15,000 ft long and improved for about 150 ft on both sides of the centerline. Typical slide-out distance was approximately 4500 ft.

# HiMAT SYSTEMS DESCRIPTIONS

## Systems Overview

In the description of the HiMAT vehicle systems, it is difficult to describe any one system independent of another owing to the requirement that both ground and airborne systems work in concert.

Under normal research flight-test conditions, the vehicles were flown via the primary control system (PCS). The PCS control laws resided in the ground-based Varian V-73 computer (Varian Associates, Inc., Palo Alto, California) in the RPRV facility with the ground-based cockpit. In the event of certain critical airborne or ground failures, transfer from PCS to the backup control system (BCS)

was usually automatic but manual transfer was possible. The BCS control laws were resident in the backup computer aboard the vehicle. Control of the BCS was via discrete signals from either the ground-based cockpit or from the TF-104G chase aircraft. Command paths, and uplink and downlink telemetry signals are shown in figure 3. All critical parameters input to the PCS were downlinked at 220 Hz. These signals included the three axis angular rates, normal and lateral acceleration, angle of sideslip, and angle of attack. Less critical parameters such as air data were downlinked at the lower rate of 55 Hz. Commands to the vehicles were uplinked at a single rate of 53.3 Hz.

## Ground Systems

### Downlink Receiving Station

Most computer-processed data to be downlinked were passed from the primary onboard computer to the flight test instrumentation system (FTIS) for transmission to the ground as a pulse-code modulation (PCM) data stream at 220 Hz. The ground station then received and decommutated the data into usable data words in counts. All these data were available to the Varian V-77 computers. The decommutation station also passed data directly to the pilot's cockpit indicators for display.

### V-77 Computer

The V-77 computer performed the necessary formatting of the vehicle sensor signals and transferred these data to the V-73 PCS computer. The V-77 also decoded a set of downlinked discrete signals to indicate status and health of various onboard vehicle systems. These signals were displayed to ground personnel by lighting a master caution and warning panel.

### Pilot's and Flight Test Engineer's Station

Figure 4 shows the cockpit instrument array, left console, and the BCS discrete command panel on the right console. Cockpit instrument displays included a forward-looking video monitor (used primarily for landing approach), attitude direction indicator (ADI), radar altimeter (0 to 5000 ft), barometric altimeter, airspeed and Mach indicators, altitude rate, engine rpm, fuel flow, fuel quantity, and exhaust gas temperature (EGT). Also included were the computer select mode control (CSMC) box and pulse panel.

The pilot's interface to the PCS was through standard fighter aircraft three-axis proportional controls consisting of a throttle lever, stick, and rudder pedals. The speed-brake switch was provided on the top of the throttle lever. The stick and rudder pedal force and displacement characteristics are presented in table 2.

The pilot's interface to the BCS was through the BCS discrete command switches on both the right and left consoles. The climb–dive, turn command switch was on the right with the other mode command switches. The speed increase–decrease command switch was on the left console. The commands from these switches were transmitted directly to the uplink encoder. Similar discrete panels were in the rear cockpit of the TF-104G chase aircraft. No HiMAT vehicle telemetry data were provided to the F-104; therefore, control and guidance from the chase aircraft was visual only.

The flight test engineer (FTE) communicated with the pilot to assist with navigation, checklist and emergency procedures, pulse panel test inputs, system gain changes, and landing energy management. The pilot and the FTE navigated using a radar-driven plot board showing ground track position. Energy was managed during landing approach when radar-driven glide slope was displayed on a plot board. Pulse panel inputs were initiated by the FTE and consisted of preprogrammed computer-generated control commands used to excite the aircraft motions independent of the pilot. System gain changes were usually reduced prior to pulse panel command inputs. Management of these tasks by the FTE greatly reduced pilot workload.

### Control Law, Maneuver, and Navigation Computers

Three separate computers (fig. 3) were used to perform the PCS control law, maneuver autopilot, and navigational computational functions in a normal mission. These computers were Varian V-73A, V-73B, and V-72 computers, respectively.

Vehicle downlinked sensor signals, processed through the V-77 computer, were combined with the pilot's stick and throttle command inputs, from the cockpit, in the V-73A PCS control law computer. The PCS command signals would then be generated and uplinked to the vehicle. The V-73A computer was synchronized at 53.3-Hz frame rate to correspond to the fixed telemetered uplink rate. In addition to the PCS control law, the V-73A computer also performed air data calculations (Mach number, altitude, altitude rate, airspeed, and dynamic pressure) for display in the ground cockpit. Some failure detection algorithms were also mechanized. In addition to the real-time in-flight computations performed by the V-73A, this computer was used to automate a systematic vehicle preflight program that tested all input and output interface parameters both statically and dynamically.

To assist in the acquisition of high-quality data, a flight test maneuver autopilot (FTMAP) control law was mechanized in a V-73B computer (Duke and others, 1986). The FTMAP was designed to provide precise, repeatable control of the HiMAT vehicle during certain prescribed maneuvers. The FTMAP operated as a non-flight-critical outer-loop controller in conjunction with the PCS. During FTMAP operation, the FTMAP computer (fig. 5) replaced the normal pilot command inputs to the V-73A PCS computer. In addition to the FTMAP control law, the V-73B computer passed to the cockpit ADI the landing guidance information generated in the V-72 computer.

The V-72 computer received and decoded tracking radar data and computed vehicle ground track information for display to the ground pilot. In addition to generating ground track information, the V-72 computed a quasi-instrument landing system (ILS) glideslope and localizer for display in the cockpit during approach and landing.

The characteristics and functions of the V-77, V-73 and V-72 ground computers are summarized in table 3.

### Uplink Encoder

The PCS command signals, from the V-73 computer, were combined with the cockpit discrete signals in the uplink encoder prior to transmission to the vehicle. The encoder was formatted to send four 16-bit words per frame at a rate of 106.6 frames/sec. Two different frames were alternately sent for a total of eight 16-bit words updated 53.3 times/sec (frame rate of 18.76 msec). The uplink data format is shown in figure 5. The first four words addressed vehicle decoder number one, and the last four words addressed vehicle decoder number two. The first 10 bits of each word were available only to the primary onboard computer and were designated proportional data. These proportional channels represented the PCS interface to the vehicle aerodynamic surfaces and throttle. The last 6 bits of each word were designated as manual command discretes and were hardwired directly to the encoder from cockpit switches. These discretes represented the pilot's discrete interface to the onboard BCS and other vehicle systems.

## Airborne Systems

Figure 6 presents an overview of the integrated airborne systems. This figure shows the major components of the airborne systems and includes the following: uplink receivers–diversity combiner–decoders, airborne computers, flight sensors, servoactuator electronics (SAE) box, and FTIS.

### Uplink Receivers–Diversity Combiner–Decoders

Dual receivers–decoders received the uplink signal and provided the command input interface to the dual onboard computers. The PCS required both receivers–decoders to be operational. If either decoder failed, an automatic transfer to BCS resulted. Early in the HiMAT program, there were frequent automatic transfers from PCS to BCS because either or both receivers–decoders received inadequate uplink signals as a function of vehicle attitude. To eliminate these nuisance transfers to BCS, a diversity-combining concept was used in the hardware to provide uninterrupted telemetry coverage (Harney, 1981). The diversity combiner continuously combined the output signals of the dual receivers so that regardless of the orientation of the airplane with respect to the transmitting antenna, the best signal was available for all uplink commands. Diversity-combining hardware was installed

in vehicle number one following the third flight, and nuisance transfers to BCS were virtually eliminated. Vehicle number two was modified in the same way.

### Airborne Computers

The dual onboard digital computers (fig. 7) were designed and built especially for the HiMAT vehicles. These computers formed the heart of the entire HiMAT system and each was designed to control the vehicle should the other fail. All critical onboard flight systems were controlled by these computers. These two computers were based on Intel 8080 microprocessors (Intel Corporation, Santa Clara, California) and operated asynchronously with respect to each other but had identical computational and memory capacities. The computers were designated primary and backup, with different resident software and input–output interfaces. Each computer contained 22,528 bytes (8 bits) of erasable, programmable, read-only memory and 1024 bytes of random access memory. Both computers were programmed entirely in 8080 assembly language and packaged in a common chassis with separate circuit card sets and connectors. The dual computer chassis weighed 40 lb and had a volume of 1198 $in^3$.

The principal functions of the primary computer were as follows: (1) uplink data processing, (2) downlink data processing, (3) failure detection for the computers, flight sensors, servoactuators, and power system (for both backup and primary flight control modes), and (4) backup IPCS. The principal functions of the backup computer were (1) uplink data processing, (2) primary IPCS, and (3) BCS control laws.

Computer interfaces with aircraft systems consisted of three types — digital, discrete, and analog. Each of the computers communicated with the outside world via the telemetry uplink and downlink systems, and with each other via an intercom. For additional details on the HiMAT airborne computers, see Myers and others (1981).

### Flight Control Sensors

Seven redundant flight-critical control system sensor sets were necessary to provide the HiMAT with the fail-safe operational capability. Five of the sensor sets were triplex and two were duplex. The seven sensor sets included the triplex three-axis angular rate gyros, normal and lateral accelerometers, and the duplex air data system(static and impact pressures). Air data rates were determined by an analog differentiation of the air data signals. A single sensor of each set was designated the backup to the BCS.

A simplex vertical gyro (all-attitude gyro) and radar altimeter were provided, however, they were not flight control system critical. The vertical gyro provided vehicle attitude information to the pilot's ADI and to a direction cosine algorithm in the BCS code. The radar altimeter provided data to the pilot at altitudes below approximately 5000 ft in the landing approach situation and was a key input to the BCS in the automatic landing mode, however, the BCS could be used to land the vehicle even if this instrument failed.

### Servoactuator Electronics Box

The servoactuator electronics (SAE) box provided the interface between the onboard computers and the control surface servoactuators and the engine nozzle. The SAE box functions included electrically closing all servo loops to the actuators, receiving all actuator commands from the computers, and feeding back all actuator positions to the computers. Another major function was the failure detection of the elevon servoactuator system, which was detected faster in hardware than software. If a failure was detected, it was communicated to the primary computer (this is discussed in the duplex actuator failure management section).

### Flight Test Instrumentation System

To complete the onboard systems, the flight test instrumentation system (FTIS) handled and processed all data to be downlinked into a digital PCM data stream. Inputs to the FTIS included both direct sensor (analog) and onboard computer (digital) inputs. Select signals were downlinked directly through the FTIS and also through the onboard computer. Onboard computer data to be downlinked were processed through the downlink processing routine. This routine processed and formatted eighteen 10-bit proportional parameters and seven 10-bit discrete words. Also included in this routine were midvalue selection of the triplex sen-

sors, synchronization logic, and the packing of vehicle status and failure indication discretes. The PCM signal to be downlinked was input to dual transmitters to be telemetered to the ground at 220 Hz.

# CONTROL SYSTEMS DESCRIPTIONS

## Systems Overview

The design goal of the HiMAT was that it should be capable of a sustained 8-g turn at Mach 0.90 at an altitude of 25,000 ft. To achieve this transonic maneuver performance goal, it was required that

1. the vehicle be ballasted to an aft center-of-gravity condition to reduce trim drag and
2. the wings be aeroelastically tailored to provide favorable spanwise twist for drag reduction.

The combination of vehicle aft center of gravity and aeroelastically tailored wings resulted in trailing edge down elevator and elevon trim with favorable wing twist at the specified design point. The aft center of gravity resulted in a longitudinal static margin of 10-percent negative at low angles of attack which increased to 30 percent at high angles of attack at low subsonic Mach numbers. These negative static margins placed unusual demands on the development of both the ground and airborne active control systems. Owing to the high-risk nature of such an approach, the HiMAT program was conducted in two phases. The first phase was a relatively conservative approach with the vehicles ballasted in a forward center-of-gravity or stable configuration. The second phase was with the vehicles ballasted at a mid or aft center of gravity or RSS configuration. This approach allowed the accomplishment of the initial objectives and provided quantitative data for the continued development of the RSS control systems. The disadvantage of this approach, however, was that the development of both stable and RSS control laws was required.

## Stable Control Systems

The basic design considerations used in the development of the ground-based PCS and airborne BCS were to provide adequate flight control over the entire flight envelope and to provide systems that would ensure completion of all program objectives.

### Stable Primary Control System

The stable PCS was a full-authority three-axis rate damper system that commanded the elevators and elevons for pitch control, the elevons and ailerons for roll control, and the rudders for yaw control and drag modulation. Petersen (1979) presents additional details of the stable PCS.

The HiMAT stable PCS longitudinal control law is shown in figure 8. The pitch rate feedback signal passed through a pilot-switchable gain and was summed with prefilter pitch stick input. The combined signal was multiplied by a gain factor scheduled as a function of static pressure and summed with a filtered angle-of-attack feedback signal. Used as an angle-of-attack inhibiting device, the angle-of-attack feedback signal commanded a nose down input whenever the vehicle's angle of attack exceeded 8°. The total-longitudinal command drove both the elevators and the symmetric component of the elevons. A launch mode input was implemented that inserted a nose down bias command during the launch sequence to ensure separation from the B-52 aircraft. Fader elements were implemented in the command paths to provide synchronization of the PCS uplink commands to the control surface positions while in the backup mode, and minimization of surface transients during a transfer from BCS to PCS. The final elevon and elevator commands were then summed with auxiliary input signals controlled from a cockpit-mounted pulse panel prior to uplink output. The pulse panel inputs were used to excite the aircraft for the extraction of stability derivatives.

The lateral-directional control laws of the stable PCS are shown in figure 9. The roll rate feedback signal was summed with the filtered roll stick input to form the basic roll command. The roll rate gain and roll stick gearing were scheduled as functions of dynamic pressure and Mach number, respectively. The roll command controlled both the aileron and asymmetric elevon commands at a ratio determined by the aileron command gain. The rudder command consisted of the combination of rudder-pedal position and high-passed yaw rate multiplied by a gain scheduled with dynamic pres-

sure. Pilot-switchable gain functions were implemented for both the roll and yaw rate feedbacks. The faders and pulse panel inputs were used for the same functions described previously.

Throttle position in the cockpit was passed through a nonlinear limiting function forming the throttle uplink command (fig. 10). Drag was modulated by deflecting the rudders asymmetrically trailing edges outboard as speed brakes. Speed brake authority was limited to 5° on each surface and was controlled using a throttle mounted discrete switch that activated an integrator within the primary control laws (fig. 11).

During the conduct of the stable phase of the flight-test program, several stable control system evaluations were conducted in support of the RSS phase. These evaluations included (1) roll control with only differential elevon (ailerons locked), (2) evaluation of an aileron-to-rudder interconnect, and (3) lateral acceleration feedback to the rudders. Because the PCS was coded in FORTRAN, these modifications to the basic stable PCS were relatively easy. Simple discrete switches were used to activate each function for evaluation. Additional details of these evaluations are presented in the flight data section of this report.

### Stable Backup Control System

The BCS was designed to recover control of the vehicle from unusual or extreme attitudes, provide well-controlled vehicle dynamics throughout the flight envelope, and provide adequate control modes and vehicle stability to land at a selected site under control of either the ground or airborne controller. Failure in any one of a variety of primary systems would normally result in an automatic transfer to BCS. Table 4 lists failures that would result in automatic transfers to BCS.

To ensure BCS versatility, a variety of automatic modes was implemented. Table 5 presents a list of the seven major modes mechanized in the BCS. Further, the BCS was required to command the vehicle to orbit at a specified altitude even in the absence of uplink or downlink carrier signals. All commands into the BCS were discrete: there were no proportional commanded inputs. Internal logic was used extensively for mode switching and control and keyed upon these discrete commands. The basic BCS loop structure provided inner-loop stabilization functions at 100-Hz execution rate, outer-loop command functions at 50-Hz execution rate, and less time-critical functions, such as some gain schedules, at 10-Hz execution rate. Further discussion of the BCS is presented in the RSS BCS section. Kempel (1982) presents additional details on the BCS.

### Degraded Primary Mode

Under certain failure conditions, such as engine failure, it was more desirable to retain proportional control rather than to be limited to discrete commands through the BCS. The pilots felt that proportional control would provide more precise control of the vehicle and should be retained if possible. The degraded primary mode, therefore, was mechanized as a subset of the normal PCS control law. The degraded primary mode (DPM) was ground-pilot selectable in the event of certain airborne failures, such as engine failure. In DPM the pilot retained his proportional stick, rudders, and throttle commands. The DPM control law was resident in the V-73A computer. When the DPM was selected, the vehicle backup systems were activated just as they would be had a transfer to BCS occurred, that is, elevator locked, elevon active for pitch and roll control, rudder for yaw control, and backup electrical and hydraulic power active.

### Integrated Propulsion Control System

The HiMAT engine was totally under control of the onboard computers. The primary IPCS control law resided in the backup computer, and the backup IPCS was resident in the primary computer. The primary IPCS was mechanized in the backup computer owing to the memory limitations in the primary computer. The IPCS emulated the conventional J85-21 engine mechanical controls, but it also provided additional control modes not found in standard engines.

The IPCS concept was based on the retention of most of the conventional engine control hardware and allowed the implementation of flight–propulsion control coupling, high and normal engine stability margin operating modes, and rapid and normal thrust response modes through the computer program. For additional details on

the IPCS, see Bayati (1976) and Baer-Riedhart (1981). Table 6 lists the IPCS commands and the engine feedback signals for both PCS and BCS operation.

In the primary IPCS, the engine was operable in either a normal or combat mode and at a high stability setting. In the normal mode, the engine operated in a conventional manner. In the combat mode, the rate of thrust response was significantly greater than that of a standard engine. The engine rotor speed was maintained at near intermediate power for all settings, and dry thrust modulation was achieved by varying the exhaust nozzle. The high-stability mode provided operation of the engine at a lower exhaust gas temperature, resulting in an increased stall margin compared to a standard engine.

The engine was controlled in PCS from the ground cockpit via the proportional throttle and discrete switches for the various engine operating modes. Cockpit discrete switches included (1) engine igniter, (2) combat mode, (3) nozzle override, (4) high stability, and (5) throttle reset. Throttle reset was used when some fault indication automatically selected the secondary throttle system. Throttle reset was used to reselect primary throttle when the fault was cleared.

Throttle commands in BCS were generated based on prescribed airspeed schedules that were a function of the BCS operating mode. In BCS the engine was limited to dry power operation with either high or normal stability mode, depending on which had been selected prior to transfer. Combat mode and afterburner operation were inhibited in BCS.

## Relaxed Static Stability Control Systems

The basic design considerations used in the RSS control systems were the same as those for the stable control systems, that is, to provide adequate flight control over the entire flight envelope and to provide systems that would ensure completion of all program objectives. The RSS control systems were designed for the 10-percent aft center-of-gravity configuration; however, operational considerations again dictated a more conservative approach and the vehicle was flown only at 5-percent aft configuration.

### Longitudinal RSS PCS

Development of a ground-based primary flight control system for a statically unstable vehicle proved difficult at best. Significant time delays from airborne sensor input to surface commands existed. Figure 12 presents significant signal paths, using the pitch rate signal input and the elevators and elevons as outputs. Delays in each element of the control loop were analyzed and included (1) sensor filter delays, (2) telemetry downlink time, (3) telemetry ground data formatting and transfer, (4) V-77 and V-73 computer processing times, (5) uplink command delays, (6) onboard uplink receiving and computer processing times, and (7) servoactuator system delays, to complete the loop. Total system time delays from sensor input to servoactuator surface command input were found to be approximately 50 to 60 msec. Delays of this magnitude in pitch rate proved unacceptable for the RSS configuration.

The solution to the problem of excessive time delays was to include aboard the vehicle a complementary fixed gain pitch rate feedback to the elevons and elevators that provided significantly less than the 50 to 60 msec time delay that existed with the ground-based PCS. The mechanization of the onboard pitch rate feedback was through the primary computer, synchronized with the PCS uplinked pitch rate command, but with a significantly decreased time delay from sensor input to command output (see fig. 12). Pitch rate sensor input to the primary computer occurred between 1.0 and 1.2 msec prior to being input to the downlink data stream routine. The downlink data routine received the pitch rate input and was executed at 220 Hz, or every 4.54 msec. This routine then passed the pitch rate information to the uplink decoder routines (decoder 1 for elevons and decoder 2 for elevators) through the computer, circumventing the ground loop. This information was then multiplied by the onboard pitch rate gain (KBQ) and summed with the uplinked pitch rate command signal for the elevons and elevator. It was determined that the maximum time required from pitch rate sensor input until this command was available as a surface

command was 5.9 msec. The onboard pitch rate surface commands were constrained to the 18.76-msec frame time (53.3 Hz) per elevon or elevator of the uplink, but alternating between the elevon and elevator frames so that a pitch rate command was sent to a pitch surface (elevons or elevator) at twice this rate or every 9.38 msec (see Uplink Encoder section). Although this time did not include the servoactuator delay, it constituted a significant improvement over the time delay through the ground path.

The onboard pitch gain was fixed at KBQ = −0.25 deg/deg/sec unless a transfer to DPM occurred and the elevators were locked. This gain was then multiplied by 2 owing to the availability of half of the pitch control surface and with an execution time of 18.76 msec.

The RSS PCS control law is shown in figure 13. The ground-based longitudinal control law consisted of two distinct parts: the first was a pitch command augmentation system, referred to as the normal controller, and the second provided angle of attack and normal acceleration limiting. The feedback signals to the normal controller consisted of (1) low-pass filtered pitch rate at a fixed gain, (2) low-pass filtered normal acceleration at a fixed gain, and (3) high-pass filtered angle of attack used only at supersonic speeds to improve command response. These signals are summed with the shaped pilot's stick command. The combined signal was then multiplied by a gain factor scheduled as a function of dynamic pressure. These signals were then output to logic that determined which commands would be honored, the normal controller's or the limiters'. Assuming that the vehicle was not at either of its limits, the signal was summed with a forward integration of the signal and a command was output to both elevators and elevons. The forward loop integrator provided longitudinal trim as long as the stick was centered. Fader elements were implemented in the command paths and provided the same function as the stable PCS. The commands were then summed with auxiliary input signals generated in the V-73A computer and controlled manually on the CSMC panel at the cockpit. These auxiliary inputs consisted of flutter excitation pulses and commanded step and pulse inputs for data analysis. In addition, each of the feedback gains could be multiplied by constants if system considerations dictated. These constants were also programmed in the V-73A computer and were manually selectable on the CSMC panel. As in the stable PCS, a launch mode input was implemented which inserted a nose down bias command for the first 3 sec following launch, thus ensuring positive separation from the B-52 aircraft. Table 7 presents all RSS PCS gains, gain schedules, and filter representations.

The angle-of-attack limiter schedule is shown in figure 14. The positive limit was constant between low Mach numbers and 0.8 at 12° and 15° between Mach 0.9 and higher. Negative angle-of-attack limit was −3°.

### Lateral–Directional RSS PCS

The lateral-directional RSS PCS control law is shown in figure 15. The roll rate feedback signal was summed with the low-pass filtered lateral stick input to form the roll command. The roll rate gain was a scheduled function of both dynamic pressure and Mach number while the lateral stick gearing gain was a function of Mach number only. The roll command controlled only the asymmetric elevon. The rudder command consisted of the combination of (1) rudder pedal position, (2) lateral stick input, (3) lateral acceleration, and (4) yaw rate. The rudder pedals in the HiMAT were seldom used. The aileron-to-rudder interconnect was a scheduled function of angle of attack. The lateral acceleration gain was a scheduled function of dynamic pressure, and the yaw rate was low-pass filtered with the gain a scheduled function of both dynamic pressure and Mach number. Manually switchable gain functions were also implemented for roll and yaw rates and lateral acceleration for use as required. Faders and pulse panel inputs were used for the same functions described previously.

## Backup Flight Control System Modes

The BCS was a full-authority, three-axis, multimode, multirate digital controller with stability augmentation functions and mode command functions. The seven BCS modes are listed in table 5. A brief discussion of these seven modes follows.

### Recovery Mode

The BCS was initialized in the recovery mode and generally every transfer to BCS sequence occurred through this mode. The recovery mode brought the vehicle to straight and level flight. If the altitude rate was greater than 12,000 ft/min when BCS was engaged, an inverted recovery would occur to preclude potential engine flameout and lubrication problems. During the recovery sequence, discrete commands were not accepted into the BCS. The BCS would not exit the recovery mode until the Mach number was less than 0.96 and until the altitude rate was less than 600 ft/min. When these conditions were satisfied, external commands were accepted and a 25-sec timer was initiated. Once recovery was complete, the mode would automatically change to heading hold and altitude hold until another command was received, or until expiration of the 25-sec timer, when the mode would go to orbit unless an exit orbit command was present.

### Orbit Mode

The orbit mode and direction of turn were selectable via the discrete panel. Orbit mode could not be entered until the 25-sec timer had expired. When the orbit mode had been entered, the vehicle would automatically climb or dive to one of three preselected orbit altitudes at a fixed altitude rate of 6000 ft/min and at a bank angle of approximately 35°. Dive to orbit altitude would occur only at altitudes above 25,000 ft; at lower altitudes, the vehicle would climb to orbit.

When orbit altitude was reached, the altitude rate was commanded to zero and the vehicle continued to orbit at constant altitude, airspeed, and bank angle until an exit orbit command was received.

If telemetered (TM) carrier signal was lost at any time, a 25-sec timer was initiated and the vehicle entered the orbit mode upon expiration of this timer; it then remained in orbit until communication was reestablished. If the engine failed during loss of communication, the vehicle would spiral to the ground.

If exit orbit had been selected, the BCS was in altitude hold, airspeed hold, and heading hold until another command was received.

### Climb–Dive Mode

All climbs or dives were done at fixed values of altitude rate and could not be adjusted by the pilot. Climbs or dives were at 6000 ft/min, with the exception of dives begun below 10,000 ft, which were at 3600 ft/min. The throttle responded to maintain the appropriate airspeed in climbs or dives. Turns could be executed while in a dive or climb.

### Turn Mode

Two types of turns were available and were pilot selectable. The first was attitude command and the second was roll rate command. In attitude command, vehicle attitudes were computed in the BCS by integrating a direction cosine set, using vehicle angular rates as inputs. In attitude command, turns were at bank angles of approximately 35°, or, if the pressure altitude was below 4000 ft, at bank angles of 20°. In roll rate command, the pilot could roll the vehicle to any bank angle at a rate of 15 deg/sec. Therefore, when in roll rate command, the pilot had to monitor vehicle bank angle by video, the attitude-direction indicator, or visually in the case of the chase controller. The roll rate command system was included to provide the pilot with the capability to make small heading corrections during final approach.

### Landing Mode

The landing mode was a pilot-selectable switch function. Vehicle airspeed and descent rate were scheduled functions within the BCS and were keyed on radar altitude. The radar altimeter range was from 0 to 5000 ft, so landing mode was usually selected at altitudes below 5000 ft above ground level (AGL). Once the vehicle had been maneuvered to a position where the landing mode could be engaged, the pilot need not provide additional inputs for landing, although the system did have the capability of modulating both airspeed and altitude rate during the landing approach. Minimum airspeed in the landing mode was 185 knots, and commanded altitude rate at zero altitude was −5 ft/sec.

### Engine-Out Mode

In the engine-out mode, the BCS used the elevons for glide airspeed control and altitude-rate

control in the landing flare. Commanded glide airspeed was 215 knots, but the pilot could control airspeed from 165 to 300 knots via the BCS throttle-control discrete switch on the left console. The BCS transferred from speed command (glide) to altitude-rate command (flare) at 550 ft AGL. Airspeed at the 550-ft point was to be no higher than 240 knots nor lower than 190 knots, with pilot commanded gear deployment at approximately 70 ft AGL. In the flare, the commanded altitude rate was ramped from the existing altitude rate at 550 ft to -5 ft/sec at 25 ft.

## Backup Flight Control System Loop Structure

### Longitudinal RSS BCS Control Law Loop Structure

The BCS longitudinal stabilization control loop is shown in figure 16. This loop consisted of direct pitch rate feedback plus an integral feedback combination of washed-out pitch rate and load factor. The direct pitch rate gains were scheduled as a function of air data parameters.

The outer-loop commands were input as a load factor command that was a function of the internal BCS logic state. The longitudinal portion of the recovery-mode command loop is shown in figure 17. Static pressure was the only input to the longitudinal path in this mode. The derived altitude rate was subtracted from the initial altitude rate to form the altitude-rate error, which was driven to zero, thus bringing the vehicle to level flight.

Figure 18 shows the altitude-hold, climb–dive, and landing mode loop structure. As in the case of the recovery mode, static pressure was the only input. The climb–dive and landing modes were altitude-rate commands so the loop structure was similar in each case. In the climb–dive mode, the commanded altitude rates were fixed; in the landing mode, they were a scheduled function of radar altitude. The altitude-hold mode maintained constant altitude based on the difference between existing static pressure and the altitude-hold pressure, as determined by the track and hold function. This difference was then multiplied by the GRAD function to determine altitude error.

Altitude rate was computed in BCS based on an analog differentiation of static pressure. Static pressure rate was then multiplied by the GRAD function, which was the gradient of static pressure with altitude, to determine the derived altitude rate. Altitude rate was not determined by a differentiation of radar altitude.

### Lateral-Directional RSS BCS Control Law Loop Structure

Figure 19 presents a simplified concept of the lateral-directional BCS. Two turn modes were available: a roll rate command mode provided the ability to command bank-angle changes of any desired magnitude at a constant 15 deg/sec roll rate, and the attitude command mode provided a wing-leveling function and a constant 35° or 20° bank-angle turn capability. To accomplish the attitude command task, a direction cosine algorithm, integrating vehicle angular rates, was mechanized in the BCS. The simplex vertical gyro was used to update the direction cosines every 5 sec. In the event of a vertical gyro failure, a manual discrete, at the pilot's station, discontinued the 5-sec update, and update was then referenced to a set of constants when wings were level, as determined by small angular rates. The direction cosines were used to calculate bank-angle error flags, which were used in the internal BCS logic to determine when and in which direction to command roll. A heading-hold function became active when the BCS was not in a turn. The BCS directional stabilization consisted of a yaw rate feedback for flights with a forward center of gravity. With 0 percent or more aft center-of-gravity positions, a lateral acceleration feedback was included.

### BCS Throttle Control Law

All airspeeds in the throttle control law (fig. 20) were determined based on an impact-pressure command. Above 20,000 ft pressure altitude, Mach number was determined by a schedule of impact-to-static-pressure ratio for the commanded Mach number. This pressure ratio was then multiplied by the measured static pressure, and the impact pressure for that Mach number at that altitude was issued as the commanded input. Below an altitude of 20,000 ft all airspeeds were determined based

on scheduled impact-pressure command schedules. Impact-pressure rate was used for airspeed damping. Above 20,000 ft, the BCS commanded a Mach number of 0.8; below 20,000 ft, it commanded a constant airspeed of 300 knots. The pilot had limited control over airspeed: to Mach 0.9 or 350 knots at the high end and to 185 knots at the low end.

Additional information concerning BCS loop structure is contained in Hoyt and others (1980) and Woolley (1978).

# FLIGHT SYSTEMS FAILURE MANAGEMENT

The dominant HiMAT systems design requirement that no single failure will result in the loss of the vehicle describes the overall failure management strategy used on the HiMAT program. Fault detection mechanisms existed in the hardware and software of the ground and airborne HiMAT systems. The hierarchy of HiMAT systems failure detection is shown in figure 21. The failures detected by the ground and airborne systems are outlined in tables 8 and 9, respectively. Most of the failure indications were displayed to the systems engineer in the control room on the master caution and warning panel (MCWP) shown in figure 22. Most of the system faults illuminated a master abort light which was used as an abort mission and return to base signal. A few of the more important failure indications were displayed directly to the pilot on cockpit annunciators.

The faults detected by the HiMAT onboard computer systems could be classified into four categories, as follows:

1. Caused automatic transfers to backup mode
2. Prevented automatic transfers to backup mode
3. Indicated mission abort conditions
4. Indicated caution conditions

The various system failures in the aforementioned categories are listed in table 9.

The failure-detection mechanisms onboard the vehicles and on the ground were similar in philosophy. Watchdog timers, digital-to-analog converter (DAC) and analog-to-digital converter (ADC) wraparound tests and loop counters were used in computer self-tests; uplink and downlink discretes had to persist through multiple frames before they were accepted. Uplink and downlink proportional data had to pass rate checks prior to acceptance. Redundant analog inputs, such as airborne sensors and ground stick, were compared with predetermined tolerances.

## Ground Failure Management

Failure detection and management in the ground-based computer software (table 8) included a variety of different tests that determined the health and validity of the downlink signal and ground systems.

### Downlink Integrity

The following tests determined the integrity of the downlink signal:

1. Downlink discrete persistence check—The downlink discretes were required to remain constant for three consecutive frames prior to being honored as a true change in state, that is, true or false.
2. Downlink parameter rate check—The rate of change of downlink parameters in excess of 100 PCM counts from one frame to the next was not honored as legitimate data.
3. Downlink word counter check—A counter in the last two words on the downlink was checked to ensure that the values were changing and that the V-77 computers had not failed.

### Uplink Integrity

The following tests determined the integrity of the uplink signal:

1. Uplink proportional rate check—The uplink aerodynamic surface commands were rate limited to ensure that these commands did not exceed the rate limits of the vehicle servoactuators.
2. Uplink discrete check—The cockpit input discretes were required to persist for two frames prior to being honored as a true change in state.

### Real-Time Loop Integrity

The V-73 computer performed a dual function of computing air data calculations for display in the cockpit and computing the PCS control law. Failure detection was mechanized for both these functions and included the following:

1. Nonsynchronous or instrument model loop check—This test checked a 10-frame counter. If the counter was not reset within 10 frames, the instrument model was declared failed.

2. Primary real-time loop check—A time-out counter was checked to determine that the primary real-time loop (PCS control law) was operating. If this counter was not reset in 20 frames, the primary loop was declared failed.

### Computer Watch-Dog Timer

The V-73 watch-dog timer consisted of missing pulse detector routine contained in the V-73 computer. This routine was called each frame, and if missing, a failure was declared.

### Stick Input Checks

The dual stick, rudder, and throttle inputs were checked to ensure that they were within tolerances. If tolerances were exceeded, stick failure was declared.

### DAC/ADC Wrap Tests

A wraparound test from DAC signals to ADC signals was made to check real-time input–output (IO). If this test failed, a stick fail annunciation was made in the cockpit.

### Air-Data Miscompares

The dual air data parameters were compared to ensure meeting tolerances. If air data miscompare was declared, air data fail annunciation was made in the cockpit.

### Angle-of-Attack Miscompares

The dual angle-of-attack signals were compared to ensure that they were within 2° of each other. If a difference of 2° was exceeded, an angle-of-attack failure was declared and the RSS PCS angle-of-attack signal was ramped to zero and held until the failure was cleared.

## Airborne Failure Management

Airborne failure was managed by airborne software when failures were detected in software or hardware. Failure consequences and failure annunciation to the ground station are summarized in table 9. Normally, failure indications were downlinked for display in the cockpit and the MCWP. Fault detection was a primary computer task, with uplink system failure and computer self-test diagnostics done in both the primary and backup computer.

### Hydraulic Systems

Failure of hydraulic systems was detected by monitoring hydraulic pressure and hydraulic fluid level in both primary and backup hydraulic systems. A primary hydraulic system failure resulted in an automatic transfer to BCS while a backup hydraulic failure inhibited automatic transfers to BCS.

### Electrical Systems

Electrical systems failure was detected by monitoring primary electrical (generator) and backup electrical (battery) voltage. A primary electrical failure resulted in an automatic transfer to BCS. Hardware was mechanized to monitor the generator bus and did an automatic bus split if the voltage fell to approximately 26 V.

### Duplex Actuators

A failure in the primary side of a duplex actuator resulted in an automatic transfer to BCS, while a failure in the secondary side inhibited a transfer to BCS. Two methods for determining failures of a duplex actuator were used. First, a failure in the duplex rudder was detected by a cross-ship comparison as in the simplex actuators. Second, failure detection in a duplex elevon servoactuator was mechanized, external to the onboard computers, in the servoactuator electronics (SAE) box. An analog model that duplicated the elevon servovalve dynamics was used to detect failures. The actual servovalve signals were combined with the modeled values to form an error signal which was then sent to the primary computer for processing.

### Simplex Actuators

Failure of the simplex actuators (elevator, canard, and aileron) was detected by a cross-ship comparison algorithm in the primary computer. In the event of a cross-ship miscompare of a simplex ac-

tuator, the primary computer commanded an automatic transfer to BCS. Upon transfer to BCS, all simplex actuators were commanded to their locked positions.

### Triplex Sensors

Triplex sensor failure was detected by comparing the output of the two nonmidvalues with the midvalue output for each of the five triplex sensor sets. Failure indications (miscomparisons) were downlinked to the ground and annunciated on the MCWP; however, no automatic action was taken, since a failed sensor would have been voted out of the system by the midvalue selection process. If the number three sensor of a triplex set failed (number three sensor outputs were input to the BCS), automatic transfers to the BCS were inhibited.

### Duplex Sensors

Air data duplex sensor faults were detected by comparing the primary static and impact pressure transducer outputs with those of the corresponding backup transducer outputs. If a disagreement existed, the state was downlinked for resolution on the ground. The static and impact pressures were also used to digitally compute predicted static and impact pressure rates. These predicted rates were then compared with the analog differentiated rates to determine if the air data pressure rate failed.

### Downlink System

A failure in the downlink system was determined by the loss of synchronization between the onboard computer and the flight test instrumentation system. A loss in synchronization would automatically result in a transfer to the BCS.

### Uplink System

The uplink monitoring logic determined whether both decoders were operational, which was a requirement to remain in the PCS mode, and whether the uplink command discretes were valid.

The PCS required a complete set of proportional commands to be available for output to the control surfaces. If missing data indicated one or both decoders failed, an automatic transfer to BCS was commanded.

As shown in figure 6, the critical uplink command discretes were sent to both decoders. Discrete validity was ensured by two methods: a persistence test guarded against noise being interpreted as a command; and if both decoders were operational, the discretes from the two decoders had to agree before they were acted upon. If a discrete difference between decoders occurred, it was possible for the ground station to command the onboard system to use the discretes from the decoder whose data were correct, based on information telemetered to the ground.

### Computer Self-Test Diagnostics

The computer intercom was checked by sending a diagnostic test message from the primary computer to the backup computer. The backup computer echoed the message to the primary computer where it was checked for accuracy. Two different messages were used so that all bits could be checked in both the on and off states.

Self-test software was used in each computer. These tests included random access memory (RAM), erasable programmable read only memory (EPROM), hardware multiplier tests, ADC and DAC tests, and instruction diagnostic tests. If a failure was detected, the failed computer would take itself off-line by turning on its computer failure discrete output and freezing its watchdog pulse output. A primary computer failure caused a transfer to BCS, while a backup computer failure inhibited automatic transfers to BCS.

## Systems Flight Qualification

### Qualification Tests

Extensive qualification testing of all aircraft systems and subsystems hardware, and ground and airborne software was required to certify a HiMAT vehicle for flight. Onboard computer hardware was qualified environmentally by the use of components meeting military specifications and by environmental tests both before and after delivery. Computer hardware was tested to the requirements of standard specifications.

The onboard computer interfaces were verified in four different test sequences (integrated systems, combined systems, iron bird, and preflight), portions of which were repeated anytime a modification was required to the interface.

The integrated systems test sequence demonstrated that each vehicle subsystem operated correctly. This test phase included signal interface and continuity checks, power system checks, the functional qualification of both the backup and primary hydraulic and servoactuator systems, vehicle telemetry uplink and downlink systems testing, and engine test runs with the engine both installed and uninstalled.

Combined system testing was conducted with the HiMAT vehicle operating in combination with the RPRV facility. All ground and airborne systems were active in these tests with the exception of the radiofrequency links, which were hard-lined with cables. This test sequence included end-to-end signal verification, closed-loop total system and subsystem time delay measurements, ground resonance tests, and automated preflight testing, both onboard and ground based. Open-loop failure modes and effects tests were conducted to validate proper system response to component and subsystem failures.

The iron bird simulation test sequence expanded the combined systems test configuration to include real-time simulation of the vehicle dynamics, aerodynamics, and engine model. Tests conducted during this phase included dynamic response for both the PCS and BCS flight modes, limit cycle, closed-loop failure modes and effects, piloted evaluation and training, and a complete mission profile simulation.

Vehicle preflights were a final check of all vehicle subsystems and were performed as close to each flight as possible. This test sequence used the interface capability resident in the onboard computers to verify interface and subsystem operation. Upon completion of the preflight check, all subsystem configurations were frozen and could not be changed without invalidating the preflight checks. If removal of hardware was required, a preflight check was performed again on that item.

### Simulation Systems

Four types of simulations were used to qualify onboard computer software (Evans and Schilling, 1983; Evans and Schilling, 1984). In each of these systems, the vehicle dynamics were simulated in the Dryden Cyber 73-28 computer (Cyber Systems, Inc., Anaheim, California). The four HiMAT simulation systems, termed ALL-Cyber, Cyber-Varian, CASH, and iron bird are described in the following paragraphs. In the order presented, each included more actual HiMAT hardware in the loop than the previous one.

The ALL-Cyber simulation (fig. 23) was the principal tool in the design and development of both the BCS and PCS software since it permitted designs to be verified in a dynamic environment before they were implemented in the ground and airborne flight computers. In this simulation, the HiMAT servoactuator system and the uplink and downlink systems were all modeled, along with HiMAT vehicle dynamics, using a Cyber 73-28 computer. This simulation was interfaced by way of the Cyber computer's real-time input–output system with a HiMAT simulation cockpit.

The Cyber-Varian simulation (fig. 24) allowed much of the HiMAT PCS software to be validated in the simulation facility with ground computers identical to those used for flight, and with a full simulation of the HiMAT vehicle dynamics. Simulation cockpit uplink and downlink interfaces permitted ground-based software to be identical to the software for the RPRV facility computers. This simulation method was the least useful for design or verification of onboard software.

The computation and simulation of HiMAT (CASH) system (fig. 25) went a step further than the Cyber-Varian simulation just described. In this simulation, the actual HiMAT onboard computer was interfaced with the Cyber and simulation facility ground computers. An uplink encoder was hard lined to an uplink decoder, bypassing only the transmitter–receiver radiofrequency link. The decoder was interfaced with the onboard computer just as in the flight configuration. A high-fidelity

electronic model of each of the HiMAT servoactuator channels was interfaced with the onboard computer, and the output of these actuator models was monitored by the Cyber computer that calculated vehicle response. This configuration was used extensively for both ground and airborne software validation and verification since both the BCS and PCS software were executed in computers identical to those used for flight.

The iron bird simulation (fig. 26) represented the most sophisticated of the HiMAT ground test phases, making maximum use of actual flight hardware by incorporating the flight vehicle in the loop. In this configuration, the aircraft and RPRV facility systems were made to function as if the HiMAT vehicles were in flight. With the HiMAT vehicle in the hangar, the telemetry downlink was hard lined to the RPRV facility, as was the uplink command system to the vehicle; all vehicle control loops were active. The simulation of the vehicle dynamics was similar to that used in the CASH system except that actual surface positions were interfaced with the Cyber 73-28 computer. Vehicle response data were trunked to the vehicle, summed with the actual vehicle transducer outputs, and input to the telemetry downlink system. The iron bird simulation provided for a full system validation of both the BCS and PCS. Additional information on HiMAT simulations can be found in Evans and Schilling (1983) and Myers (1979).

Initial attempts to accomplish satisfactorily an iron bird simulation with the vehicle in the RSS configuration were unsuccessful owing to the slow frame rate of the Cyber computer of only 18.75 msec per frame. Several approaches were attempted to eliminate the limit cycles caused by the total system delays (see Myers, 1979, for additional details). The slow frame rate was solved by including an array processor that executed the aerodynamic model and computed the vehicle airframe dynamics. The array processor, in conjunction with one of two new main simulation computers, was synchronized to the onboard computers at 4.54 msec per frame (220 Hz) and provided sufficient update rates critical to the onboard pitch rate feedback loop. The array processor enabled the RSS PCS and BCS to be flight qualified in the iron bird configuration.

### Software Qualification

Flight software underwent two types of testing during the process of flight qualification: verification and validation testing. Verification testing checked software performance by devising individual tests for each specified software task, conducting the test, and observing that the task met the specification. Validation testing was the broader task that sought to determine if the system, of which the software was a part, met flight requirements. Failure modes and effects tests (both open loop and closed loop) were among the techniques used in software validation. In these tests, failures were artificially induced, and a proper system response to those failures was verified.

The onboard flight software was developed and verified using a microprocessor development system (MDS) and the airborne computer test set, which was a stand-alone bench facility that simulated the HiMAT systems–computer interfaces. Software was validated primarily with CASH and iron bird simulations.

### Ground Test Requirements

Adequate ground test and computer interface equipment was essential to qualify the airborne system in the operational configuration. As delivered, computer memory display consisted of a three-digit octal display addressable by thumbwheel switches. Only 1 byte of RAM at a time could be interrogated while many parameters were stored as 16-bit (2-byte) quantities. This minimal capability was inadequate to verify hardware interfaces, or software.

As a result, the aircraft interrogation and display system (AIDS) was developed to provide increased onboard computer system visibility. The AIDS was an independent microprocessor-based system that interfaced with the HiMAT onboard computer. Any data available in the onboard computer memory could be displayed on a dynamically refreshed cathode ray tube (CRT) monitor. Up to 20 individually labeled parameters could be displayed at a time in either raw input form or engineering units. This system also contained a printer that could be used to provide hard copy of any CRT display. The AIDS greatly reduced the hours required to conduct failure modes

and effects testing and systems hardware and software validation.

### Configuration Control

Rigorous configuration control procedures were used to track both ground and onboard flight hardware and software changes. An outline of the configuration control process is shown in figure 27. Hardware and software changes resulted from changes in requirements or from system discrepancies. Procedures were provided for documenting and tracking all discrepancies and changes. All changes, including those associated with discrepancies, were approved by a configuration control board before they could be implemented for flight. Hardware changes were tracked by the NASA work order and the HiMAT discrepancy report systems. Software changes were tracked by the program change–program verification and validation paperwork and procedures. Each change was verified and validated and software documentation updated before the change was approved for flight.

Changes to onboard software required the manufacture of a new flight release. Source code changes were incorporated in a source file maintained on the Cyber computer; then the new total program was assembled by the cross assembler on the Cyber computer. The Intel hexadecimal format object code was transported and loaded into the MDS to program the EPROMs used in the flight computer. An octal memory check sum was computed from the assembled output on the Cyber computer and compared with that computed in the HiMAT onboard computer as part of its self-test; this process partially verified that the cross-assembler output had been accurately transferred to the flight computer. Software verification and validation test procedures used the flight release. These tests were performed in a laboratory environment using the in-circuit emulator and the computer test set, in the simulation laboratory using the CASH simulation, or on the aircraft using the iron bird simulation or a stand-alone configuration. Primary and backup onboard computer flight releases were manufactured independently, although in practice, both computers were updated in the same time period. Further information on the qualification procedures used for HiMAT can be found in Myers and Sheets (1980).

## PRIMARY CONTROL SYSTEM FLIGHT TEST RESULTS

### Verification of Vehicle Aerodynamics

During the 26-flight test program on the two HiMAT vehicles, 12 flights were devoted to the acquisition of aerodynamic data to verify wind tunnel data. This series of flights was flown with the vehicles ballasted in a stable or forward center-of-gravity configuration ensuring stable open-loop vehicle dynamics. This configuration was flown, using the stable PCS, so that the flight control system gains could be greatly reduced or set to zero during stability and control maneuvers, resulting in minimum control surface motion during the transient portion of these maneuvers. With the stable PCS mechanized in FORTRAN, it was relatively simple to write code to generate specific inputs to the control surfaces. These inputs included independent control surface steps and pulses of various amplitudes and decoupling elevon inputs from the elevators or ailerons. The acquired flight data were then used as inputs to a maximum likelihood estimator for estimating the flight aerodynamic stability and control derivatives (Matheny and Panageas, 1981). Using the flight-determined aerodynamic data, the RSS PCS was then configured for the RSS portion of the flight test program.

In addition to determining stability and control data, various control system configurations were evaluated. These evaluations included the rolling capability of the airplane with differential elevon only and aileron-to-rudder interconnect.

### Control Surface Pulse Command Inputs

Pulse magnitude, direction, and duration were controlled from the pulse panel by a flight test engineer. Figures 8 and 9 show pulse inputs to the flight control system. The pulse inputs were independent of each other, as in the case of the elevon and elevator, which normally operated in unison, so the effects of each could be determined independent of the other. In this configuration, system feedback gains were usually set to zero for the pulse sequence. Typical pitch elevon and elevator pulse inputs and vehicle transient response are shown in figure 28.

These pulses were at 1-g trim condition. Elevator and elevon amplitudes were 3° The vehicle pitch angular rate, angle of attack, and elevator and elevon surface positions are illustrated (fig. 28).

A lateral-directional pulse set is shown in figure 29. Differential elevon and aileron pulses were independent of each other, as shown in the figure. Illustrated are vehicle bank angle, roll rate, sideslip angle, yaw rate, differential elevon, aileron, and rudder position (fig. 29).

### Aileron Active and Inactive

The outboard ailerons produced large adverse yawing moment characteristics that were undesirable from both a control system and a handling qualities viewpoint. Within the scope of the HiMAT program, there was no specific requirement for the roll control power provided by the ailerons. It was felt that only differential elevon could provide the required roll control power while significantly reducing adverse yaw and simplifying the flight control system. Therefore, it was proposed that a piloted evaluation be made with the ailerons locked and unlocked on the same flight. With the PCS mechanized in software, it was relatively simple to include FORTRAN code that eliminated the ailerons from the PCS with a discrete command switch on the pulse panel. Figure 30 presents the time response of a piloted evaluation of aileron control using both aileron and differential elevon. Adverse yaw can be seen with the sharp left (right) roll command input and the corresponding right (left) induced sideslip. Figure 31 is a similar time response (on the same flight) with the ailerons locked. In this time response, the magnitude of the adverse yaw was greatly reduced. From these evaluations and assessment of other aerodynamic data, it was decided to lock mechanically the ailerons on all flights after the eighth flight of vehicle number one.

### Aileron-to-Rudder Interconnect

To further reduce adverse yaw owing to differential elevon, an aileron-to-rudder interconnect (ARI) was mechanized in software and was evaluated in flight. Figure 32 shows the time response of a 5° differential elevon step input with aileron-to-rudder interconnect gains (KARI) of zero and -0.133 deg/deg, respectively. Note that as the KARI gain was increased, the induced sideslip was reduced and the steady state roll rate response was improved from approximately 16 deg/sec to 32 deg/sec. With KARI at -0.133 deg/deg, the induced sideslip was zero and the roll rate response was first order. As a result of this study, an ARI gain schedule was developed for the RSS flight control system.

## Relaxed Static Stability Configuration

Using the data acquired from the stable portion of the flight test program, the RSS PCS was configured and the second phase of the flight test program was conducted. The following discussions present situations encountered in the RSS portion test program and the results of concerns such as control surface rate adequacy.

### Lateral Acceleration Aliasing

The phenomenon of aliasing is fundamental in the sampling of data at equally spaced time intervals such as in the 220-Hz PCM downlink system aboard the HiMAT vehicles. In actuality, a high frequency can be aliased into a low frequency as a result of sampling the data. During the first aft center-of-gravity flights (the 10th flight of vehicle number one), a low-frequency (0.67 Hz) oscillation appeared on the lateral acceleration input to the PCS. This low-frequency oscillation (fig. 33) was interpreted by the PCS as a rigid body aircraft mode and commanded rudder inputs to damp the motion. However, vehicle motion was induced rather than damped. This indication of a pseudolow-frequency lateral oscillation was attributed to a high-frequency engine vibration being aliased via the lateral accelerometer through the PCM system to the ground-based PCS.

The lateral accelerometer was provided with a first-order antialiasing filter with a break frequency of 25 Hz and was sampled at 220 Hz or samples per second. It was determined that the HiMAT engine idle speed was approximately 220 rev/sec. Figure 33 presents a 16-sec time interval of lateral-directional flight data shortly after launch. Initially, the throttle was at idle as indicated by the 14° of throttle position. The 0.67-Hz oscillation can be seen on yaw rate, lateral acceleration, and rudder position. As the throttle was advanced from 14° to about 34°, the frequency of the lateral acceleration

changed from 0.67 Hz to approximately 3.3 Hz. The rudder response was seen to increase in frequency, however, the amplitude was significantly reduced as was the resulting vehicle motion. As throttle was increased toward 50°, the lateral acceleration frequency increased to approximately 10-Hz. Again, the rudder response also increased in frequency, but the amplitude was again reduced. Throughout the entire time interval, the lateral acceleration amplitude remained about the same, which suggested a very large mechanical vibration at the accelerometer package location. This problem was solved by mechanizing of a second-order antialiasing filter with 25-Hz break frequency and 0.5 damping ratio in the lateral acceleration channel and no further problems were encountered.

### Angle-of-Attack Limiter

To protect against a predicted severe increase in the longitudinal instability, or pitchup, as a function of angle of attack and Mach number, an angle-of-attack limiter was mechanized in the RSS PCS (see fig. 14). This angle-of-attack instability was believed to increase significantly between 13° and 17° angle of attack at Mach 0.85 and to be significantly improved at Mach 0.90. At lower Mach numbers, this increase in longitudinal instability was predicted to exist at lower angles of attack, resulting in the the PCS angle-of-attack limiter shown in figure 14. Figure 34 presents a flight test experience of this increase in longitudinal instability (illustrated as a pitchup) and the effectiveness of the angle-of-attack limiter to recover the airplane.

The maneuver shown in figure 34 was a transonic windup turn. The pitchup occurred at the 4.4-sec point with the vehicle at 11.8° angle of attack, Mach 0.87, 7.2-g normal acceleration, 15 deg/sec pitch rate, 83° bank angle. The maneuver was progressing smoothly until the pitchup at the 4.4-sec point. At this point the elevator began to move in a positive or nose down command direction. The vehicle, however, continued to pitch up even though there was a significant increase in the nose down elevator command. At the 4.9-sec point, the airplane entered the angle-of-attack limiter and even more nose down elevator was commanded. Between 5.1 and 5.2 sec, the maximum angle of attack of 14.5° and normal acceleration of 8.7 g were reached with a maximum nose down elevator command of +4.2°. At this point the vehicle pitched down and recovered as illustrated by the pitch rate (fig. 34). This maneuver was a good example of the effectiveness of the angle-of-attack limiting logic.

### Surface Angular Rate Probability Distribution

During the course of the HiMAT program, a question was raised concerning aerodynamic control surface angular rates achieved in the RSS configuration as compared with the stable configuration. To answer this question, the landing approach flight condition was selected from comparable flights because the vehicle was predicted to be the most aerodynamically unstable as compared to other flight regimes. Table 10 presents the center-of-gravity location for the two 20-sec time intervals selected. Center of gravity was presented in percentage of mean aerodynamic chord (MAC) with respect to the reference center-of-gravity position. Aerodynamic static margin was also presented. In this flight condition, the vehicle was never actually statically unstable, as indicated in table 10. Figure 35 presents the time response from two flights with the landing gear transient selected for analysis. The effect of center-of-gravity location can clearly be seen in the elevator position trace as indicated by the more positive (trailing edge down) position with the aft center of gravity.

For this study, three individual surface positions were selected for analysis as being representative—left elevator, left elevon, and left rudder. Figure 36 presents the surface position time response for each of the flights; and figure 37 presents the surface angular rates for the same time interval. Qualitative examination of the data indicated a significant increase in angular rates achieved for all surfaces for the aft center-of-gravity configuration as compared with the forward center-of-gravity configuration. Figure 38 presents the probability distribution for each of the configurations. The data for these curves were obtained for each of the three surfaces over a 20-sec time interval at a sample rate of 220 Hz for a total of 4400 data points. The curves are plotted as percentages of occurrence against angular rate. Perhaps the most significant

result was the rudder rate activity in the aft center-of-gravity configuration. Note in figure 38(a) that for the forward center-of-gravity case the vast majority of time, the rudder was at zero or at very low rates, and for the aft center-of-gravity case even through the rates were relatively low, activity was significant. This general trend was evident for both elevon and elevator as shown in figures 38(b) and 38(c), however, the trend was not as dramatic as the rudder. The highest angular rates during the time intervals of interest are presented in table 11. These results were consistent and were in the direction expected, that is, increased angular surface rates for the aft center-of-gravity configuration. None of the angular rates approached the maximum rate capability as indicated in table 1.

### Flight Test Maneuver Autopilot

To meet the needs of the HiMAT program, a flight test maneuver autopilot (FTMAP) was developed. This FTMAP was designed to provide precise vehicle control during required test maneuvers, such as pushover–pullups, windup turns, and "rocking-horse" maneuvers (Duke and others, 1986). Figure 39 presents three examples of FTMAP generated high-g windup turns. Mach number and altitude were to be held constant while angle of attack was increased until normal acceleration of 8 g was achieved. Mach number was to be held to 0.90 $\pm$0.01. As the maneuvers progressed, Mach number was held constant until the later portion of the maneuver, when engine thrust limit was reached and Mach number decreased and the maneuvers terminated. These maneuvers were of high quality, repeatable, and typical of the results obtained from the FTMAP. Figure 40 presents two pilot-flown windup turns from similar initial conditions of figure 39. Pilot difficulty in flying these maneuvers is apparent from the time histories. Each of the maneuvers, by comparison with FTMAP results, was irregular and erratic with little repeatability. The FTMAP was capable of obtaining high-quality data in relatively short intervals and greatly unburdened the pilots.

## BACKUP CONTROL SYSTEM FLIGHT TEST RESULTS

During the 26-flight test program on two HiMAT vehicles, there were a total of 24 transfers to BCS. There were a total of 16 transfers to BCS on vehicle number one with 12 of these transfers occurring on the first three flights. Only one transfer was owing to a hard system (number 1 decoder) failure that precluded a transfer back to PCS and resulted in the only BCS landing. There were 8 transfers to BCS on vehicle number two with one manual transfer. Vehicle number two did not land with BCS.

All BCS modes except engine-out mode were exercised during BCS operation and all operated satisfactorily; no anomalies were observed.

### Stable Configuration

#### Transfer to BCS Recovery Mode

Each transfer to BCS resulted in a normal sequence through the recovery mode. Figure 41 illustrates three subsonic transfers from PCS to BCS. Figures 41(a) and 41(b) show a transfer from 90° right and left climbing turns at two airspeeds; the airspeed for the data in figure 41(a) was approximately 260 knots and in figure 41(b) was 360 knots. Transfer to BCS occurred when the elevator went to its locked position, as shown in the figures. During the recovery sequence, the bank angle was brought to zero and zero altitude rate was achieved within about 8 sec of transfer. In figure 41(b), a PCS elevator-pitch pulse (for data purposes) was just completed when transfer occurred. Figure 41(c) illustrates a wings-level transfer. These recoveries were relatively typical of most transfers to BCS and occurred as predicted in closed-loop analysis.

#### Orbit Mode

The orbit mode was entered only once, when the pilot inadvertently left the cockpit orbit switch in the orbit position following a transfer to BCS. Figure 42 shows an entry into left orbit following expiration of the 25-sec recovery timer. When or-

bit mode was entered, the vehicle was in a 47° right bank and entry into this mode was inadvertent; consequently, the left orbit was not fully developed. Approximately 2 sec following entry into orbit, exit orbit was selected and the pilot reestablished his right turn. The orbit mode 20 deg/sec roll rate command can be seen in the roll rate trace, as can the 15 deg/sec roll rate command initiated by the pilot's discrete turn switch. From the altitude rate trace, it can be seen that the BCS initiated a climb-to-orbit discrete.

### Dive Mode

Figure 43 shows two relatively typical BCS dives initiated from the altitude-hold mode. Both examples are initiated from a wings-level condition. Figure 43(a) represents a dive from above 10,000 ft and figure 43(b) represents a dive from below 10,000 ft where the commanded dive rates are 6000 ft/min and 3600 ft/min, respectively. In both figures, the desired dive rate was achieved; however, as shown in figure 43(b), the desired dive was not achieved until about 16 sec after dive initiation, as a result of lateral maneuvering. The lateral maneuvering shown in these figures was in the roll rate commanded mode.

### Turn Mode

Figure 44 presents examples of the two types of turn modes: attitude command and roll rate command. In the attitude-command turn shown in figure 44(a), the pilot initiates and maintains the turn command as the vehicle rolls (at the commanded 20 deg/sec roll rate) to a bank angle of approximately 30°. When approaching the desired bank angle, as determined by the direction cosine set, the roll rate command was released in the BCS logic. At this point, a bank angle of 37° was established and maintained by the BCS as the pilot continued to command a turn. In this mode, the bank angle and turn rate were maintained until the pilot released his turn command.

Figures 44(b) and 44(c) present examples of turns in the roll rate command mode. In this mode, the pilot commanded a 15 deg/sec roll rate when he commanded turn and no limit was imposed on bank angle. These two examples of roll rate command mode were relatively typical of the pilot's use of this mode at lower altitudes in preparation for landing.

### Transfer From BCS to PCS

Figure 45 shows the transfer from BCS to PCS. These transfers were relatively typical with an acceptable level of resulting transients. Note the level of vehicle activity as the pilot assumed control.

### Powered-Landing Mode

On one flight an automatic transfer to backup occurred when an uplink receiver–decoder failed and a return to PCS was not recommended, thus committing the airplane to a BCS landing. Before touchdown, it was determined that the landing gear could not be lowered; therefore, the vehicle was committed to a gear-up landing. The subsequent gear-up landing was smooth and resulted in only minor damage to the lower external skin, antennas, and air scoops. The engine was not damaged.

Figure 46 presents a comparison between flight-measured airspeed and descent rate with the BCS-scheduled commands for a powered landing. The dashed lines indicate the commanded values and the solid lines indicate flight-measured values, all as a function of radar altitude. Generally, good agreement exists between the BCS-commanded inputs and the flight data. Landing mode was selected at 2900 ft AGL, and both airspeed and descent rate approached the scheduled commands. The deviations between 2900 ft and 1000 ft may have been caused by lateral maneuvering as the pilot flew the final approach in roll rate command. Touchdown airspeed appears to have been fast.

### Pilot Comments

General pilot comments indicated that the BCS performed well throughout the flight-test program. In the landing mode with BCS, the approach to landing was very good, and the landing schedule provided a smooth touchdown.

## Relaxed Static Stability Configuration

### Aeroservoelastic Instability

During flight testing, the HiMAT vehicle was monitored for possible aeroservoelastic (ASE) in-

stability. Such instabilities occur when the flight control system dynamically interacts with structural modes. Adverse structural coupling of the BCS was observed with the first wing-bending mode (9 Hz) on two occasions (Kehoe, 1984).

Following a transfer to BCS at approximately Mach 0.9 at 37,000 ft altitude, a high-frequency low-amplitude pitch oscillation developed and sustained itself. Upon transfer back to PCS, this oscillation damped out. Transfer to BCS at 25,000 ft altitude, at approximately the same Mach number, did not excite this 9-Hz mode. Figure 47 presents a time history of this oscillation. After transfer to BCS, the amplitudes of this oscillation became limited and remained at relatively low amplitudes as can be seen in all the traces (fig. 47). Maximum amplitudes of normal acceleration were 0.2 g peak-to-peak and maximum pitch rates of 1.5 deg/sec peak-to-peak. The normal acceleration and pitch rates were approximately 180° out of phase with the wingtip accelerations. With the transfer to BCS, the system loop gain was such that the 9-Hz wing-bending mode was sustained through the pitch rate gyro.

The BCS pitch rate gain was computed in the BCS control law and was a function of impact pressure with lower gains for higher pressures and higher gains for lower pressures. If the Mach number was 0.9 and remained fixed for altitudes of 25,000 ft and 37,000 ft, the impact pressure would be in the ratio of 1.74:1. In the BCS control law with Mach 0.9 and the lower altitude of 25,000 ft and higher impact pressure, the resulting BCS pitch gain was significantly lower than for the same Mach number at 37,000 ft. For this Mach number at 37,000 ft altitude, the BCS pitch rate gain was approximately twice its value at 25,000 ft. At the lower altitude of 25,000 ft when a transfer to BCS occurred, at a similar Mach number but higher airspeed (higher impact pressure) and lower pitch gain, this ASE problem was not observed. Therefore, with a lower BCS pitch gain, the ASE instability was not a problem. A pitch rate notch filter was designed for this 9-Hz mode but never implemented, because this problem was observed late in the flight program and little flight test data was collected at altitudes higher than 25,000 ft.

### Transfer to BCS Recovery Mode at Supersonic Speed

One supersonic transfer to BCS occurred when the HiMAT vehicle was at Mach 1.29. Figure 48 presents the flight-recorded longitudinal parameters of this transfer. As the vehicle decelerated, a relatively large static pressure rise, as a result of the passing shock wave, was sensed at the static pressure orifice. The BCS recovery mode interpreted this large pressure rise as a rapid descent and sent a relatively large nose up command to counter the pseudoloss in altitude. Transfer occurred at about 1.4 sec at 1-g normal acceleration. The rapid pitchup resulted as the elevators moved to their 2.5° locked position and the elevons assumed full control. At the 10-sec point, the shock wave passed over the static pressure orifice and the BCS commanded nose up for about 2 sec, following which the recovery maneuver was completed. Also shown in figure 48 is a similar time response recorded from the HiMAT real-time CASH simulation. The initial conditions were the same as the flight data. Initial observation of the simulator data indicates that the flight time response was relatively good, but there were some differences. At BCS transfer, the simulator initial pitch was down as compared to up for flight. The large nose up command in the simulation data occurred about 11.5 sec after transfer to BCS as compared to 9 sec for flight. The nose up time response for both the simulator and flight were in good agreement, while the following nose down simulator response was larger in amplitude than in flight, as was the subsiding motion. Elevon response through the dynamic or transonic portion of the response showed relatively poor agreement with flight. The simulator elevon response at supersonic and subsonic speeds (the initial and final portion of figure 48), although biased, was comparable with flight data. The differences between simulator and flight data can be attributed to transonic aerodynamic modeling errors in the simulator data. This problem could have been eliminated in the BCS if the transonic static pressure error inverse had been mechanized as part of the control law.

## CONCLUDING REMARKS

The HiMAT program was successfully completed in 1983 with a total of 26 flights on two vehicles and approximately 11 hr of total flight time. All programmatic and design goals were either achieved or exceeded. These included a sustained 8-g turn at Mach 0.9 and 25,000 ft altitude and a sustained straight and level dash to Mach 1.4.

The requirement that no single failure result in loss of the vehicle dictated a complex approach to the development of all flight systems. Virtually all HiMAT systems were dualized and fully flight qualified. Few failures occurred in flight and none were serious enough to threaten loss of a vehicle. A single decoder failure resulted in a transfer to the backup flight control system and brought about the only landing with this system.

Each of the flight control systems and associated subsystems performed exceptionally well over the course of the program. Hard failures of ground systems were nonexistent and only a few airborne systems failed. Not a single ground or airborne computer failed during a flight, and each control system performed as specified.

Inclusion of a flight test maneuver autopilot enhanced the acquisition of high-quality flight data and holds great promise for future applications in both manned and unmanned aircraft.

*Ames Research Center*
*Dryden Flight Research Facility*
*National Aeronautics and Space Administration*
*Edwards, California, June 11, 1987*

## REFERENCES


Baer-Riedhart, Jennifer L.: *The Development and Flight Test Evaluation of an Integrated Propulsion Control System for the HiMAT Research Airplane.* AIAA-81-2467, Nov. 1981.

Bayati, Jamal E.: *The HiMAT RPRV Propulsion Control System.* Aerospace Engineering and Manufactoring Meeting, SAE 760887, San Diego, California, 1976.

Duke, Eugene L.; Jones, Frank P.; and Roncoli, Ralph B.: *Development and Flight Test of an Experimental Maneuver Autopilot for a Highly Maneuverable Aircraft*, NASA TP-2618, 1986.

Evans, Martha B.; and Schilling, Lawrence J.: *Simulations Used in the Development and Flight Test of the HiMAT Vehicle.* AIAA-83-2505, Oct. 1983.

Evans, Martha B.; and Schilling, Lawrence J.: *The Role of Simulation in the Development and Flight Test of the HiMAT Vehicle.* NASA TM-84912, 1984.

Harney, Paul F.: *Diversity Techniques for Omnidirectional Telemetry Coverage of the HiMAT Research Vehicle.* NASA TP-1830, 1981.

Hoyt, Carl E.; Kempel, Robert W.; and Larson, Richard R.: *Backup Flight Control System for a Highly Maneuverable Remotely Piloted Research Vehicle.* AIAA-80-1761, Aug. 1980.

Kehoe, Michael W.: *Highly Maneuverable Aircraft Technology (HiMAT) Flight-Flutter Test Program.* NASA TM-84907, 1984.

Kempel, Robert W.: *Flight Experience With a Backup Flight Control System for the HiMAT Research Vehicle.* AIAA-82-1541, Aug. 1982.

Matheny, Neil W.; and Panageas, George N.: *HiMAT Aerodynamic Design and Flight Test Experience.* AIAA-81-2433, Nov. 1981.

Myers, Albert F.: *Simulation Use in the Development and Validation of HiMAT Flight Software.* AGARD 28th Guidance and Control Panel Symposium, Ottawa, Canada, AGARD-CP-272, May 1979.

Myers, Albert F.; Earls, Michael R.; and Callizo, Larry A.: *HiMAT Onboard Flight Computer System Architecture and Qualification.* AIAA-81-2107, Oct. 1981.

Myers, Albert F.; and Sheets, Spencer G.: *Qualification of HiMAT Flight Systems.* Proceedings of the 7th Annual Symposium of the Association for Unmanned Vehicle Systems, Dayton, Ohio, June 1980.

Petersen, Kevin L.: *Flight Control Systems Development of Highly Maneuverable Aircraft Technology (HiMAT) Vehicle.* AIAA-79-1789, Aug. 1979.

Woolley, M.: *The Evolution of a Remotely Piloted Vehicle Microprocessor Flight Control System.* A Collection of Technical Papers, AIAA Guidance and Control Conference, AIAA-78-1273, 1978, pp. 208–225.

TABLE 1—HiMAT PRIMARY AND BACKUP CONTROL SURFACE AUTHORITIES, ANGULAR RATES, AND CONTROL SYSTEM FUNCTION

| Control surface | Control mode | Angular surface rate, deg/sec | Maximum surface authority, deg | Surface function | |
|---|---|---|---|---|---|
| | | | | Primary control | Backup control |
| Elevator | Primary | 76.6 | +28 to -21 | Symmetric pitch control | Locked at +2.5° |
| Elevon | Primary | 87.2 | +27.5 to -20 | Symmetric pitch and asymmetric roll control | Symmetric pitch and asymmetric roll control |
| | Backup | 86.9 | | | |
| Rudder | Primary | 65.6 | ±10 | Yaw control and speed brake | Yaw control |
| | Backup | 64 | | | |
| Aileron | Primary | 86.8 | ±20 | Roll control | Locked at 0° |
| Canard | Primary | 87.3 | +18 to -20 | Symmetric pitch and asymmetric roll control | Locked at 0° |

TABLE 2—HiMAT PILOT'S GROUND COCKPIT STICK AND RUDDER PEDAL CHARACTERISTICS

| Pilot's control | Airplane axis | Break-out force, lb | Force gradient, lb/in | Displacement, in |
|---|---|---|---|---|
| Stick | Pitch | 3.5 | 3.92 | 5 aft, 6 forward |
| | Roll | 1.0 | 3.71 | ±4.25 |
| Rudder pedal | Yaw | 8.5 | 8.5 | ±3.25 |

TABLE 3—HiMAT GROUND-BASED COMPUTERS' FUNCTIONS AND CHARACTERISTICS

| Computer | Characteristics | Functions |
|---|---|---|
| V-73A | Hardware floating-point<br>32K 16-bit memory<br>Full set of peripherals<br>Real-time FORTRAN | Primary control laws<br>Cockpit display computation<br>Preflight test<br>Fault detection |
| V-73B | | Maneuver autopilot control law<br>Transfer guidance data to cockpit |
| V-77 | 32K 16-bit memory<br>Limited peripherals<br>Slower than the V-73 | Telemetry interface with V-73 computer<br>Caution–warning display |
| V-72 | Same as V-77 | Navigation and ILS computation from tracking radar |

TABLE 4—HiMAT ONBOARD SYSTEMS AND HARDWARE FAILURES WHICH CAUSE AUTOMATIC TRANSFER TO BACKUP CONTROL

| Sensed failure |
|---|
| Decoder number 1 |
| Decoder number 2 |
| Primary electrical system |
| Primary hydraulic system |
| Simplex actuator: elevator, aileron, or canard |
| Primary computer |
| Uplink system |
| Downlink system |

TABLE 5—HiMAT BACKUP FLIGHT CONTROL SYSTEM MODES AND MODE FUNCTIONAL CHARACTERISTICS

(a) Recovery, Orbit, Straight and Level, and Turn Modes

| Mode | Mode function |
|---|---|
| Recovery | BCS initialized in this mode |
| | Brings the vehicle to level flight (altitude rate = 0) |
| | Reduces airspeed to subsonic Mach numbers |
| | Provides inverted recovery if altitude rate is above 12,000 ft/min |
| | External discrete commands not honored until altitude rate is ±600 ft/min |
| | Will reenter recovery mode if Mach number exceeds 0.96 or if altitude rate exceeds 12,000 ft/min |
| Orbit | Orbit mode will be entered at expiration of 25-second timer following transfer to BCS unless orbit has been deselected |
| | Vehicle will climb to one of three orbit altitudes or dive to 25,000 ft if BCS entered above this altitude |
| | Orbit altitudes are 25,000 ft, 10,000 ft and 5,000 ft |
| | Bank angles are 35° above 4,000 ft and 20° below |
| | Left or right orbits are pilot selectable |
| Straight and level | Altitude, quasi-heading, and speed or Mach hold $M \approx 0.8$ above 20,000 ft and $V_c \approx 300$ knots below |
| Turn | Attitude command with a roll rate of 20 deg/sec to ±35° bank angle above 4,000 ft and ±20° below |
| | Roll rate command mode roll rate is 15 deg/sec with no bank angle limit |
| | Automatic turn rate commanded as a function of airspeed |

TABLE 5—COMPLETED

(b) Climb–Dive, Land, and Engine Out Glide and Flare Modes

| Mode | Mode function |
|---|---|
| Climb–dive | All climbs at 100 ft/sec |
| | Dives above 10,000 ft at 100 ft/sec and dives below at 60 ft/sec |
| Land | Scheduled airspeed and altitude rate command as a function of radar altitude |
| | Pilot modulation of airspeed and altitude rate within limits; minimum airspeed is 185 knots |
| | Maximum radar altitude is 5000 ft |
| | Alternate land mode provided if radar altimeter failed |
| | Pilot can select roll rate command for precise heading control |
| Engine out | Commanded airspeed of 215 knots with modulation capability |
| | Flare initiated at 550 ft radar altitude when elevon control transfers from airspeed command to altitude rate command for the flare; the initial altitude rate for the flare was the existing rate at 550 ft; commanded altitude was then ramped to -5 ft/sec at 25 ft |

TABLE 6—HiMAT AIRBORNE INTEGRATED PROPULSION CONTROL SYSTEM COMMAND AND FEEDBACK FUNCTIONS

| Function | Onboard computer control mode | |
|---|---|---|
| | Backup/PCS | Primary/BCS |
| Command function | | |
| Power lever angle | X | X |
| Variable nozzle area | X | X |
| Engine igniter | X | |
| Throttle feedback select signal | X | |
| Variable nozzle area override | X | X |
| Feedback function | | |
| Compressor inlet total pressure | X | X |
| Compressor discharge total pressure | X | X |
| Turbine discharge static pressure | X | |
| Turbine discharge temperature (EGT) | X | X |
| Rotor speed (rpm) | X | |
| Main fuel control throttle position | X | X |
| Exhaust nozzle area | X | |

TABLE 7—HiMAT RELAXED STATIC STABILITY PRIMARY FLIGHT CONTROL SYSTEM GAINS, SCHEDULES, AND FILTER DESCRIPTIONS

(a) Normal Controller and Alpha Limiter

| Symbol | Name | Value–function–comments | Units |
|---|---|---|---|
| | | Normal controller | |
| KNA | Alpha gain | 0.0 for $M < 1.0$<br>-5.0 for $M \geq 1.0$ | deg/deg |
| KNQ | Pitch rate gain | 0.5 | deg/deg/sec |
| KNNZ | Normal acceleration gain | 4.3 | deg/g |
| KND | Longitudinal stick command gain | -11.25; for landing -7.5 | deg/in |
| LDEP | Launch stick command | -0.75<br>fades to zero after 3 sec | in |
| DEP | Pilot's stick command | DEPOUT<br>= DEPIN {ESLOPE<br>+ [(1 - ESLOPE)/4.5]\|DEPIN\|} | in |
| ESLOPE | Nonlinear parameter | 0.4 | |
| KNT | Total controller gain | $(0.46 - 0.0004 * \bar{q})$ for $\bar{q} < 400$ lb/ft$^2$<br>0.30 for $\bar{q} \geq 400$ lb/ft$^2$ | deg/deg |
| KPMPC | Variable test gain | Pilot-selectable gain for test<br>0 to 0.7 | |
| | | Alpha limiter | |
| KALM | Positive alpha limit | 12.0° for $M < 0.8$<br>$0.8 \leq M \leq 0.9$, $12 + 30 * (M - 0.8)$<br>15.0° for $M > 0.9$ | deg |
| KAA | Alpha gain | 1.26 | deg/deg |
| KAQ | Pitch rate gain | $0.1875 + 150/\bar{q}$ for $\bar{q} > 100$<br>1.6875 for $\bar{q} \leq 100$ | deg/deg/sec |
| | Negative alpha limit | -3° | |
| KLA | Negative alpha gain | 1.26 | deg/deg |

TABLE 7—Continued

(b) Normal Acceleration Limiter and Onboard Pitch Rate Loop

| Symbol | Name | Value–function–comments | Units |
|---|---|---|---|
| | | Normal acceleration limiter | |
| KGLM | Normal g limit | 10 g | |
| KGNZ | Normal g gain | 103.14/g for $\bar{q} \geq 100$ lb/ft$^2$<br>1.0314 for $\bar{q} < 100$ lb/ft$^2$ | deg/g |
| KGQ | Pitch rate gain | $3.51/q$ for $\bar{q} \geq 100$ lb/ft$^2$<br>0.351 for $\bar{q} < 100$ lb/ft$^2$ | deg/deg/sec |
| | | Onboard pitch rate loop | |
| KBQ | Pitch rate gain | 0.25<br>In degraded primary = 0.50 | deg/deg/sec |

TABLE 7—Continued
(c) Roll and Yaw Axes

| Symbol | Name | Value–function–comments | Units |
|---|---|---|---|
| | | Roll axis | |
| KRP | Roll rate gain | $-60/\bar{q}$ for $M < 1.0$ | deg/deg/sec |
| | | $-120/\bar{q}$ for $M \geq 1.0$ | |
| KRD | Lateral stick command gain | $1800/\bar{q}$ for $M < 1.0$ | deg/in |
| | | $3600/\bar{q}$ for $M \geq 1.0$ | |
| | | 4.0 for landing | |
| KRMCP | Variable test gain | Pilot select for test 0 to 0.9 | |
| KARI | Aileron-to-rudder-interconnect | $-0.5[(0.00933)\text{alpha}+0.015]$ | deg/deg |
| | | Yaw axis | |
| KYAY | Lateral acceleration gain | $1489.8/\bar{q}$ for $\bar{q} < 744.9$ lb/in$^2$ | deg/g |
| | | 2.0 for $\bar{q} \geq 744.9$ lb/in$^2$ | |
| KYR | Yaw rate gain | $35/\bar{q}$ | deg/deg/sec |
| | | $(35.0)M/\bar{q}$ for $M > 1.0$ | |
| KYD | Rudder pedal command gain | 0.858 | deg/in |
| KYMCP | Variable test gain | Pilot select for test; 0 to 0.9 | |

TABLE 7—Continued
(d) Default System Gains

| Symbol | Name | Value and units |
|---|---|---|
| | Normal controller | |
| KNA | Alpha gain | 0 |
| KNQ | Pitch rate gain | 0.5 deg/deg/sec |
| KNNZ | Normal acceleration gain | 4.3 deg/g |
| KND | Longitudinal stick command gain | -11.25 deg/in |
| KNT | Total controller | 0.414 deg/deg |
| | Alpha limiter | |
| KALM | Positive alpha limit | 12° |
| KAA | Alpha gain | 1.26 deg/deg |
| KAQ | Pitch rate gain | 1.50 deg/deg/sec |
| KLA | Negative alpha gain | 1.26 deg/deg |
| | Normal acceleration limiter | |
| KLGM | Normal g limit | 10 g |
| KGNZ | Normal g gain | 0.906 deg/g |
| KGQ | Pitch rate gain | 0.03078 deg/deg/sec |
| | Roll axis | |
| KRP | Roll rate gain | -0.526 deg/deg/sec |
| KRD | Lateral stick command gain | 4.0 deg/in |
| | Yaw axis | |
| KYAY | Lateral acceleration gain | 13.06 deg/g |
| KYR | Yaw rate gain | 0.307 deg/deg/sec |
| KYD | Rudder pedal command gain | 0.858 deg/in |

TABLE 7—Concluded
(e) Systems Filter Representations*

| Filter identification | Type | Transfer function |
|---|---|---|
| | Normal controller | |
| PN01 | High pass | $s/(s+5.0)$ |
| PN02 | Low pass | $1/(s/15+1)$ |
| PN03 | Low pass | $1/(s/15+1)$ |
| | Alpha limiter | |
| PA01 | Lead-lag | $(s/10+1)/(s/5+1)$ |
| PA02 | Lead-lag | $(s/10+1)/(s/2.5+1)$ |
| PA03 | Lead-lag | $(s/15+1)/(s/60+1)$ |
| PA04 | High pass | $s/(s+5.0)$ |
| PL01 | Lead-lag | $(s/10+1)/(s/5+1)$ |
| | Normal acceleration limiter | |
| PG01 | Lead-lag | $(0.8275s+1)/(0.2s+1)$ |
| PG02 | High pass | $s/(s/30+1)$ |
| | Pitch integrator | |
| P01 | Integrator | $5/s$ |
| | Roll axis | |
| R01 | Low pass | $1/(s/5+1)$ |
| | Yaw axis | |
| Y01 | high pass | $s/(s+1)$ |
| Y02 | Low pass | $1/(s/5+1)$ |
| Y03 | Low pass | $20/(s+20)$ |

*All filters are presented in continuous s-plane representation. Filters were transformed to digital form using Tustin's method.

TABLE 8—HiMAT GROUND COMPUTER FAILURE DETECTION AND ANNUNCIATION

| Fault category | Cockpit annunciation indication |
|---|---|
| Downlink integrity | Input–output fail |
| Uplink integrity | Input–output fail |
| Real-time loop integrity | Computer fail |
| Computer watch-dog timer | Computer fail |
| Stick input checks | Stick fail |
| DAC/ADC wrap tests | Stick fail |
| Air data miscompare | Air data fail |
| Angle-of-attack miscompare | Angle-of-attack fail |

TABLE 9—HiMAT ONBOARD FAILURE CONSEQUENCES AND MISSION IMPACT ANNUNCIATION OF SYSTEMS' CONDITIONS

| Automatic transfer to backup failure | Mission abort annunciation |
|---|---|
| Primary hydraulic system | Backup computer uplink fail |
| Primary electrical system | Intercom failure |
| Duplex actuator (primary side) | Engine fire–overheat |
| Simplex actuator | Engine flameout |
| Primary computer downlink or uplink | IPCS sensor fail |
| | Low-fuel warning |
| Primary computer power monitor | Engine shutdown command |
| | Battery on line fail |
| Primary computer | Avionics temperature high |

| Inhibit auto. transfer to backup failure | Caution condition annunciation |
|---|---|
| Backup hydraulic system | Primary sensor fail |
| Duplex actuator (secondary side) | Radar altimeter fail |
| Backup sensors (no. 3 unit) | Attitude gyro fail |
| Backup computer real-time clock | Primary duplex actuator fail |
| | Backup 28-V power on fail |
| Backup computer power monitor | Decoder unreliable |
| | Generator voltage alert |
| Backup computer | Uplink discrete differences |

TABLE 10—HiMAT CENTER OF GRAVITY AND STATIC MARGINS FOR THE RELAXED STATIC STABILITY CONFIGURATION IN THE LANDING APPROACH FLIGHT CONDITION

(Center-of-gravity location with respect to the reference center-of-gravity location at fuselage reference station is 134.26)

| Case | Landing gear up | | Landing gear down | |
|---|---|---|---|---|
| | Center-of-gravity location, percent chord | Static margin, percent chord | Center-of-gravity location, percent chord | Static margin, percent chord |
| Forward c.g. | 7.0 | 12.23 | 8.1 | 12.83 |
| Aft c.g. | 5.2 | 0.06 | 4.2 | 0.58 |

TABLE 11—MAXIMUM ANGULAR SURFACE RATES ACHIEVED IN EXAMPLE TIME INTERVAL

| Surface angular rate, deg/sec | Forward c.g. | Aft c.g. |
|---|---|---|
| $\dot{\delta}_{r_L}$ | +1.5 | +5.0 |
| | -1.0 | -7.0 |
| $\dot{\delta}_{v_L}$ | +9.0 | +12.0 |
| | -6.0 | -10.0 |
| $\dot{\delta}_{e_L}$ | +6.0 | +9.5 |
| | -7.5 | -5.0 |

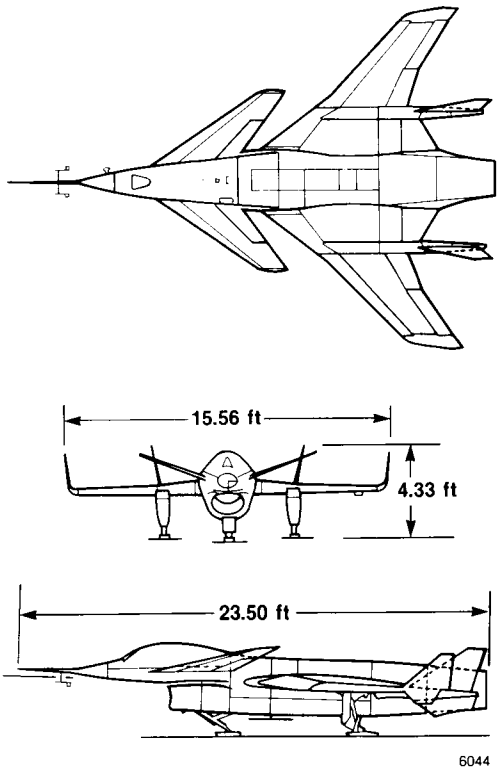


*Figure 1. Three-view drawing of HiMAT vehicle.*

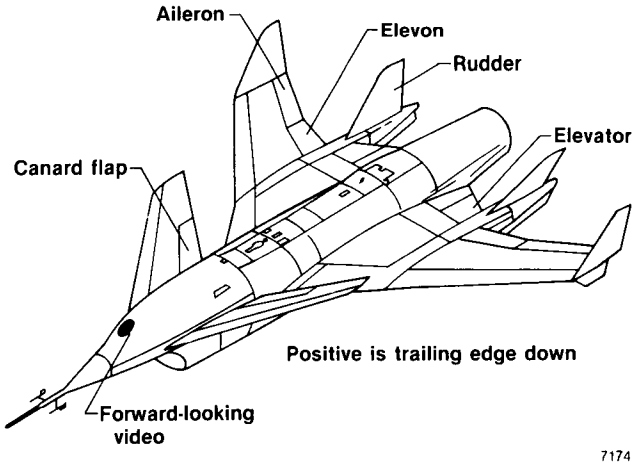


*Figure 2. HiMAT vehicle control surfaces.*

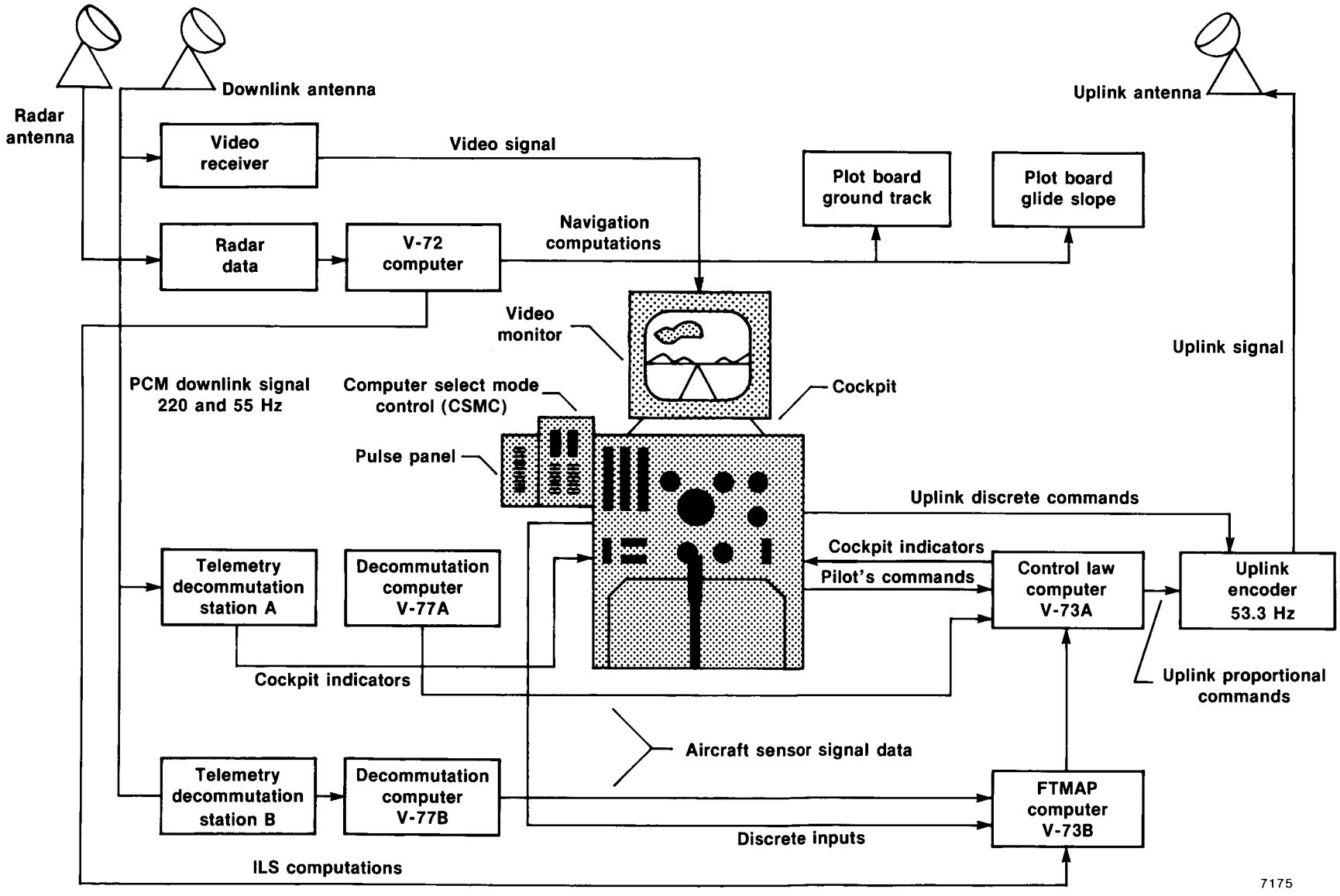


*Figure 3. Simplified HiMAT downlink, radar, video signal paths, ground computers, cockpit, and uplink command signal path.*

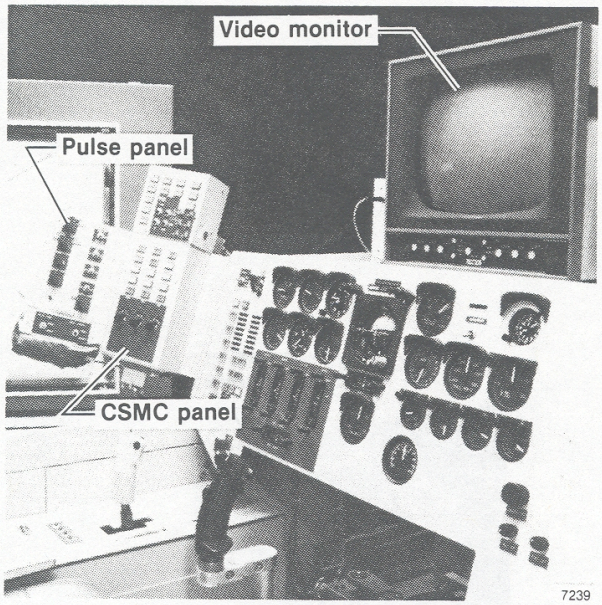


ECN 10906

*(a) Pilot's instrument panel.*

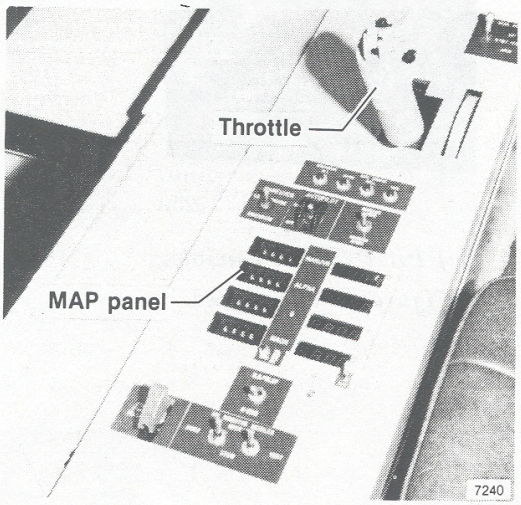


ECN 18180

*(b) Pilot's left console.*

*Figure 4. HiMAT ground-based RPRV cockpit.*

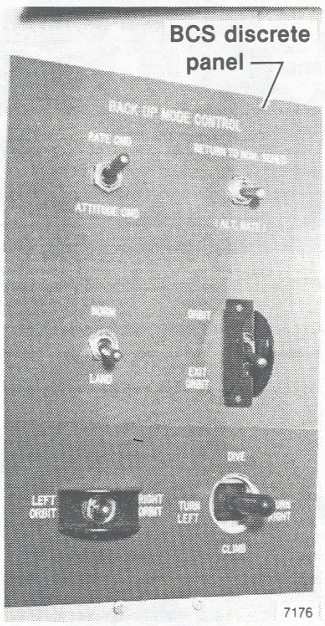


E 37250

*(c) Pilot's right console.*

*Figure 4. Concluded.*

| Word | Decoder number 1 word bits | | | | | | | |
|---|---|---|---|---|---|---|---|---|
| | 1 to 10 | | 11 | 12 | 13 | 14 | 15 | 16 |
| 1 | Left elevon | | Engine operation on-off | Ignitor on-off<br>Integ. eng.-dis. | Landing gear down-off | Combat-norm.<br>Ret. to norm.-off | Eng. stability high-norm. | Nozzle override-normal |
| 2 | Right elevon | | Climb-off | Descend-off | Bank right-off | Bank left-off | Speed increase-off | Speed decrease-off |
| 3 | Left and right rudders | | Landing-standby | Exit orbit-orbit | Reset buss tie-off | Backup select-mode | Smoke gen. on-off | Rate-attitude command |
| 4 | Rudder drag modulation | Bit 10 parity check | Receiver manual mode-off | Receiver select pri.-sec. | Decoder discrete select-off | Discrete select #1 #2 | Gryo erect-off | Reset generator-off |

| Word | Decoder number 2 word bits | | | | | | | |
|---|---|---|---|---|---|---|---|---|
| 1 | Left and right elevators | | | | | | | |
| 2 | Right aileron | | | Bits 11 to 16 | | The same as above | | |
| 3 | Right canard | | | | | | | |
| 4 | Throttle-computer discretes (Bits 1 to 8) | Mux. cont. 9 / Parity check 10 | | | | | | |

| Throttle reset reset-off 1 | Battery on-off 2 | Bendix status norm.-fail 3 | Spare 4 | Canard sym.-diff. 5 | Degraded primary mode 6 | Backup select-normal mode 7 | Test mode active-off 8 |
|---|---|---|---|---|---|---|---|

7177

*Figure 5. HiMAT uplink 16-bit digital word format.*

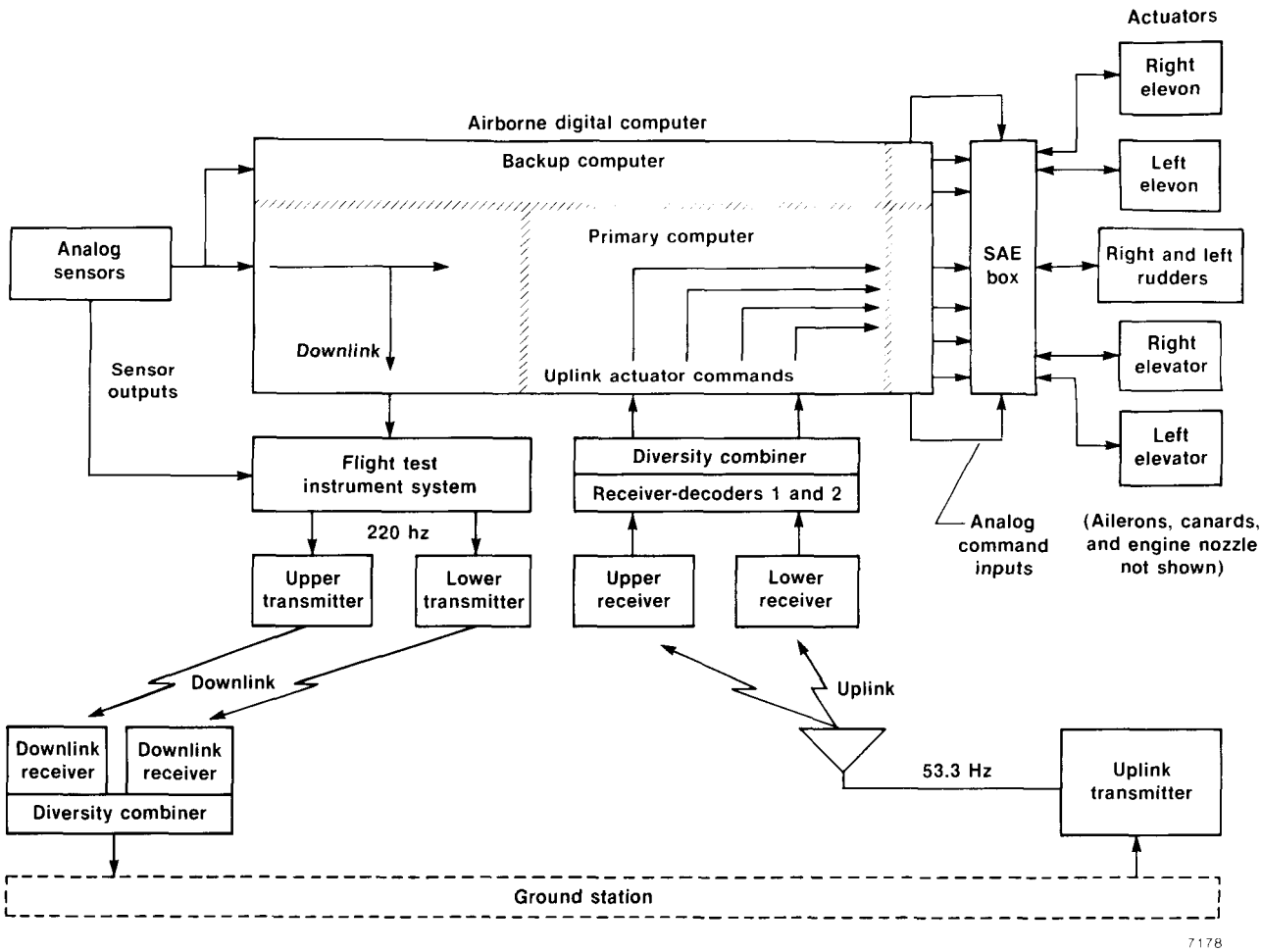


*Figure 6. Major components of the HiMAT airborne flight systems.*

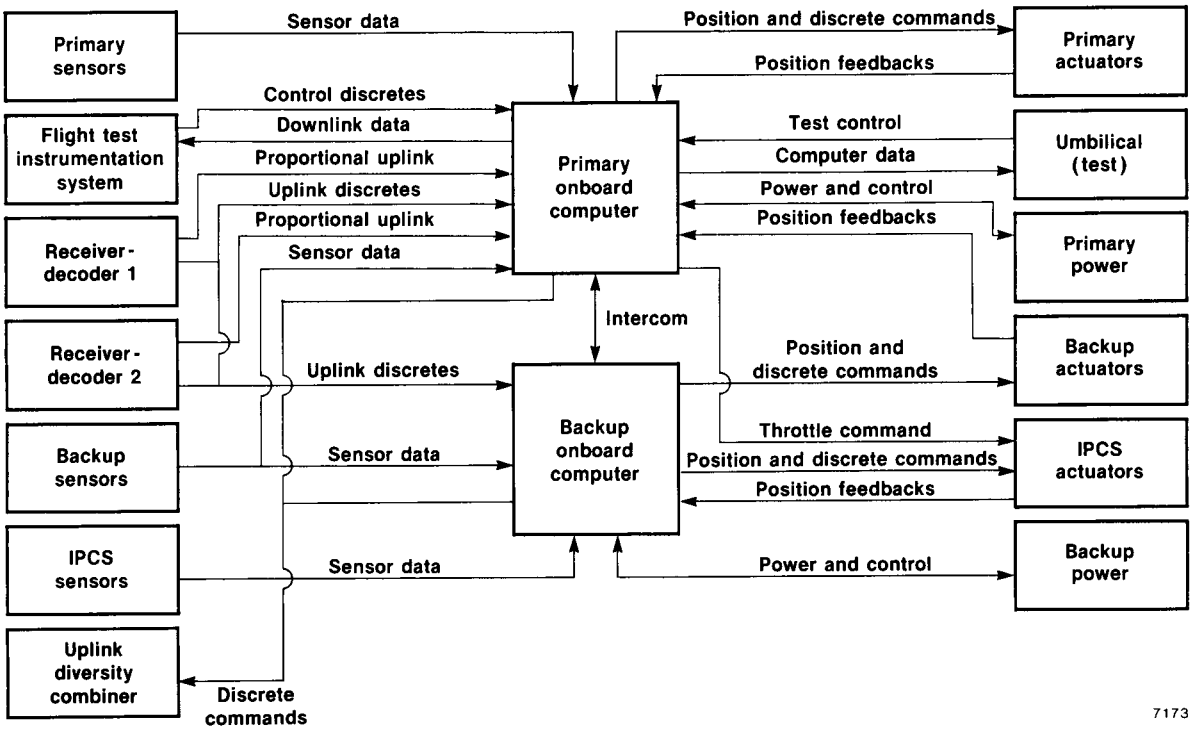


*Figure 7. Airborne computer–aircraft systems interface diagram.*

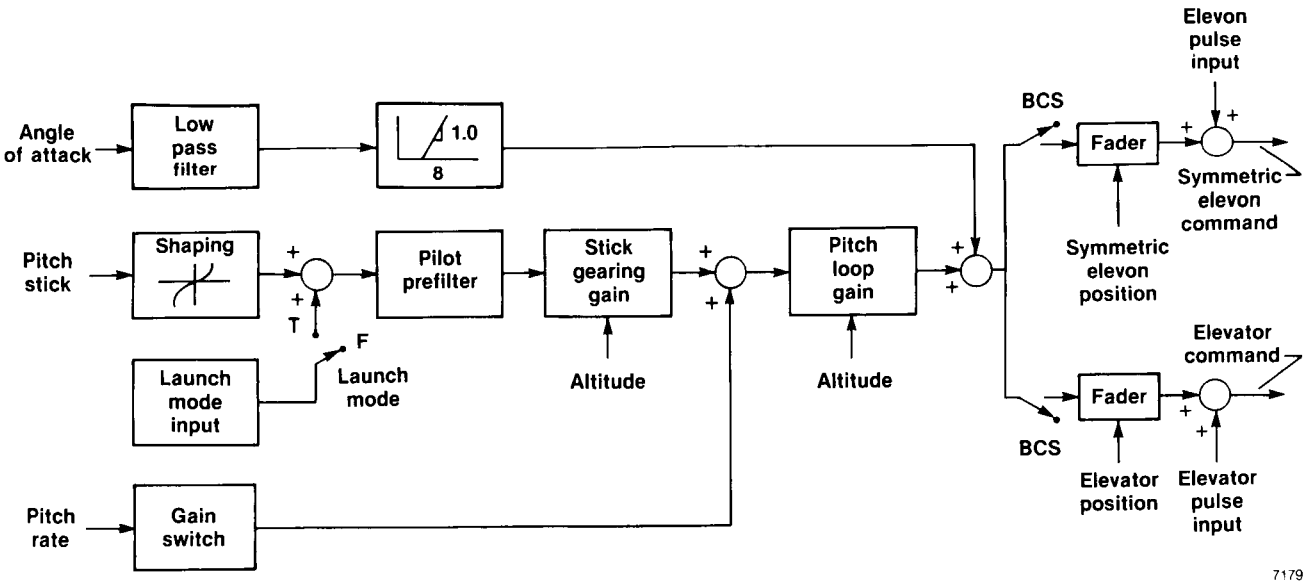


*Figure 8. HiMAT stable PCS longitudinal control law.*

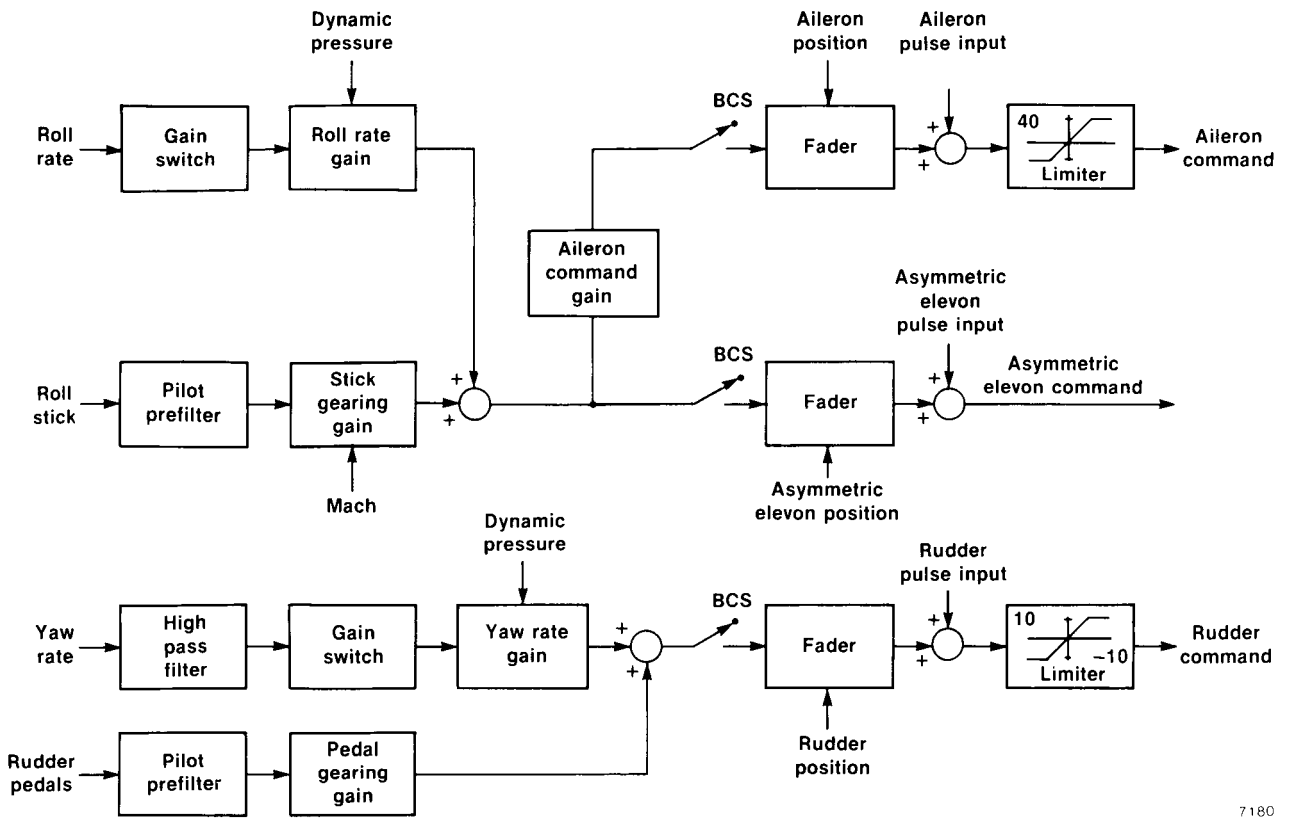


*Figure 9. Stable PCS roll–yaw axis control laws.*

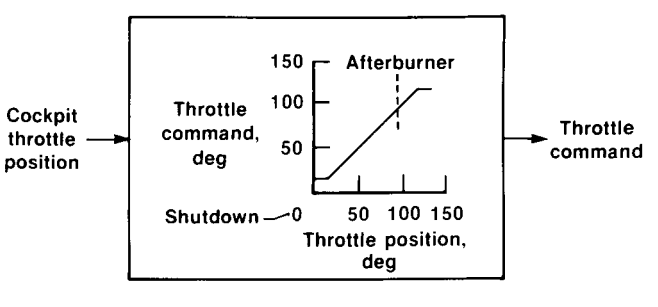


*Figure 10. Throttle control law.*

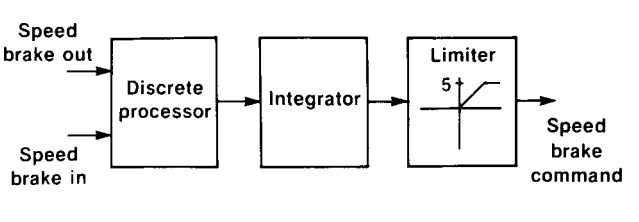


*Figure 11. Speed-brake control law.*

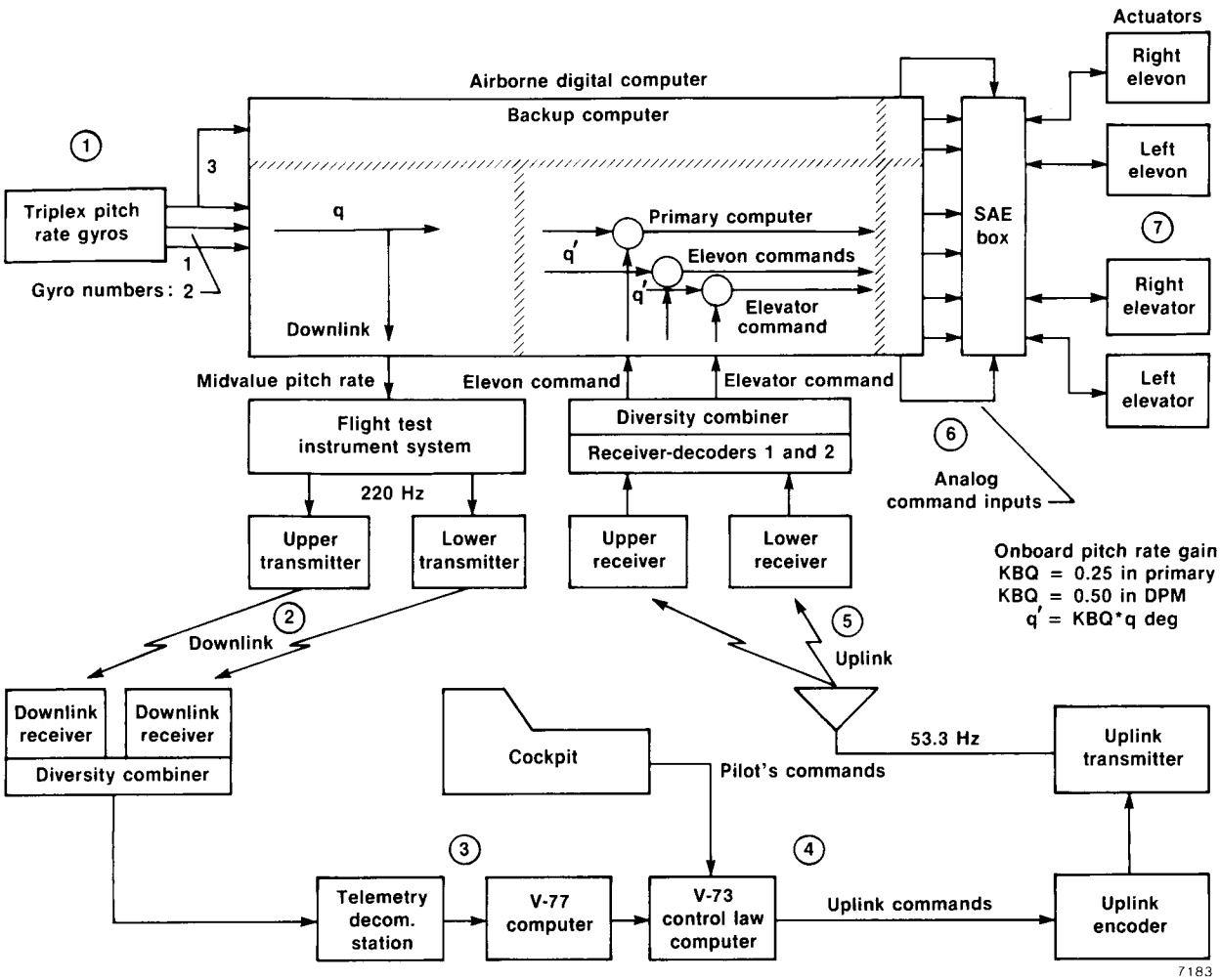


*Figure 12. HiMAT time delays from airborne sensors to surface commands and mechanization of onboard pitch rate feedback.*

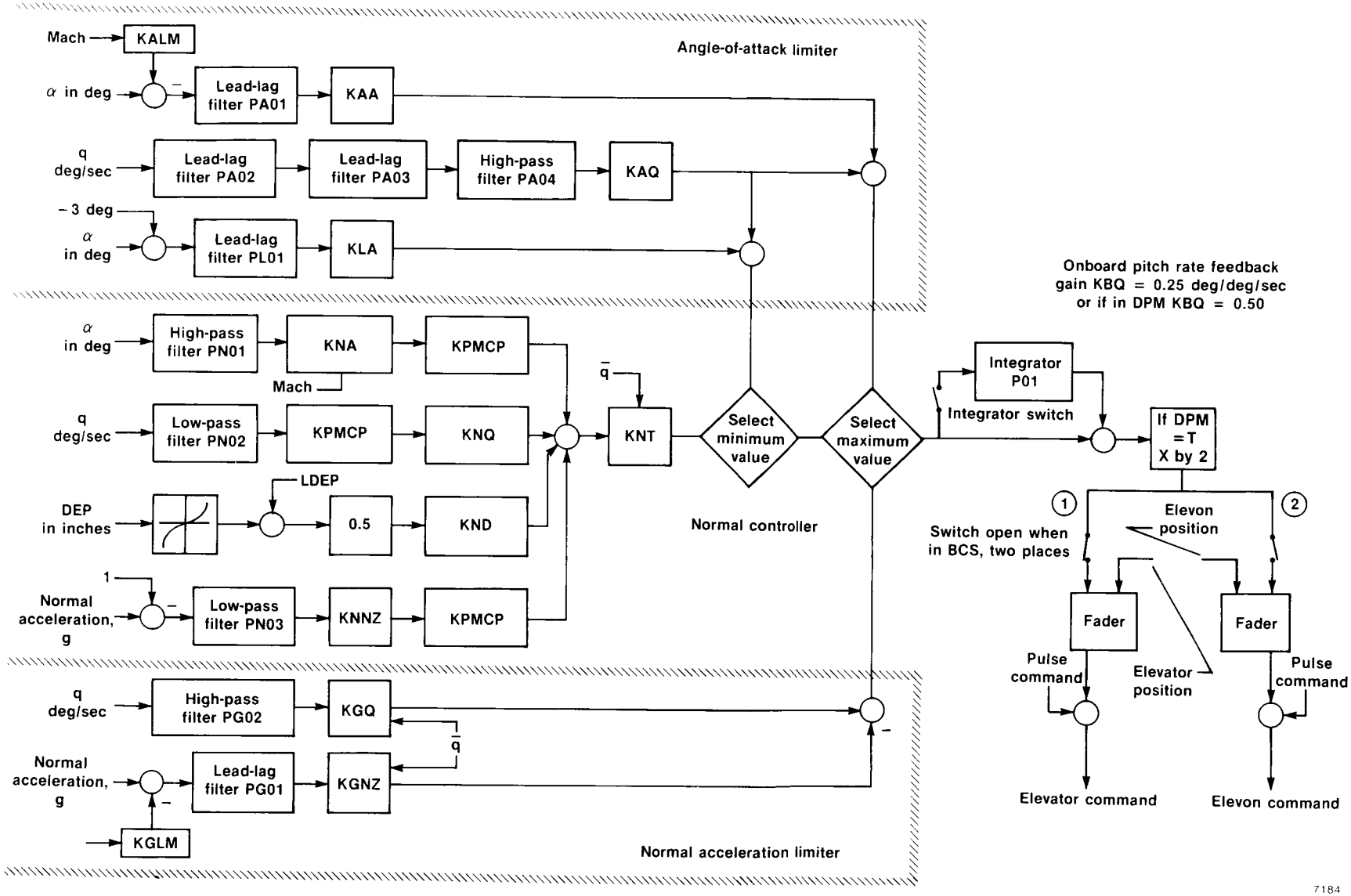


*Figure 13. HiMAT ground-based relaxed static stability longitudinal primary flight control system.*

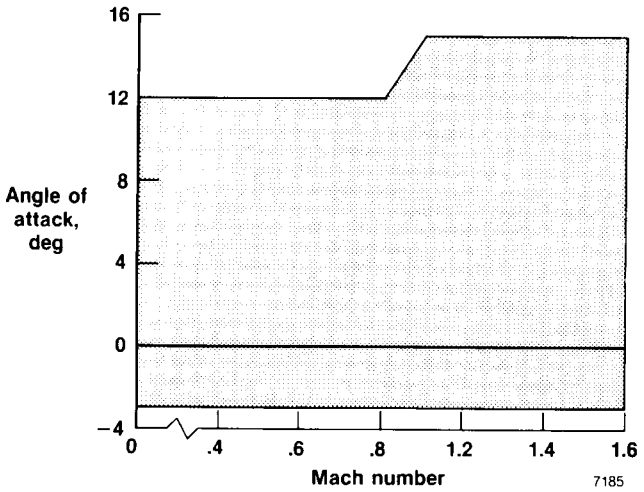


*Figure 14. HiMAT relaxed static stability, primary flight control system angle-of-attack limiter limits.*

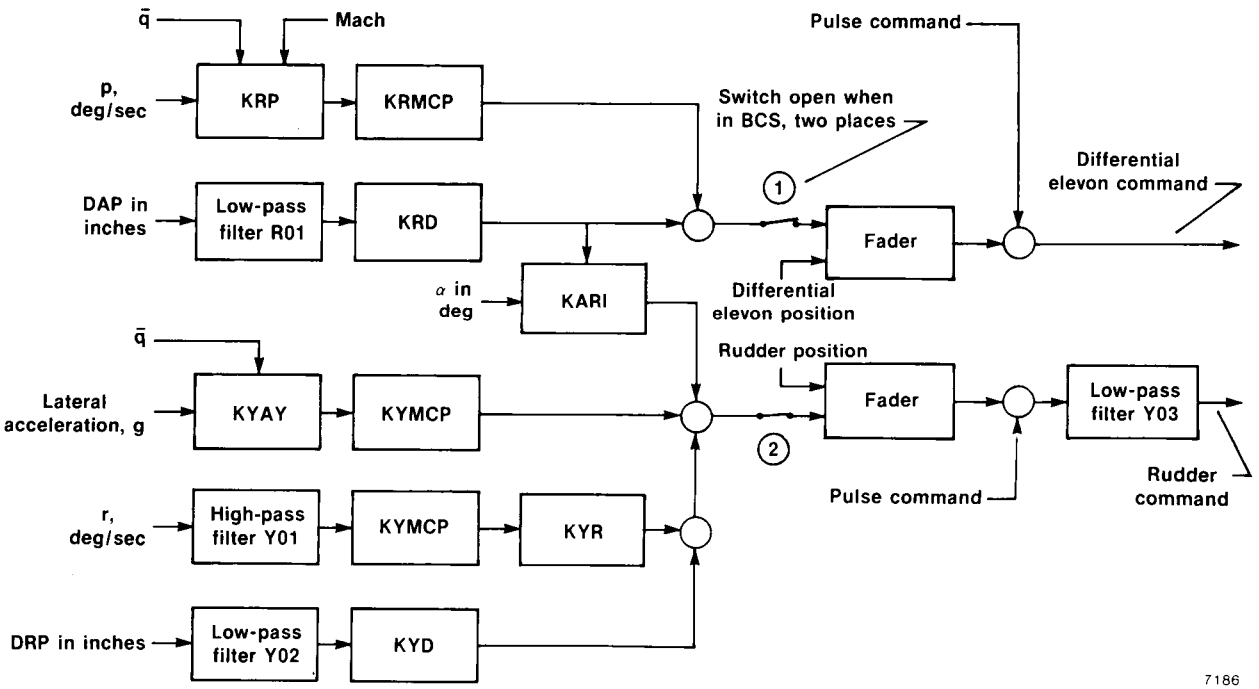


*Figure 15. HiMAT ground-based relaxed static stability lateral-directional primary flight control system.*

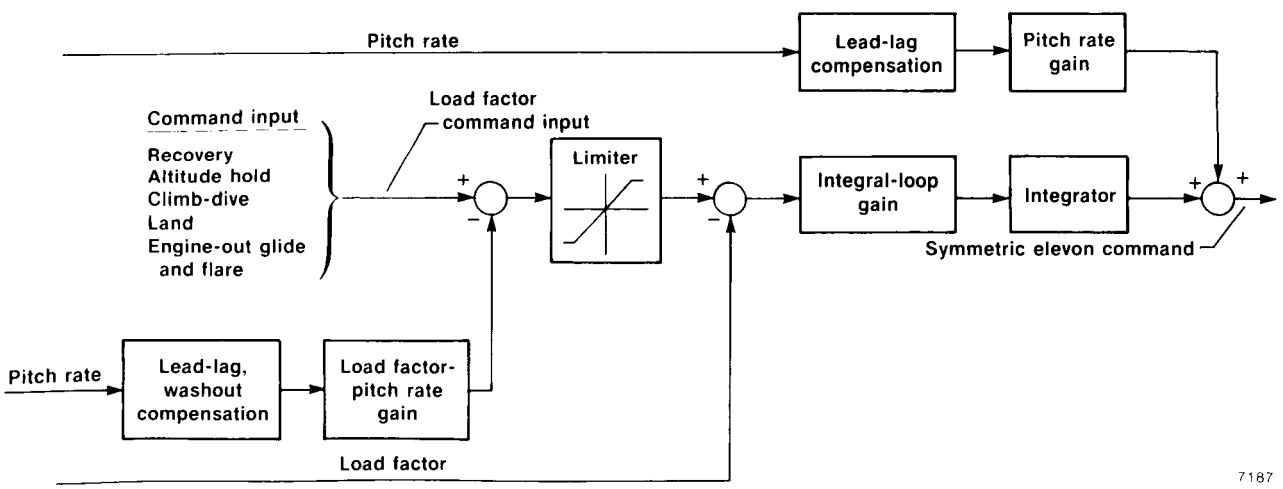


*Figure 16. BCS longitudinal stabilization control law and command inputs.*

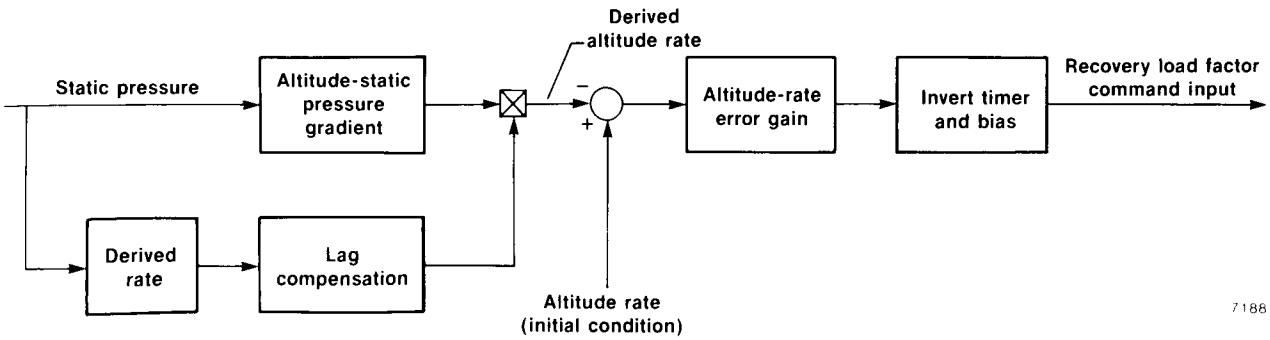


*Figure 17. BCS longitudinal recovery-mode command loop.*

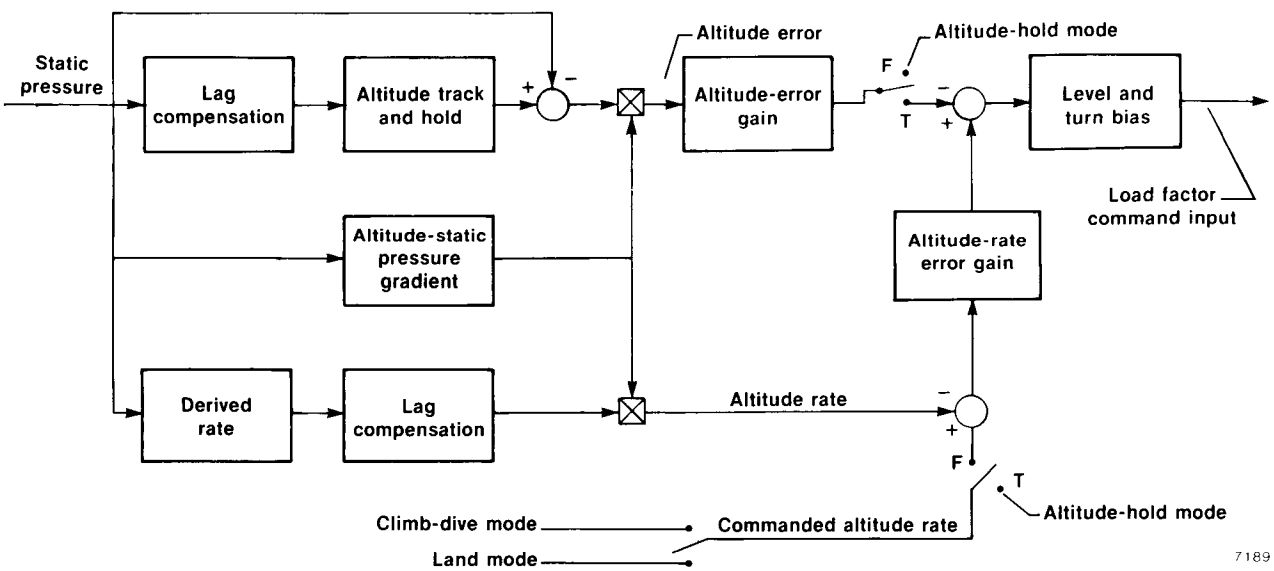


*Figure 18. BCS longitudinal command modes.*

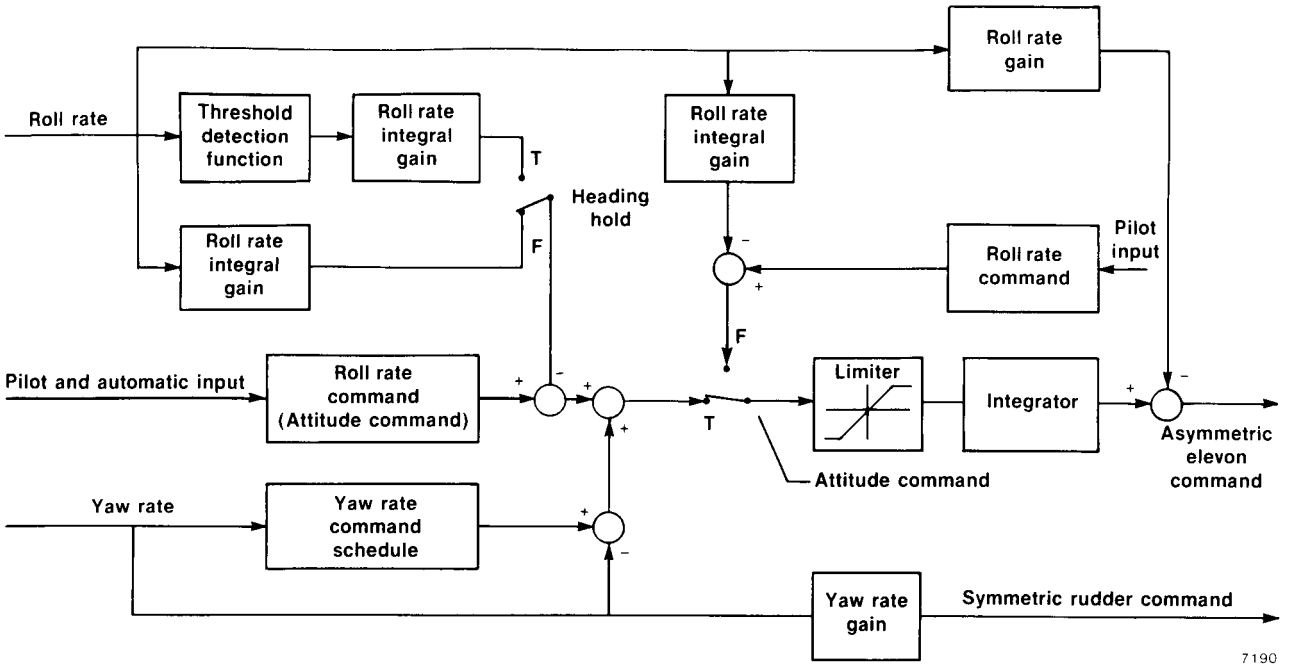


*Figure 19. BCS lateral-directional control laws.*

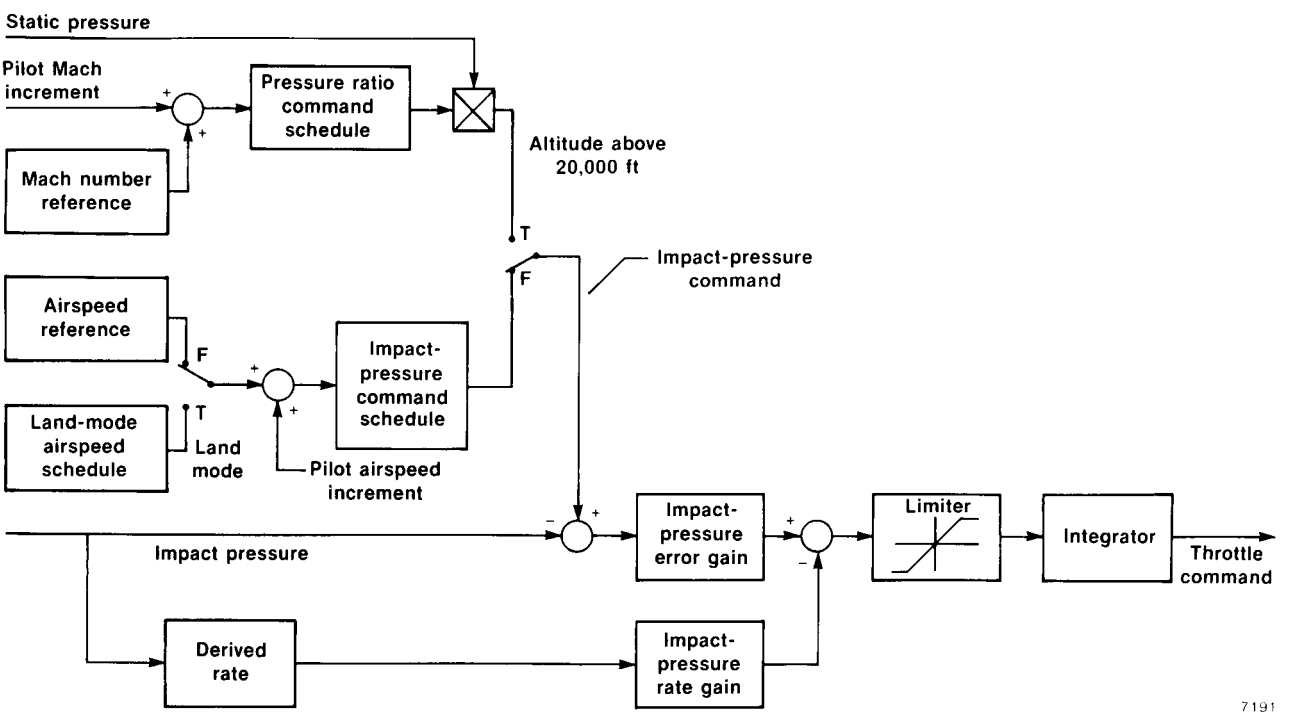


*Figure 20. BCS throttle control law.*

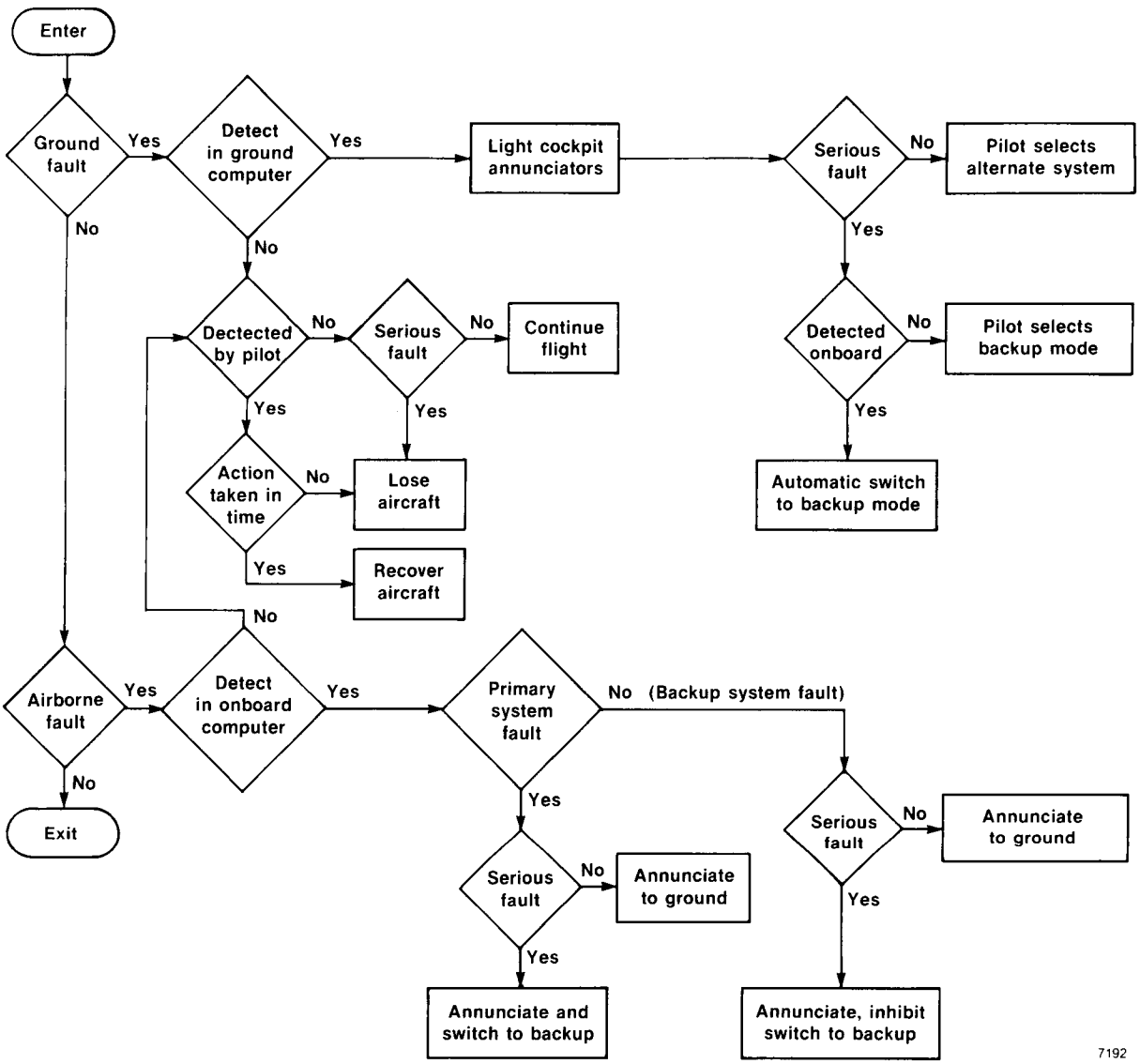


*Figure 21. HiMAT systems failure-detection hierarchy.*

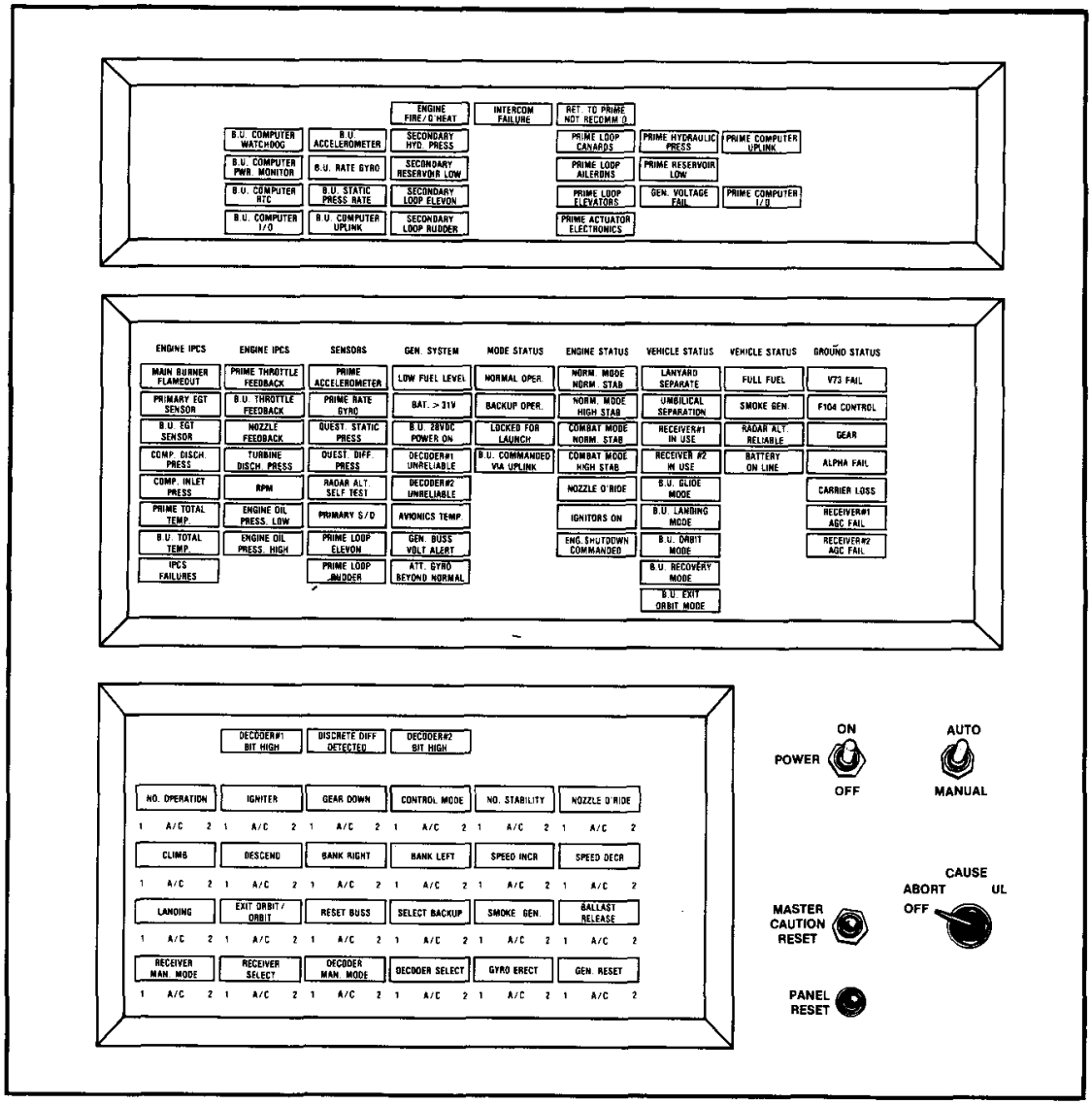


*Figure 22. HiMAT master caution–warning (MCW) panel.*

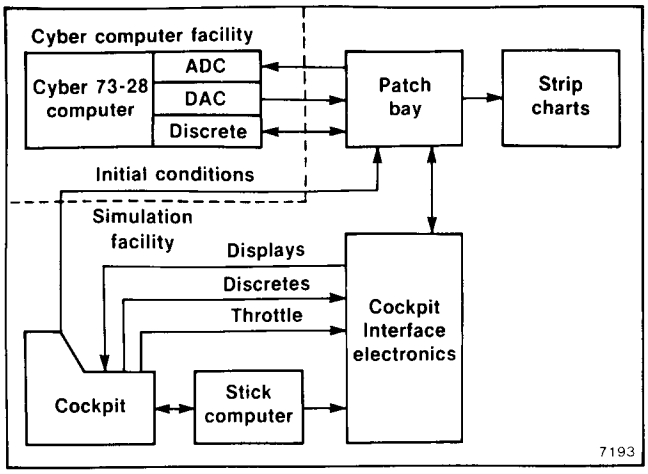


*Figure 23. HiMAT all-Cyber simulation.*

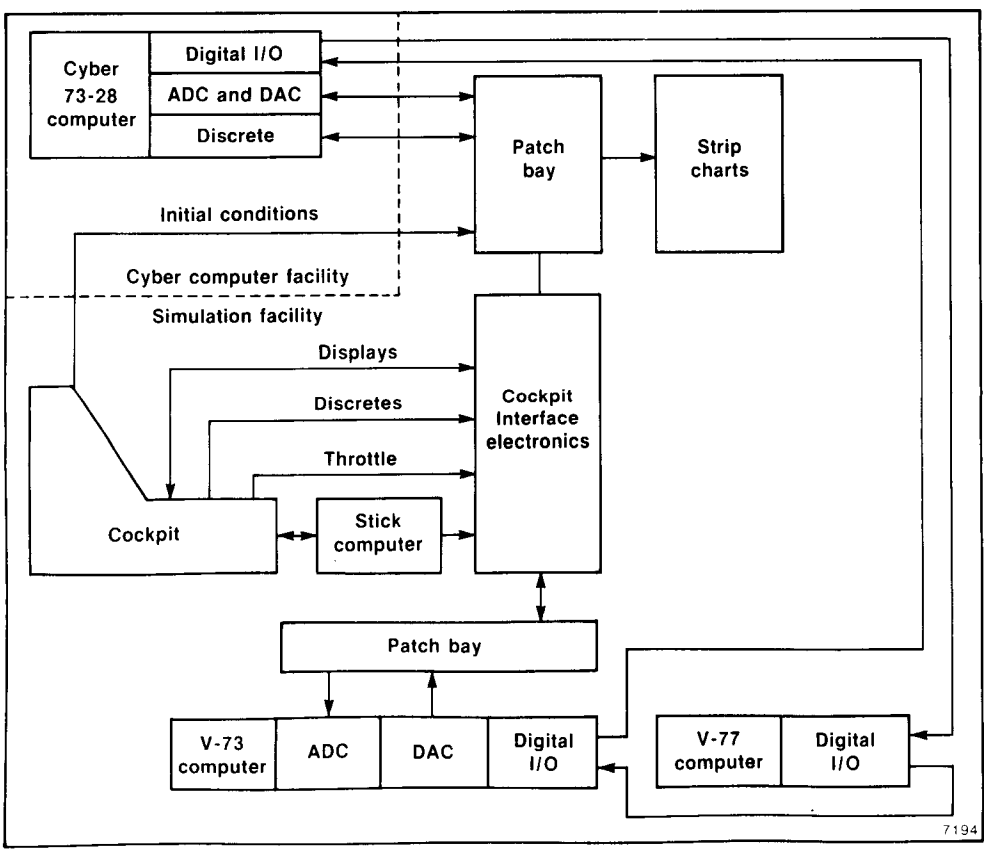


*Figure 24. HiMAT Cyber-Varian simulation.*

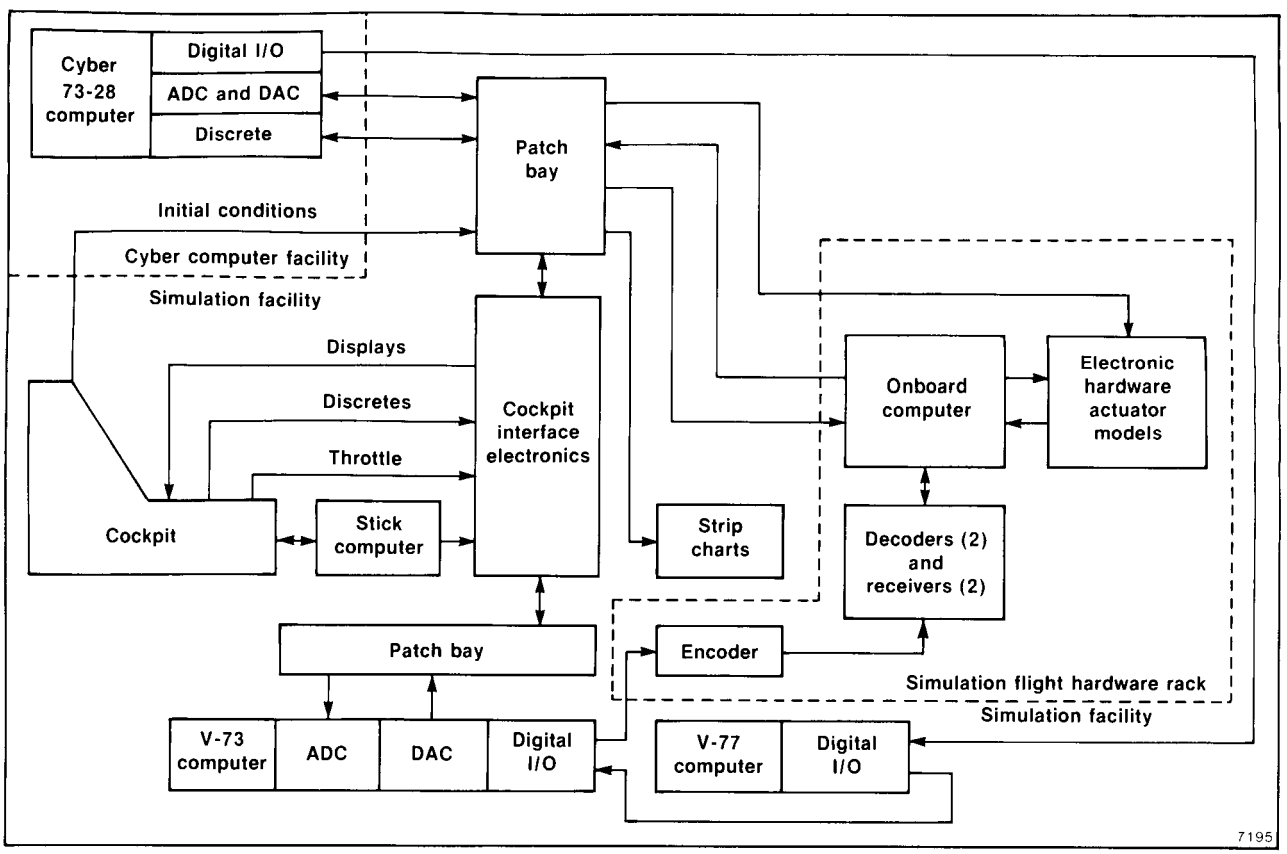


*Figure 25. HiMAT CASH simulation.*

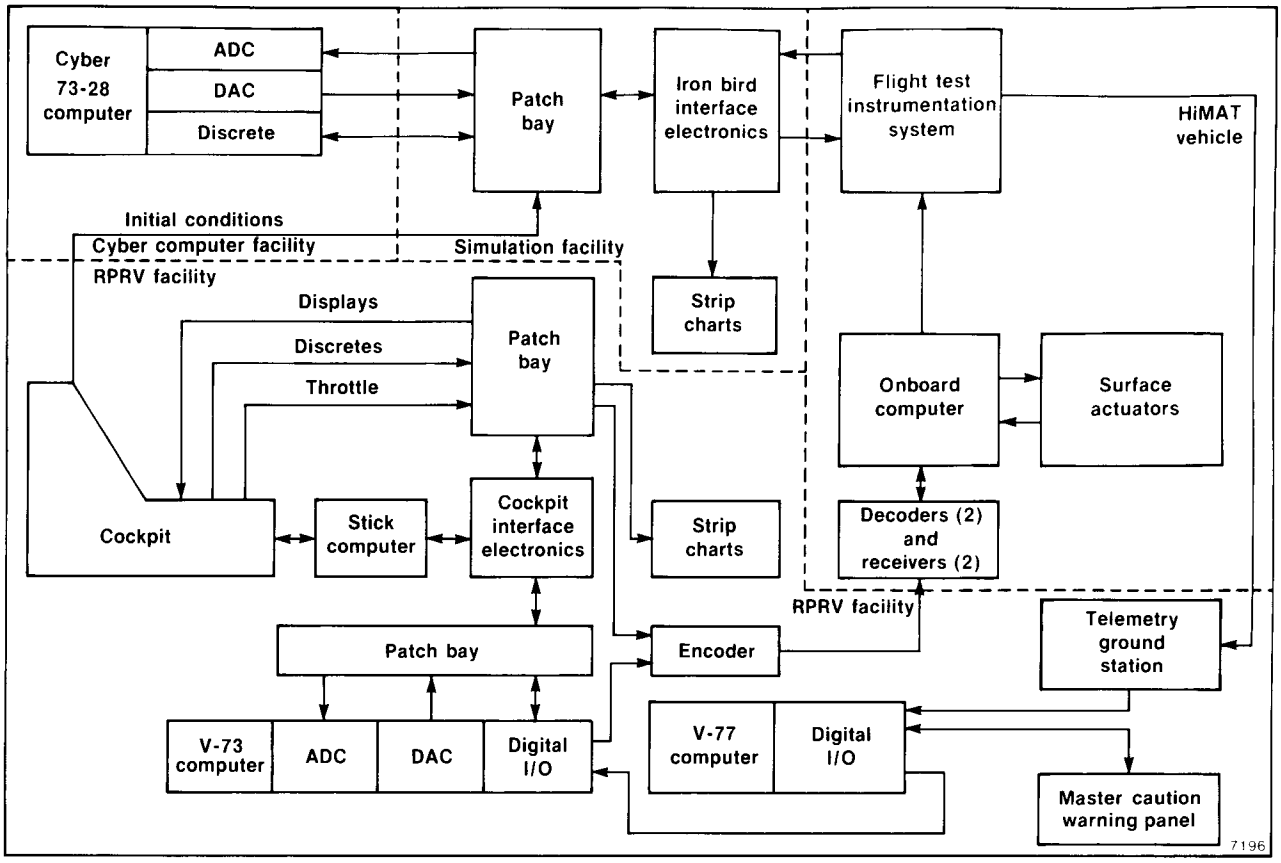


*Figure 26. HiMAT iron bird simulation.*

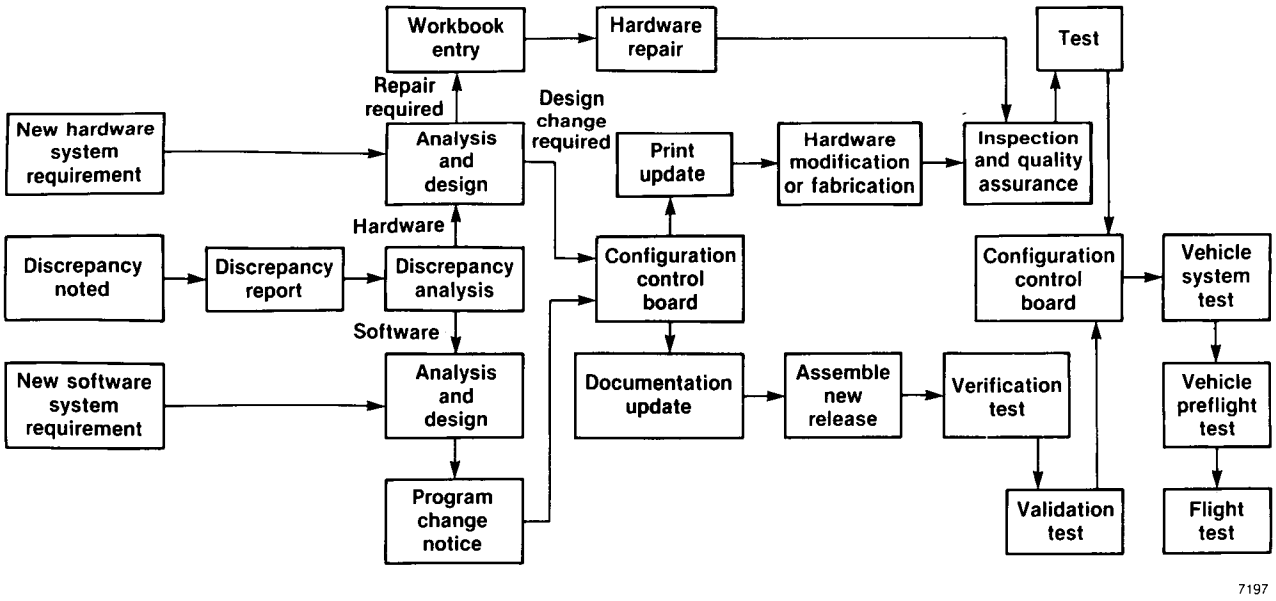


*Figure 27. HiMAT configuration control process.*

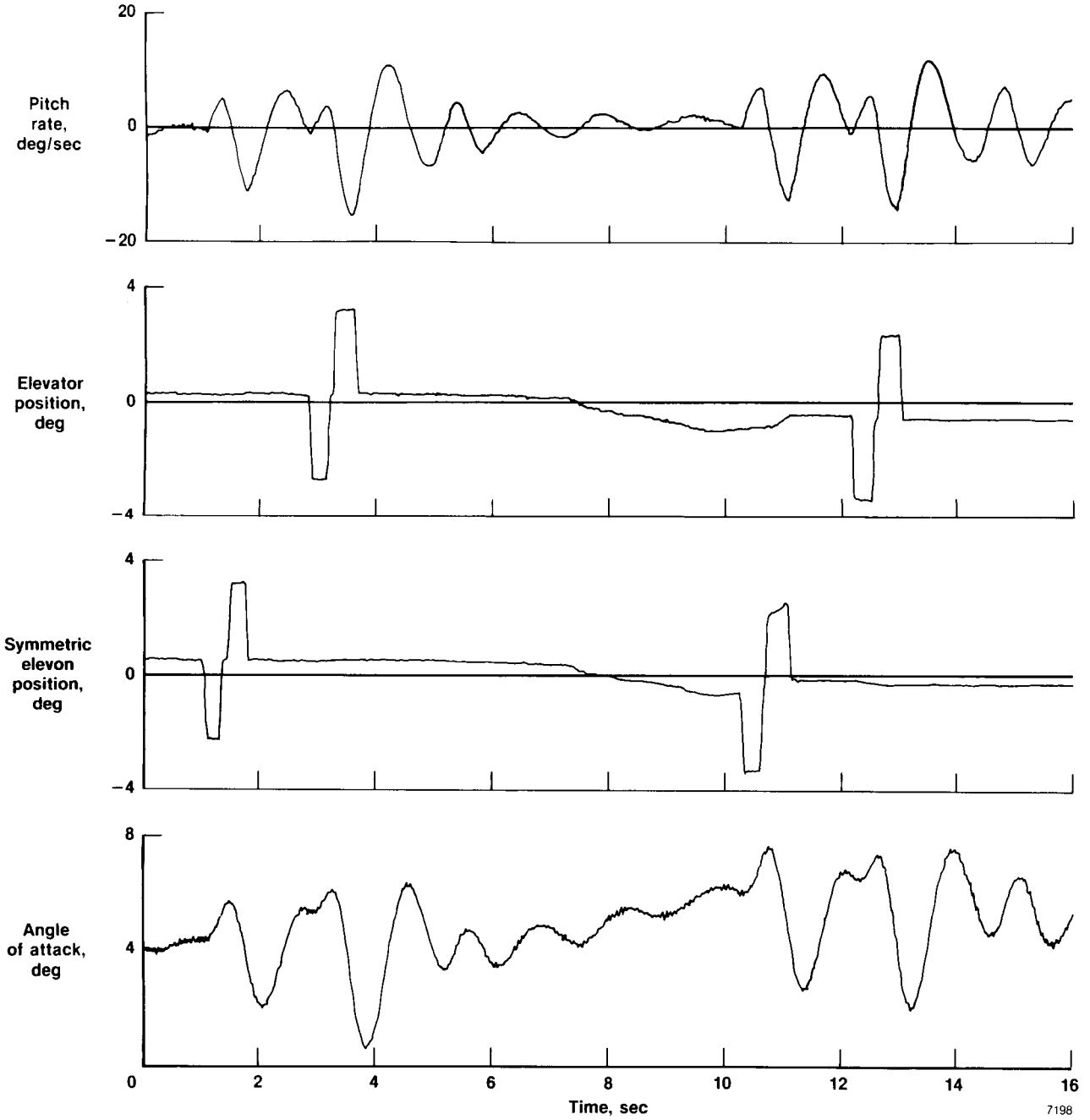


*Figure 28. HiMAT pitch pulse inputs of the elevon and elevator at zero pitch gain. $M = 0.9$, $h = 25{,}000$ ft.*

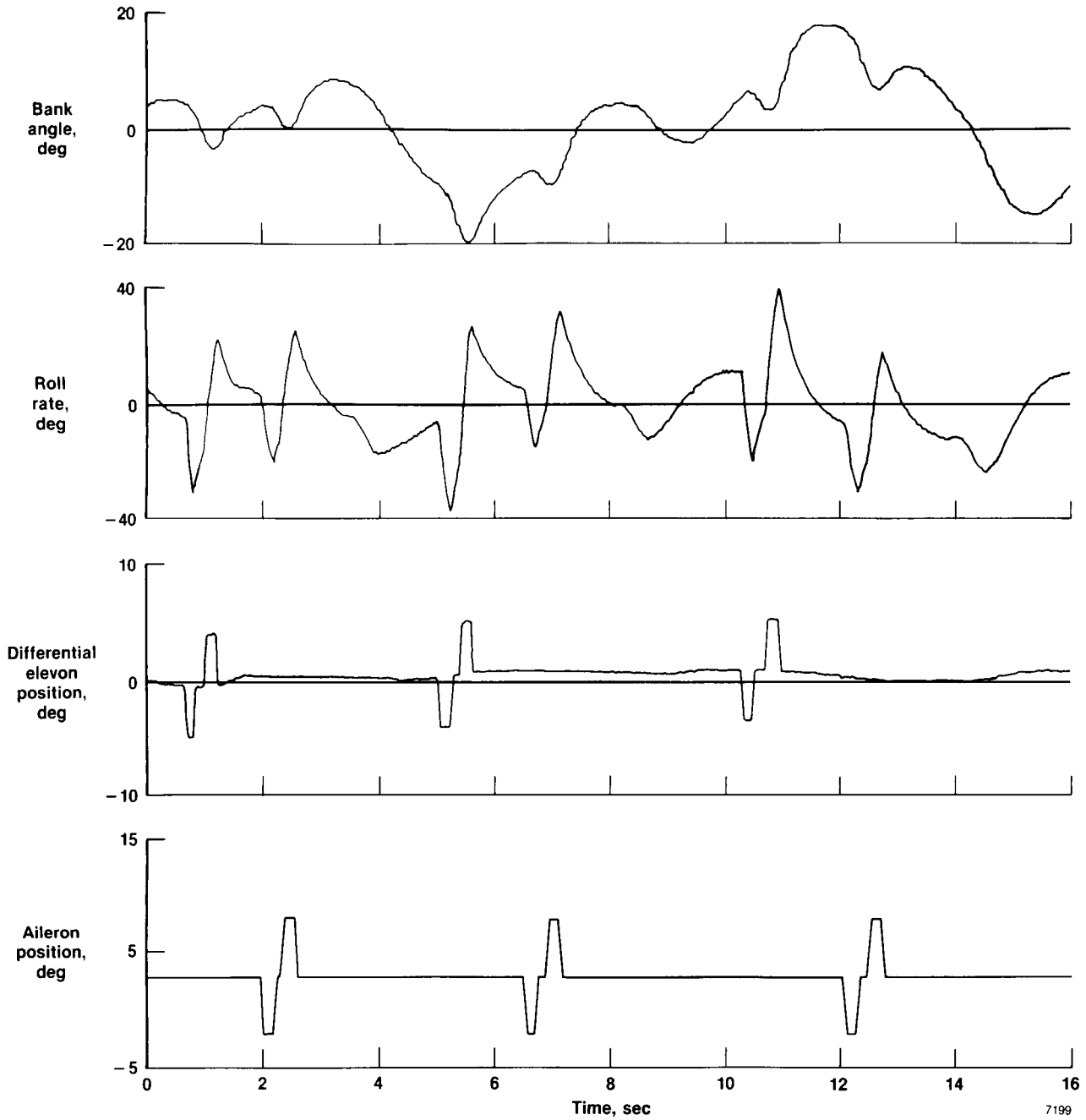


*(a) Differential elevon and aileron inputs.*

*Figure 29. HiMAT lateral-directional pulse inputs at zero roll and yaw gain. $M = 0.9$, $h = 25{,}000$ ft.*

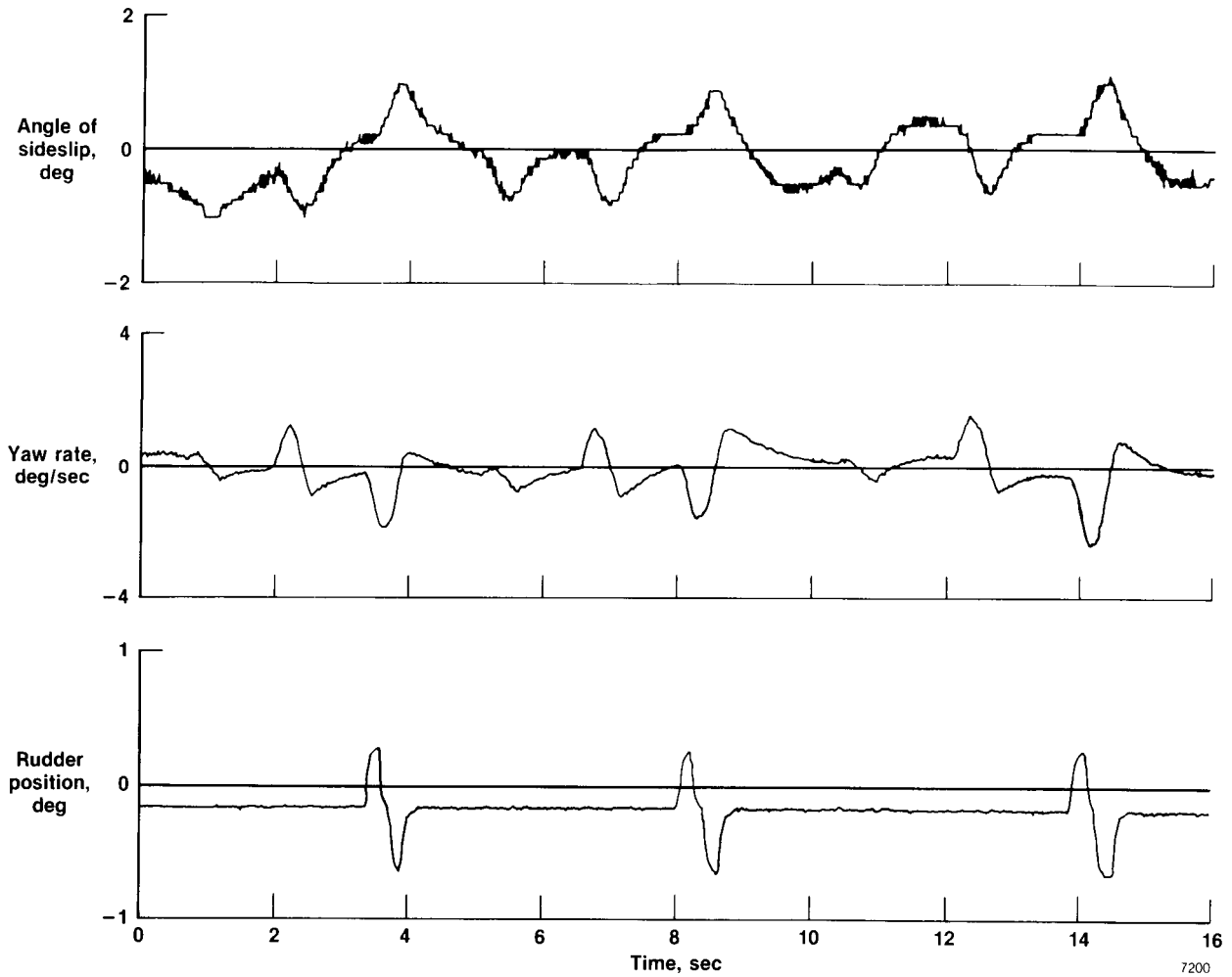


*(b) Rudder inputs.*

*Figure 29. Concluded.*

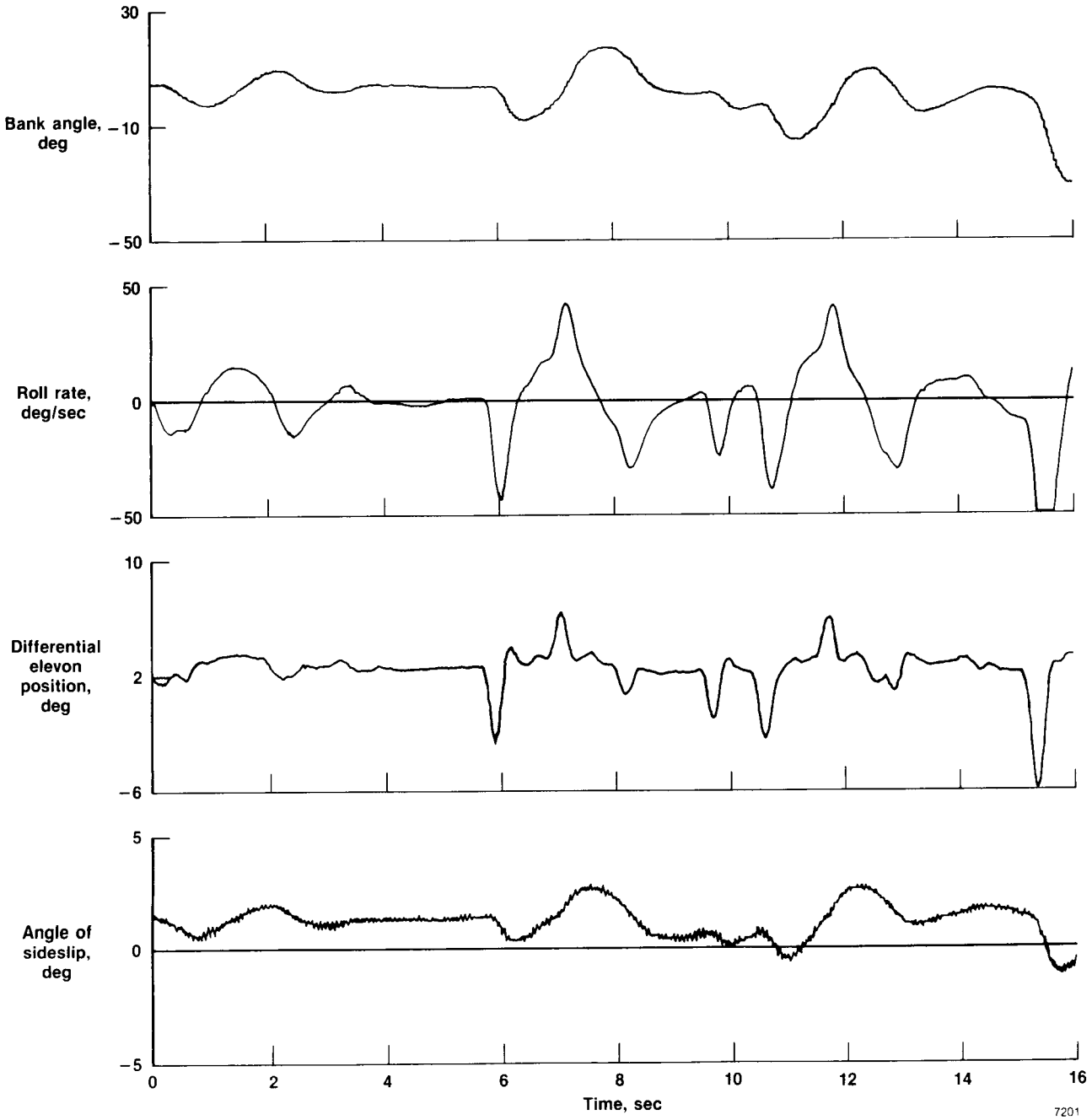


*Figure 30. HiMAT roll control evaluation using both differential elevon and aileron. $M = 0.5$, $h = 15{,}000$ ft, $\alpha = 4°$.*

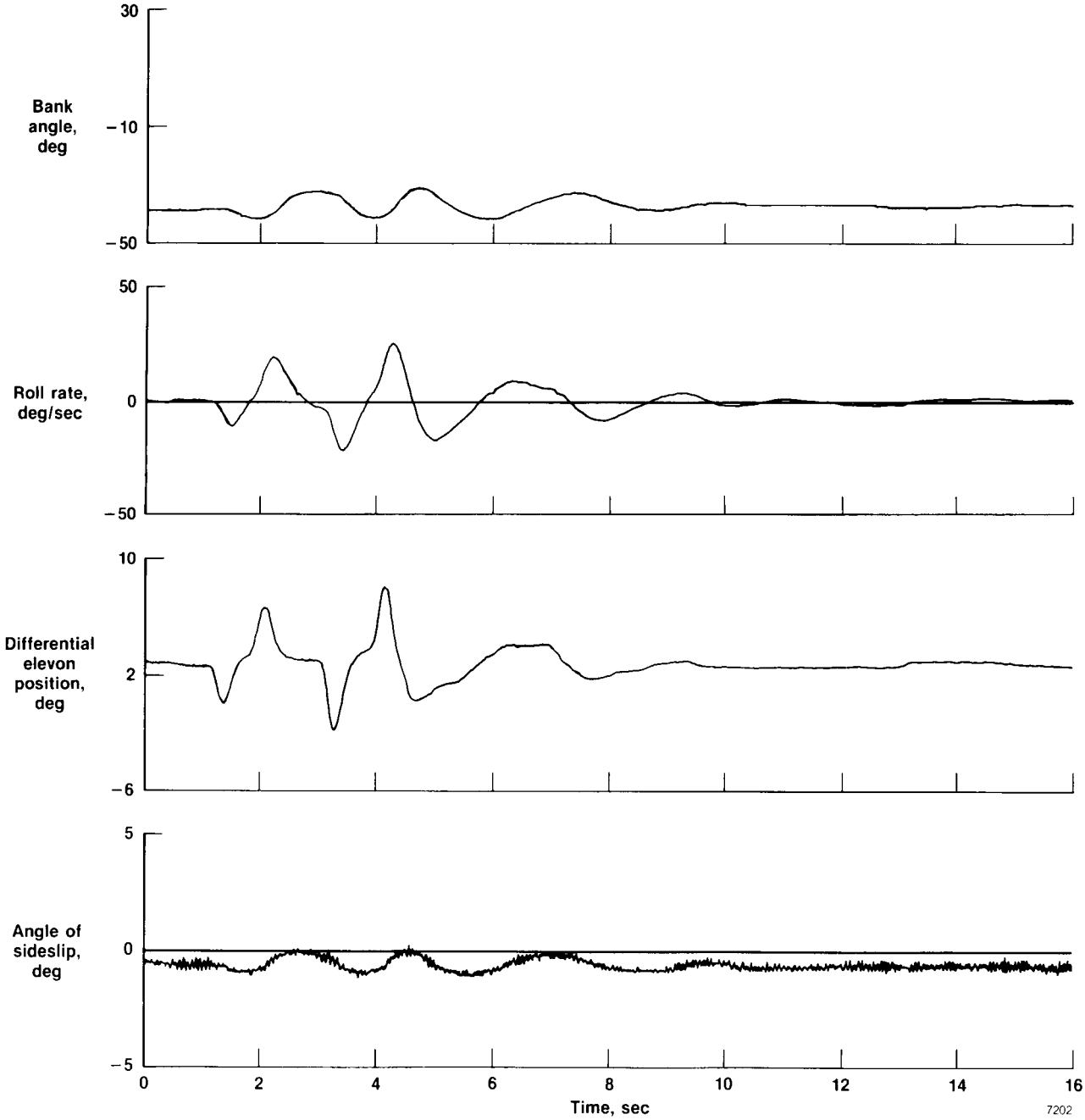


*Figure 31. HiMAT roll control evaluation using differential elevon only. $M = 0.5$, $h = 10{,}000$ ft, $\alpha = 4.5°$.*

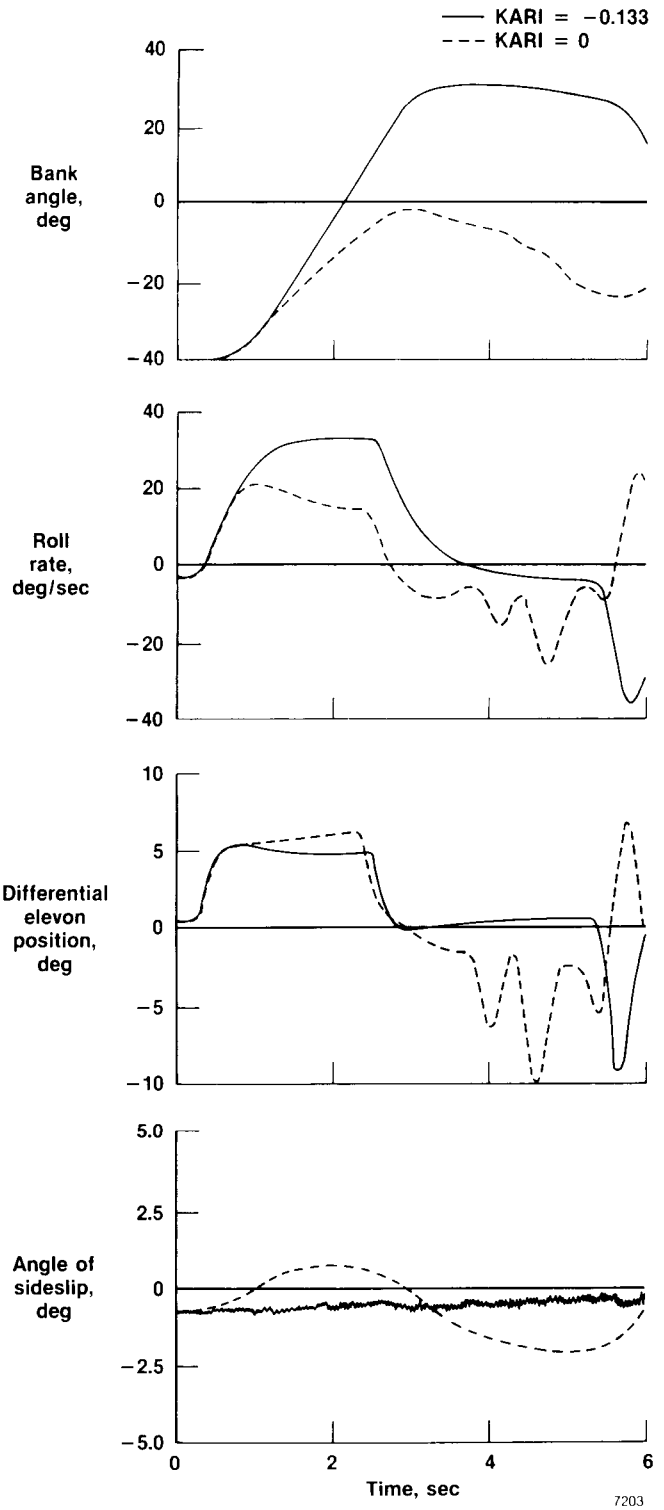


*Figure 32. HiMAT aileron-rudder-interconnect in-flight evaluation. $h = 15{,}000$ ft, $M = 0.43$, $\alpha = 5.5°$.*

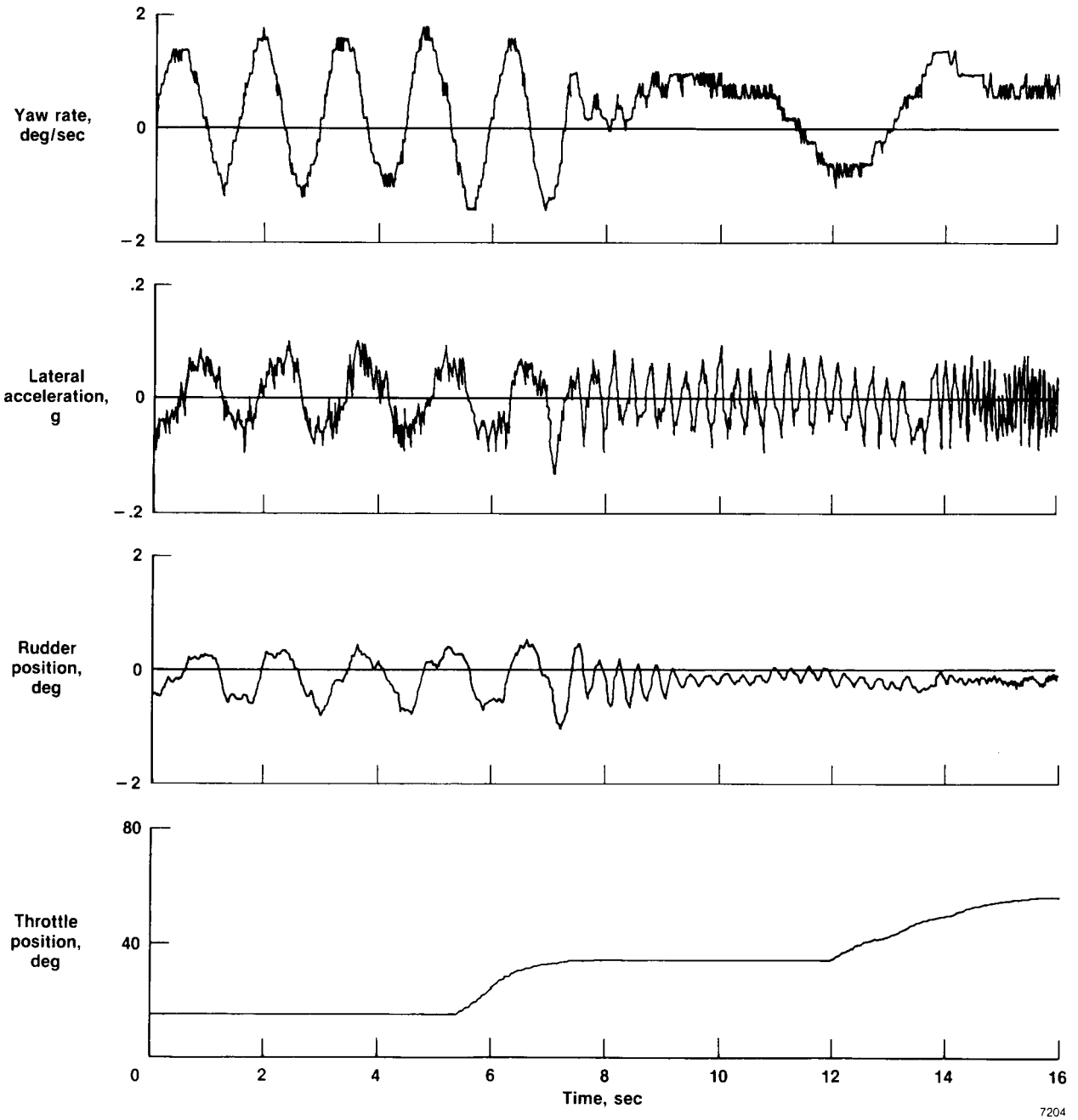


*Figure 33. HiMAT lateral-directional oscillation induced by engine vibration being aliased through the lateral accelerometer to the rudder. M = 0.72, h = 40,000 ft.*

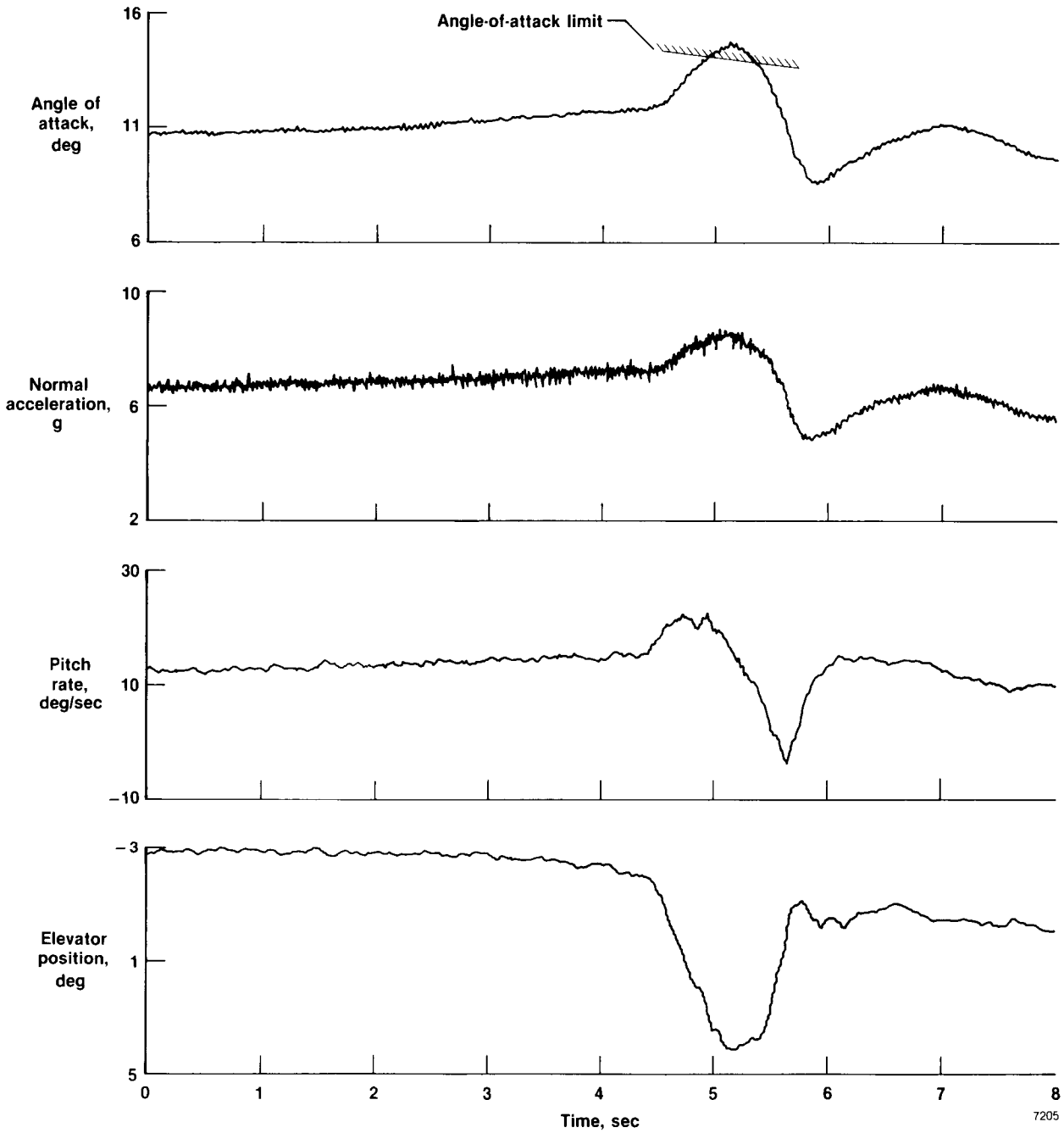


*Figure 34. HiMAT transonic pitch-up through the angle-of-attack limiter. $0.85 \leq M \leq 0.90$, $26{,}000\ ft \leq h \leq 27{,}100\ ft$.*

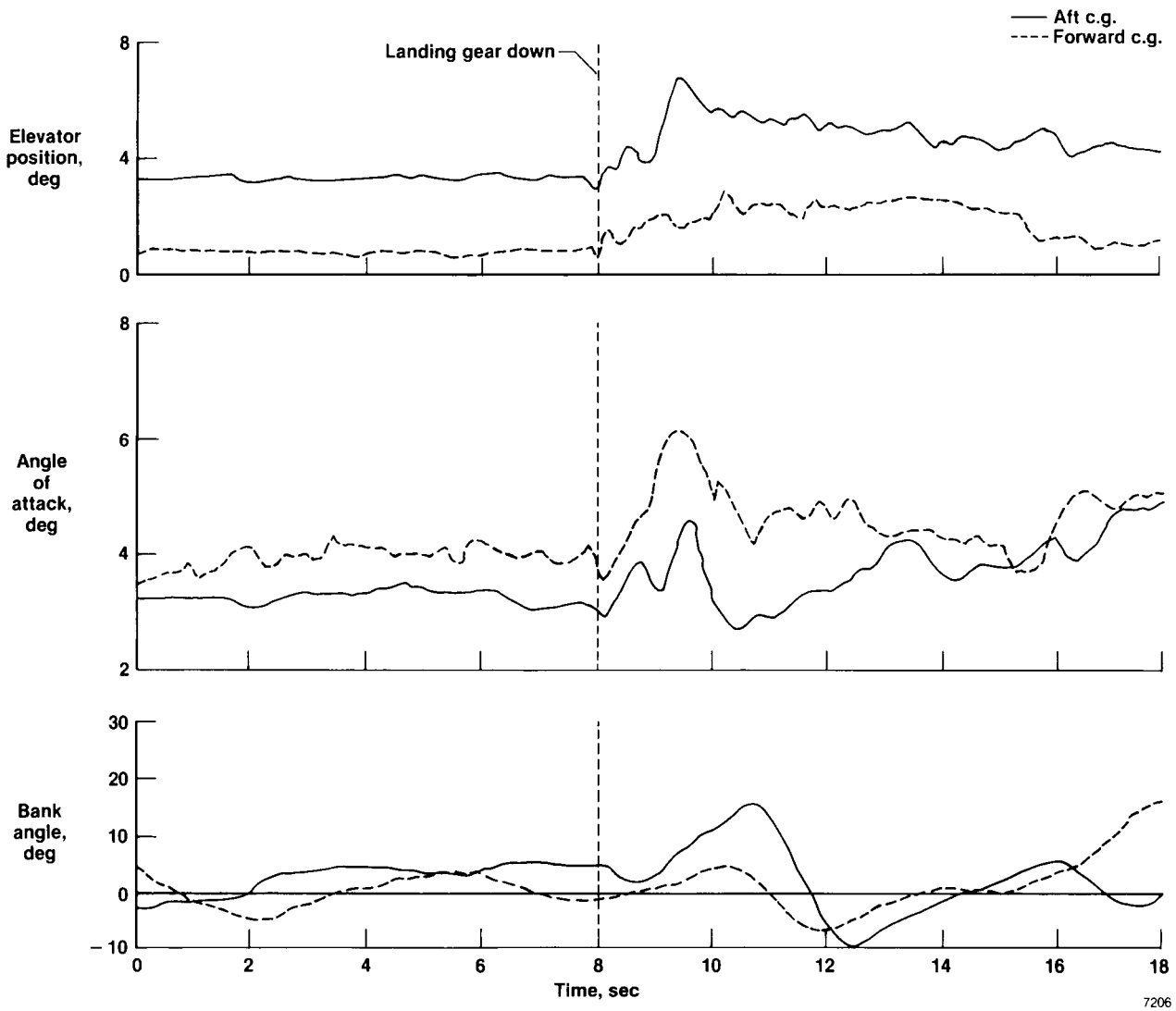


*Figure 35. HiMAT landing gear extension transient comparison between forward and aft center-of-gravity location.*

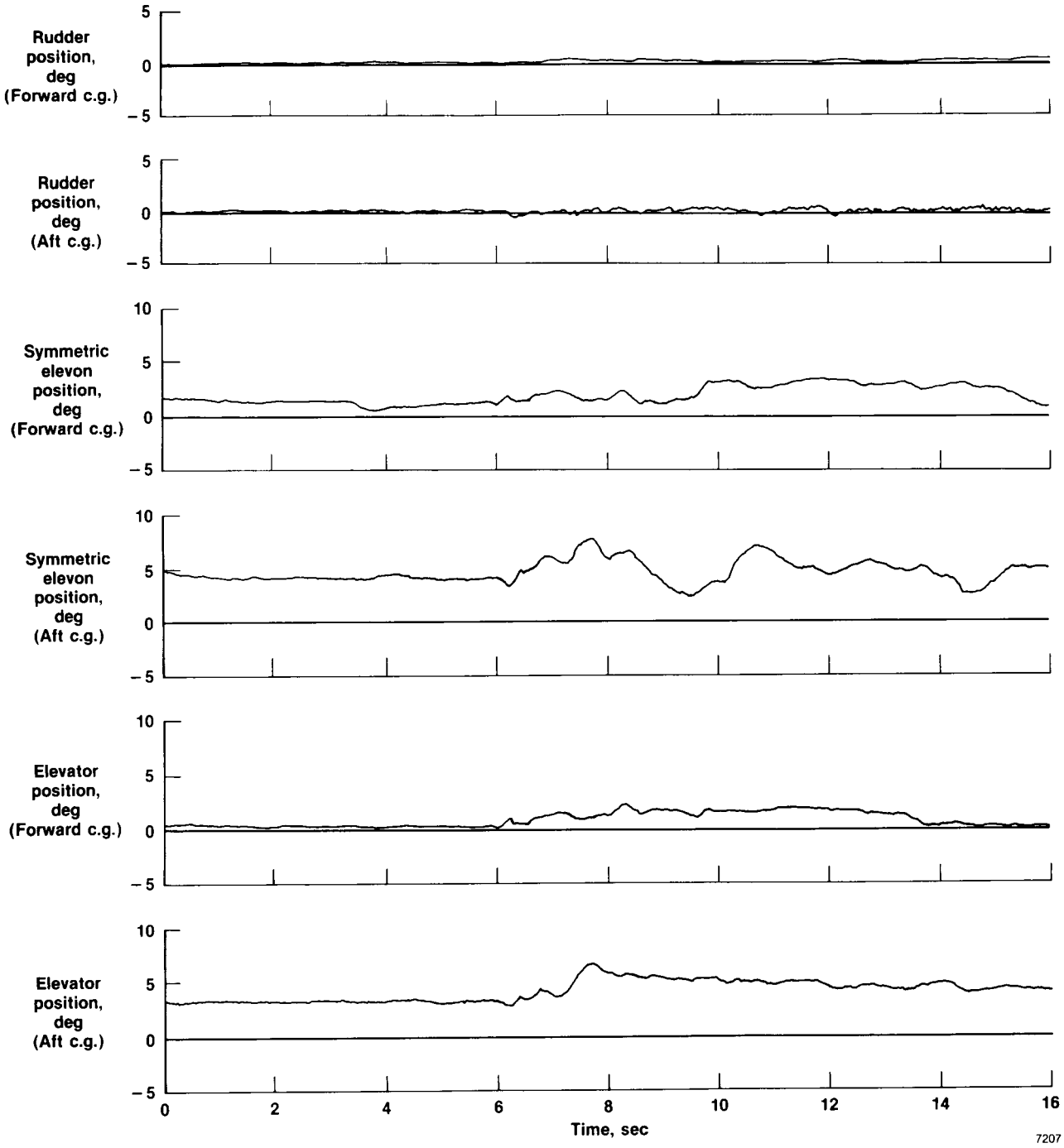


*Figure 36. HiMAT left control surfaces at landing gear extension for aft and forward center-of-gravity locations.*

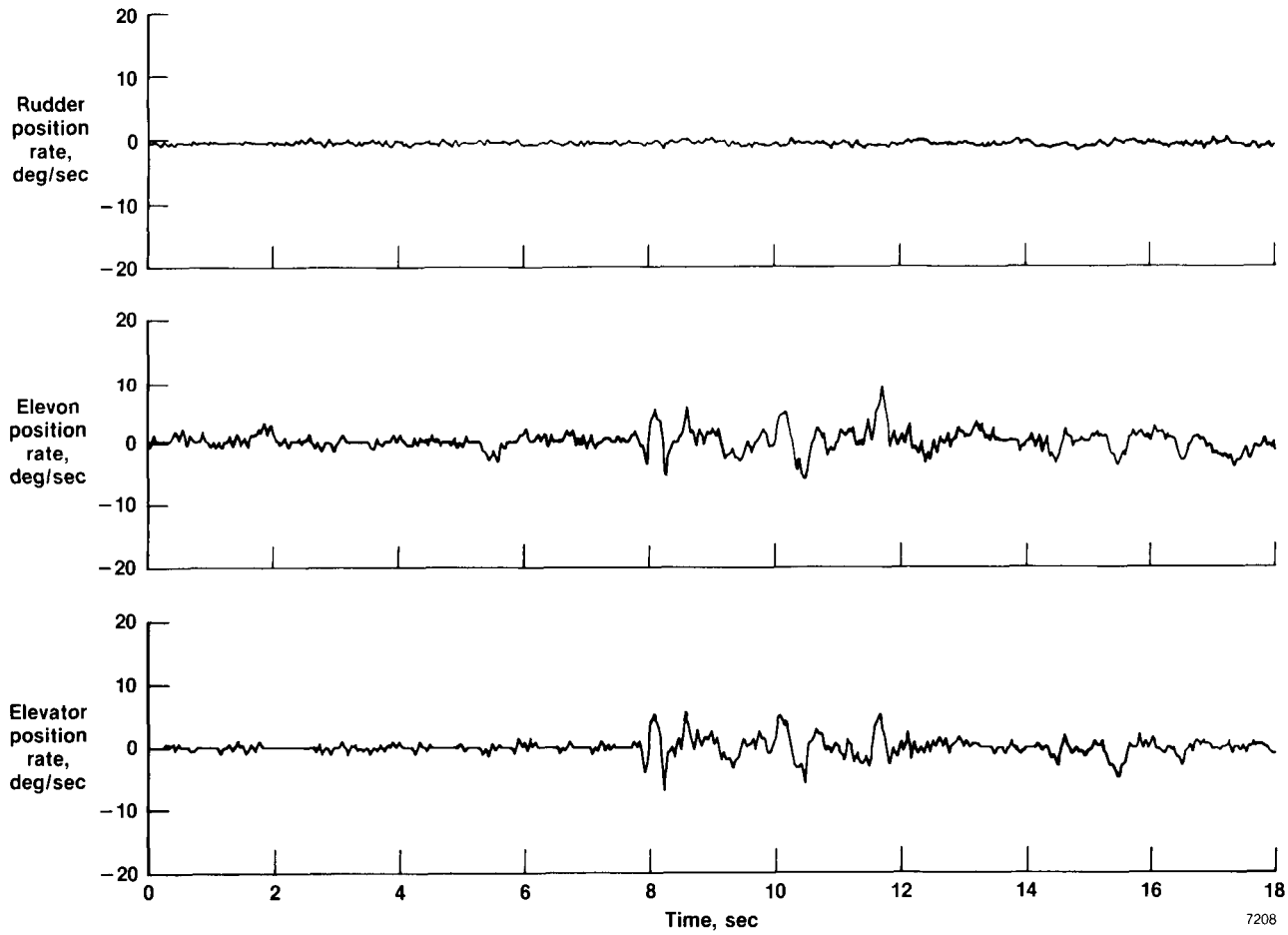


*(a) Forward center-of-gravity location.*

*Figure 37. HiMAT left control surface position angular rates at landing gear extension.*

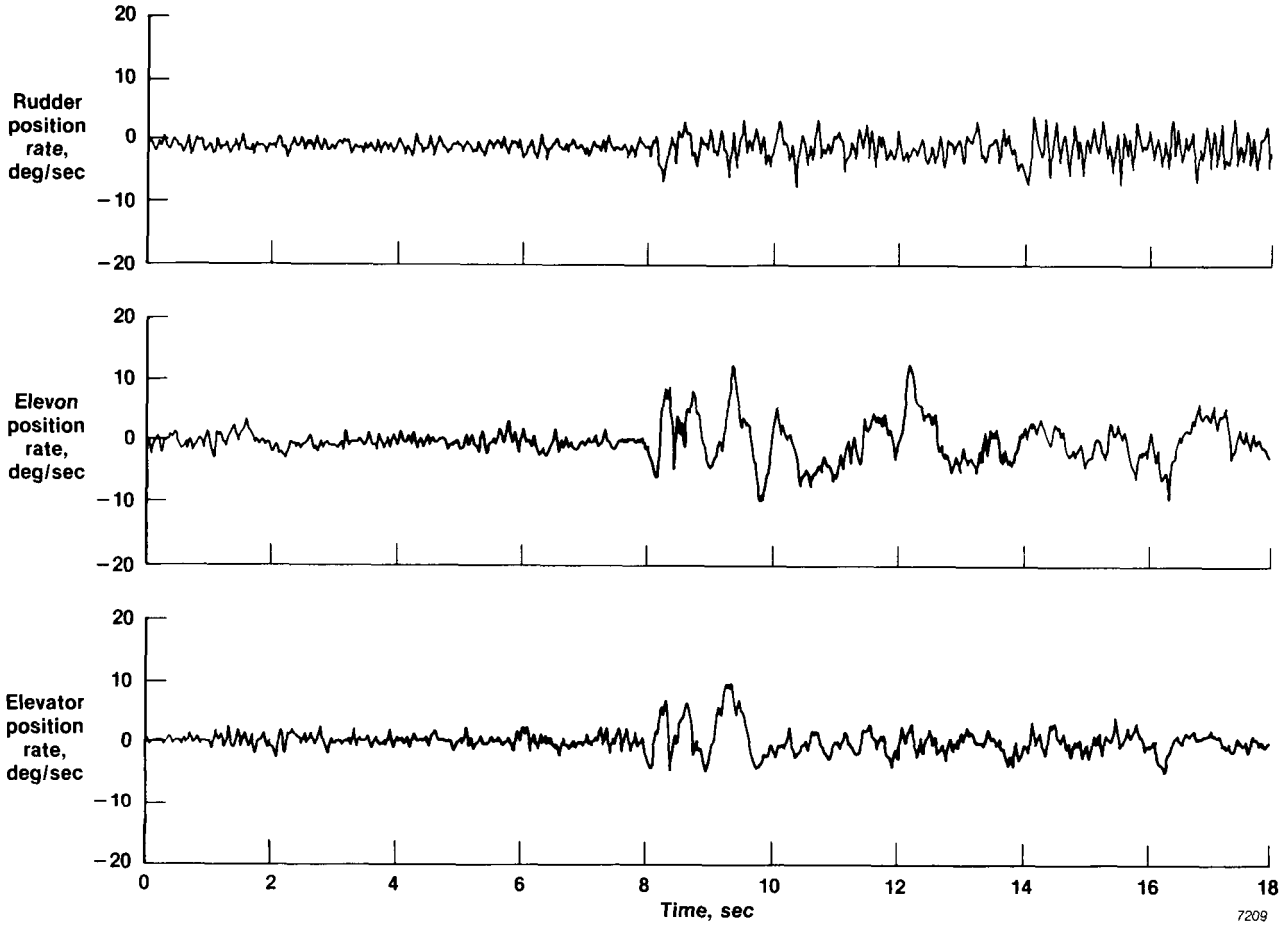


*(b) Aft center-of-gravity location.*

*Figure 37. Concluded.*

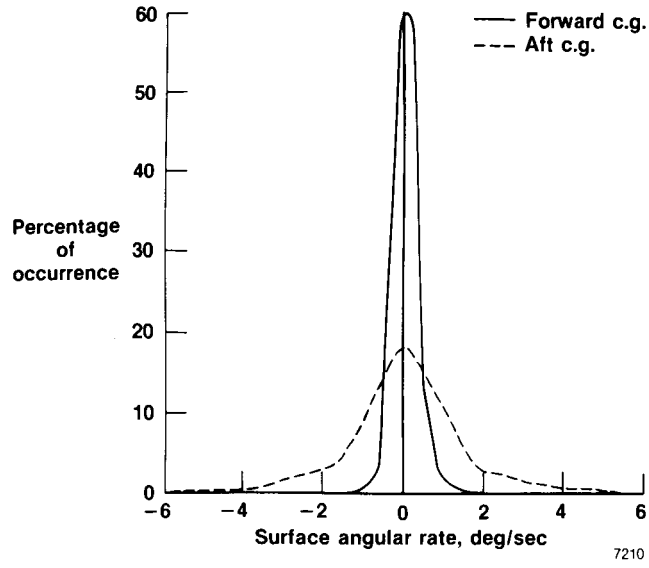


*(a) Left rudder.*

*Figure 38. HiMAT control surface probability distribution using 4,400 data points for a 20-sec time interval.*

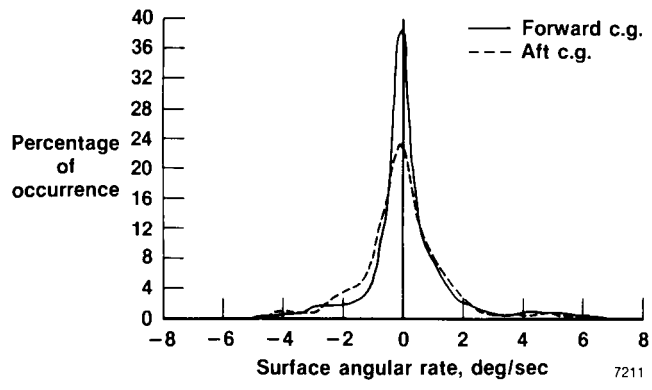


*(b) Left elevator.*

*Figure 38. Continued.*

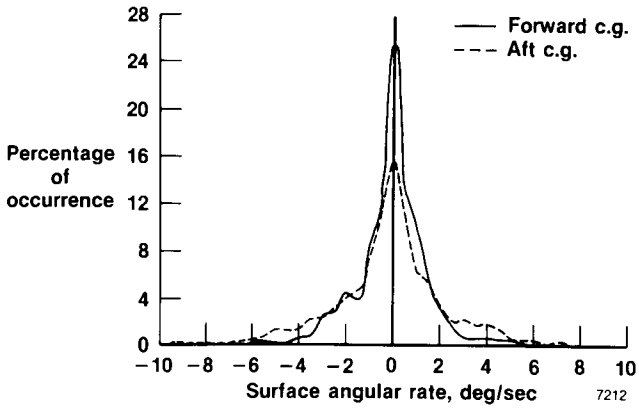


*(c) Left elevon.*

*Figure 38. Concluded.*

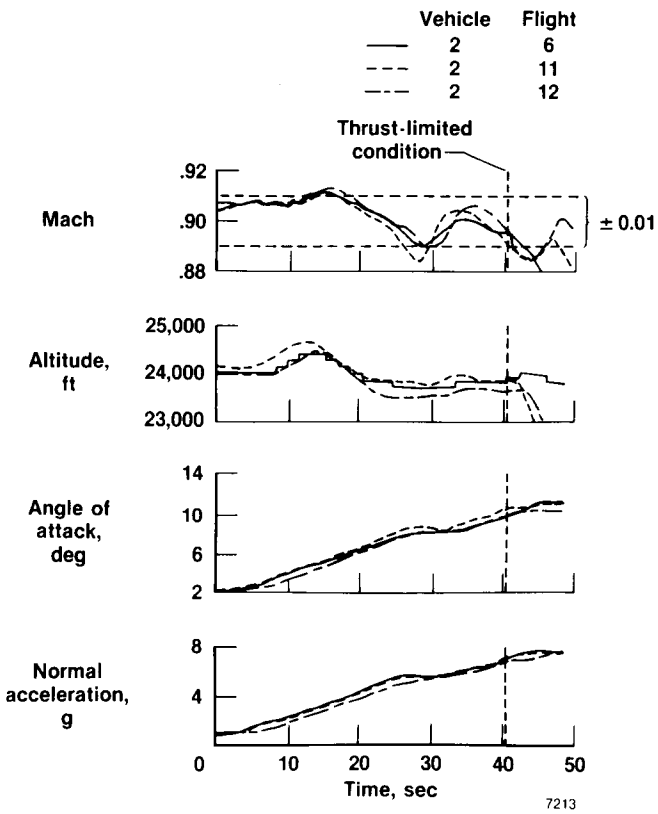


*Figure 39. Comparison of three FTMAP-flown windup turns at nominal conditions of Mach 0.90 and 25,000-ft altitude.*

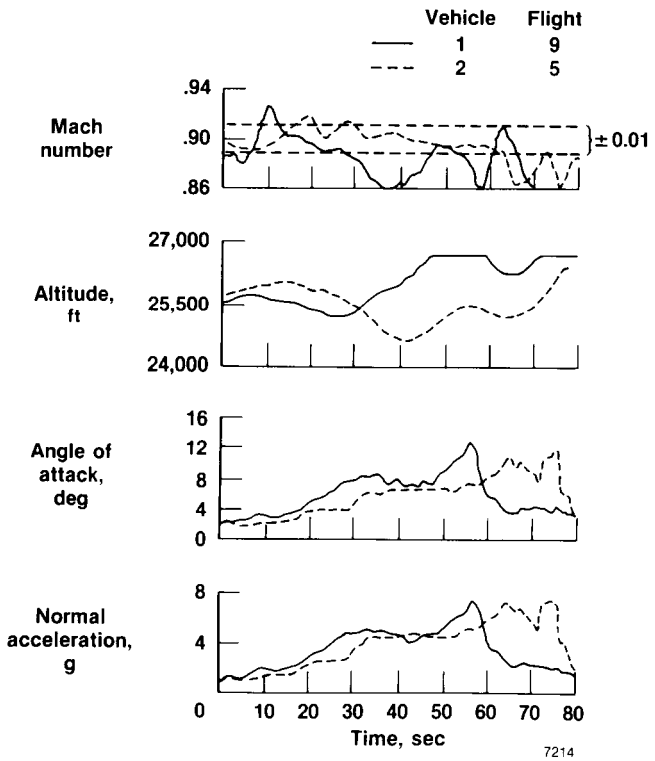


*Figure 40. Comparison of two pilot-flown windup turns at nominal conditions of Mach 0.90 and 25,000-ft altitude.*

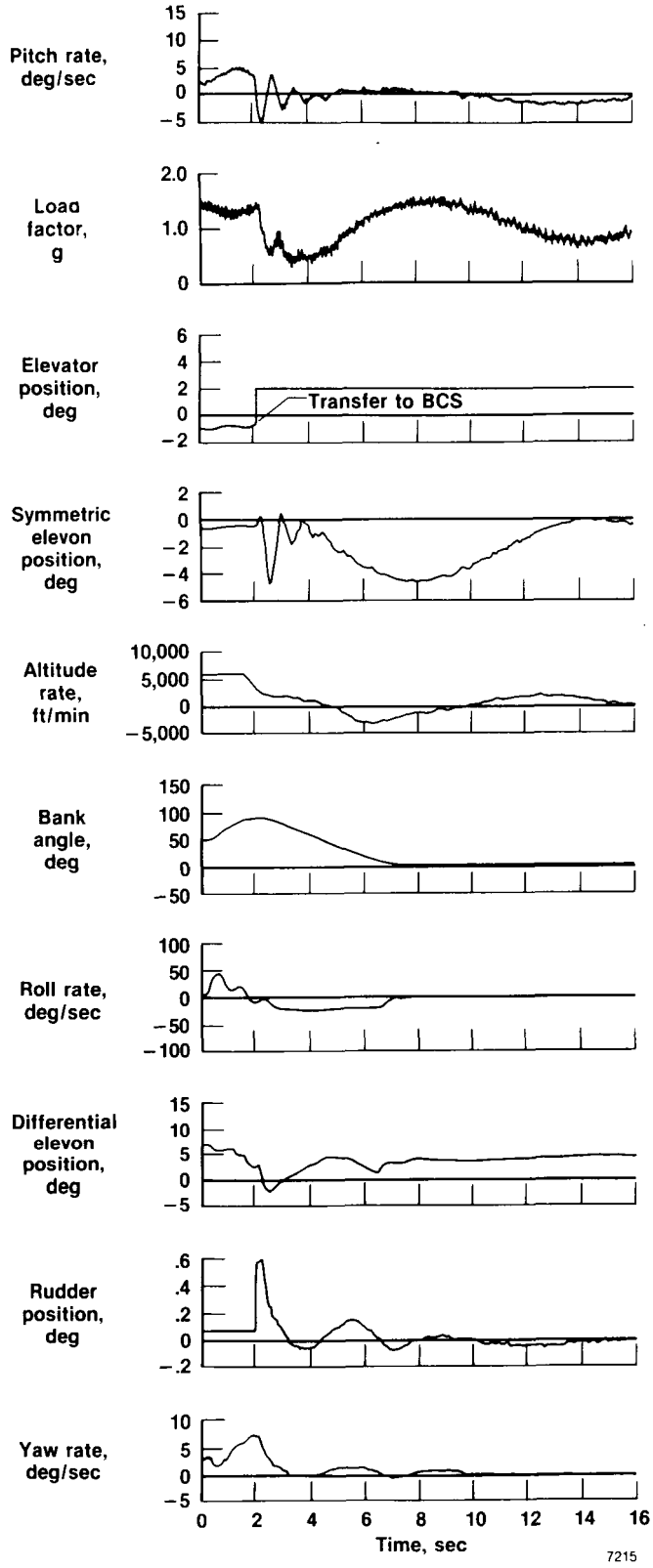


*(a) Mach number = 0.65, h = 26,000 ft, $\bar{q}$ = 220 lb/ft$^2$, $V_c$ = 260 knots.*

*Figure 41. HiMAT transfer from primary control to backup control, recovery mode.*

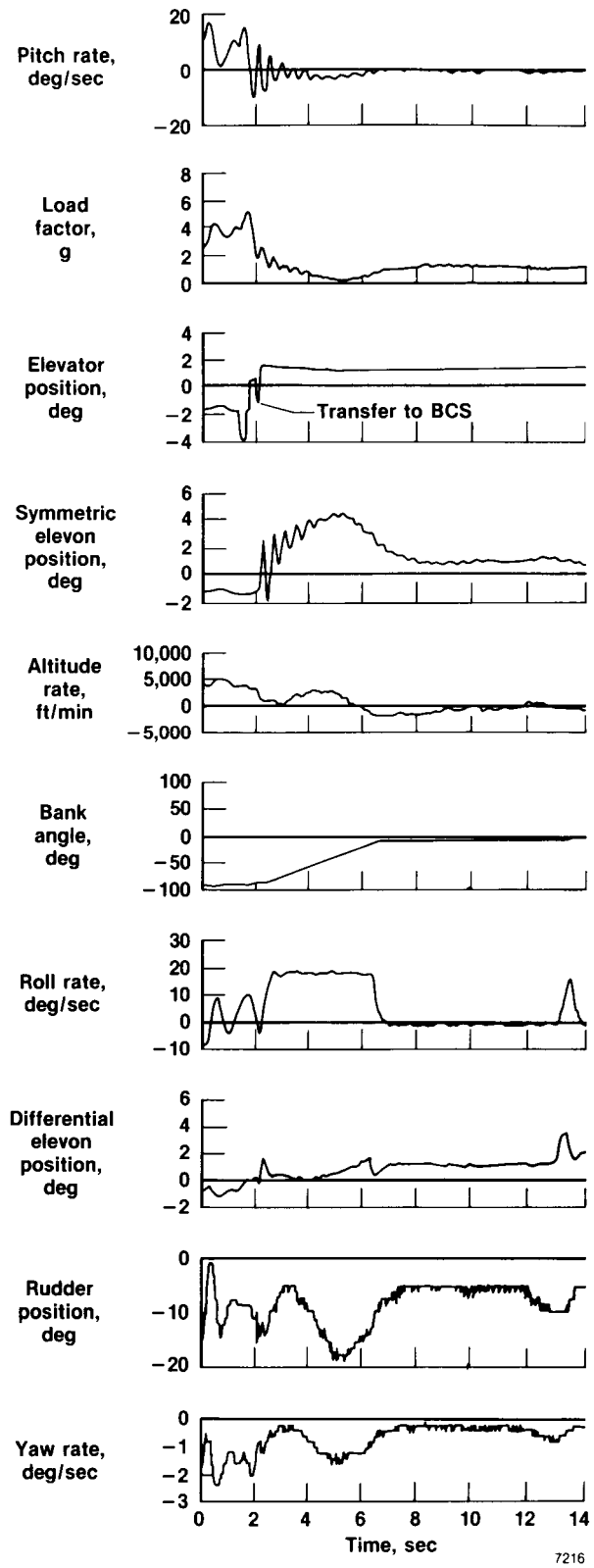


*(b) Mach number = 0.85, h = 25,450 ft,* $\bar{q}$ *= 390 lb/ft*$^2$*,* $V_c$ *= 360 knots.*

*Figure 41. Continued.*

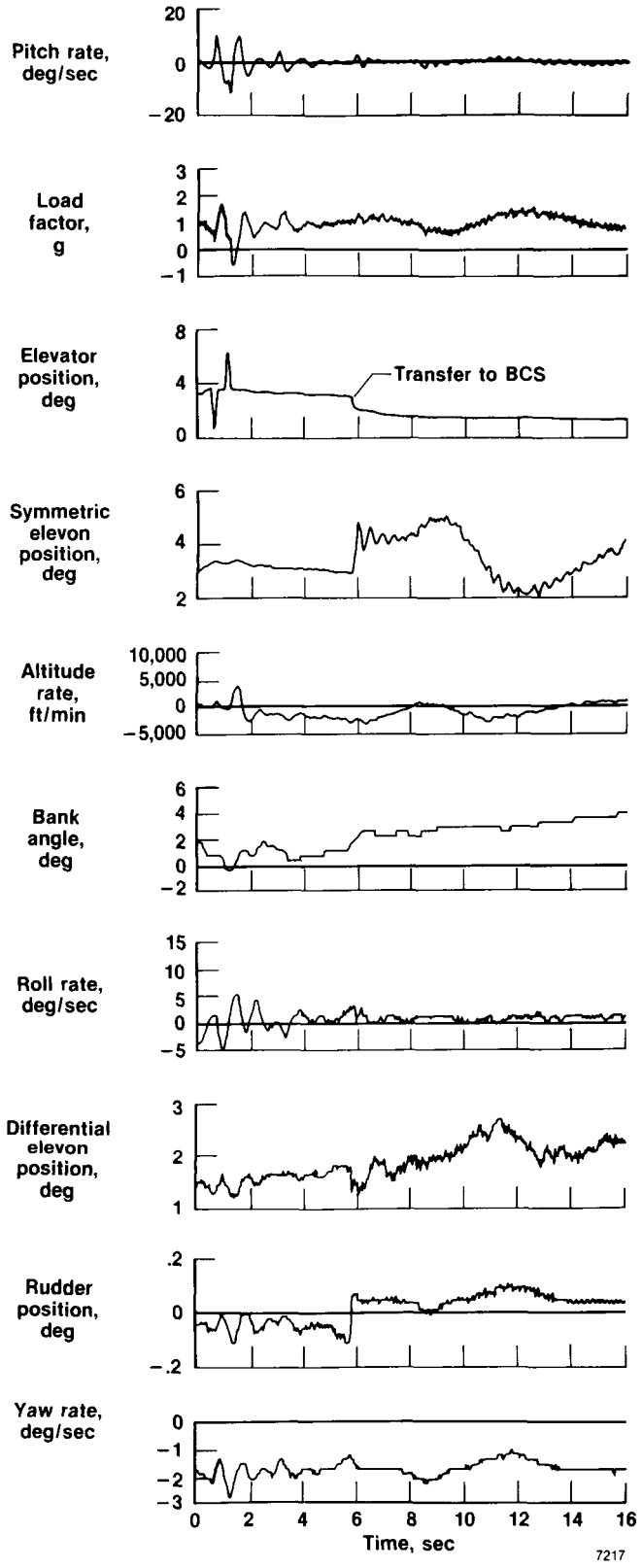


*(c) Mach number = 0.88, h = 25,100 ft, $\bar{q}$ = 430 lb/ft$^2$, $V_c$ = 375 knots.*

*Figure 41. Concluded.*

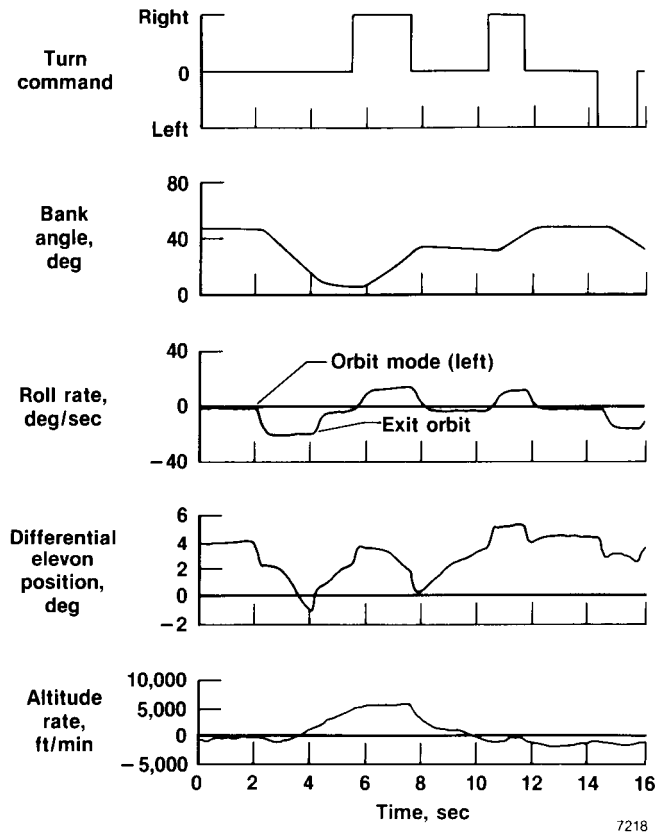


*Figure 42. HiMAT backup control, orbit mode Mach number = 0.82, h = 25,400 ft,* $\bar{q}$ *= 360 lb/ft*$^2$, $V_c$ *= 343 knots.*

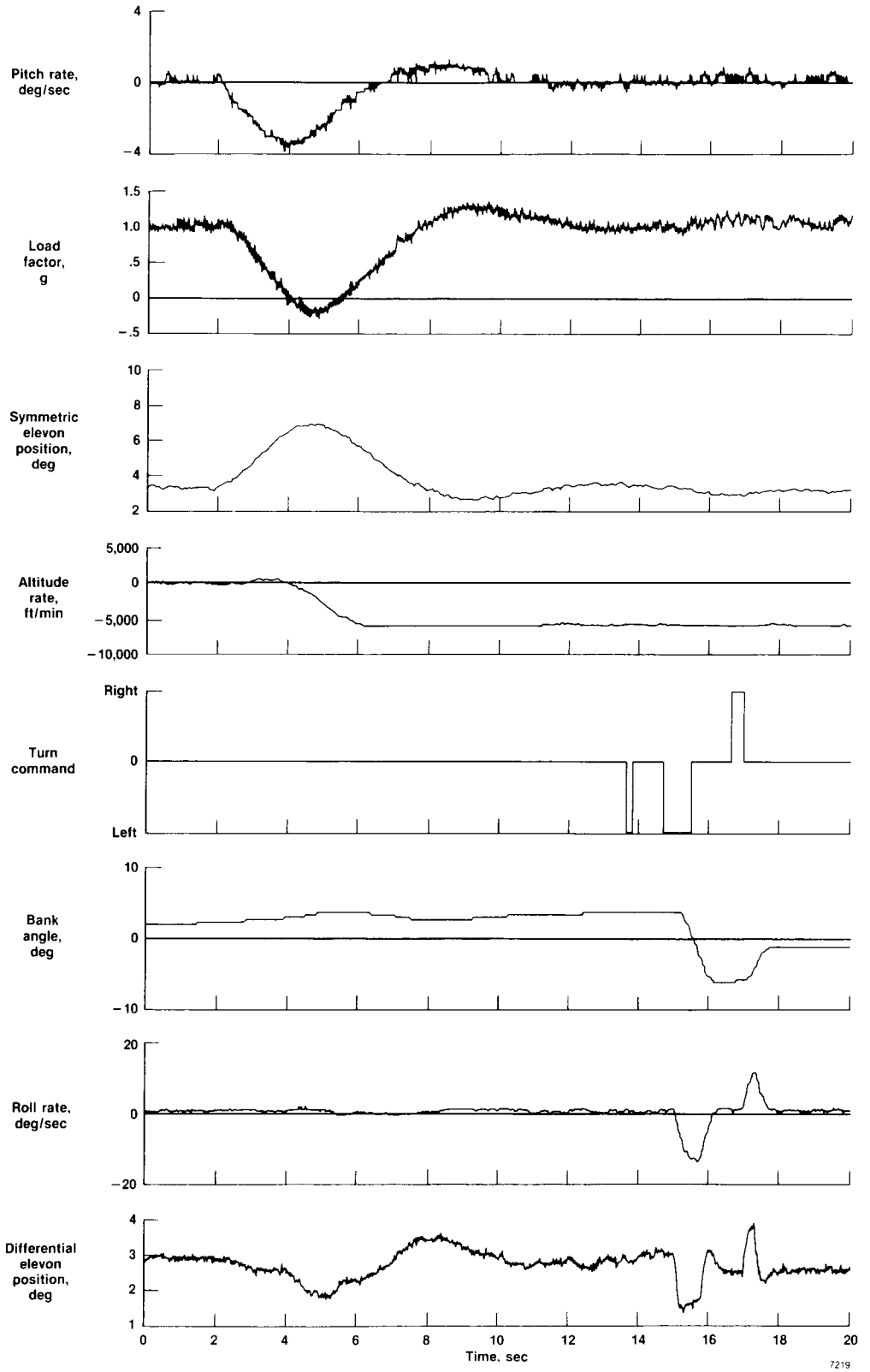


*(a) Mach number = 0.76, h = 24,000 ft, $\bar{q}$ = 330 lb/ft$^2$, $V_c$ = 325 knots.*

*Figure 43. HiMAT backup control, dive mode.*

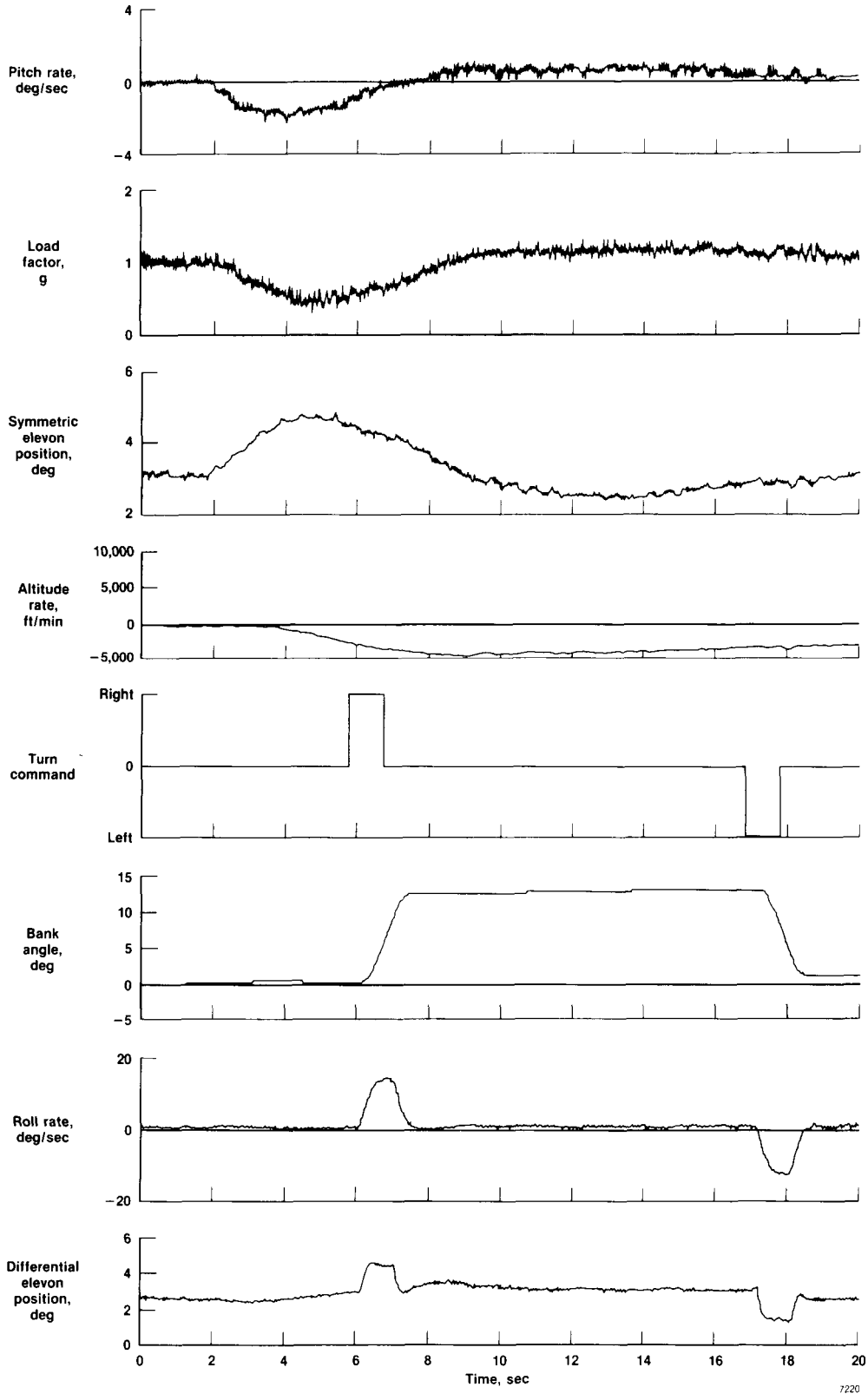


*(b) Mach number = 0.55, h = 9,600 ft, $\bar{q}$ = 213 lb/ft$^2$, $V_c$ = 307 knots.*

*Figure 43. Concluded.*

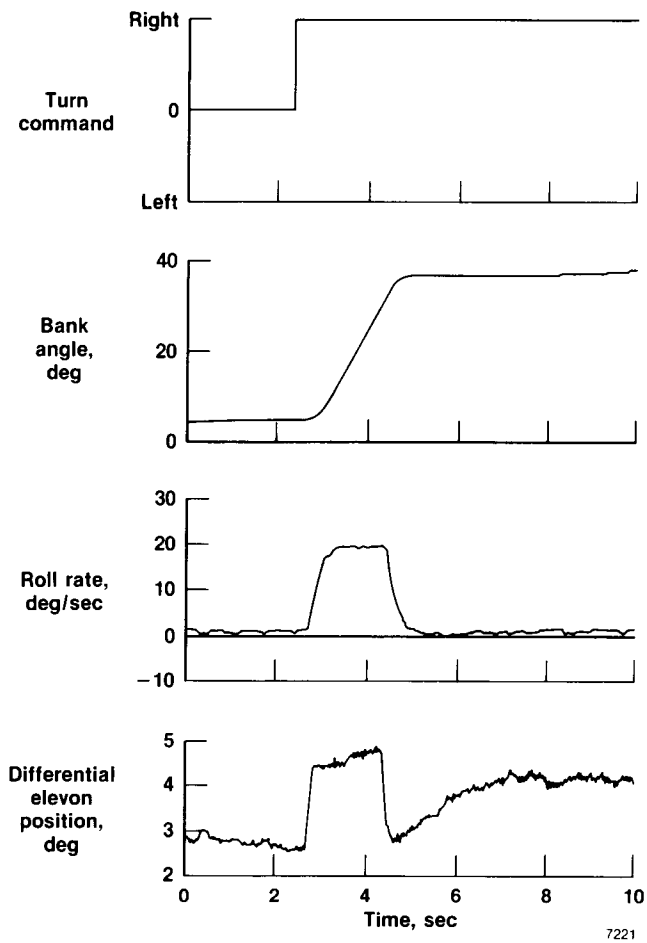


*(a) Attitude command, Mach number = 0.82, h = 24,900 ft, $\bar{q}$ = 373 lb/ft$^2$, $V_c$ = 348 knots.*

*Figure 44. HiMAT backup control, turn mode.*

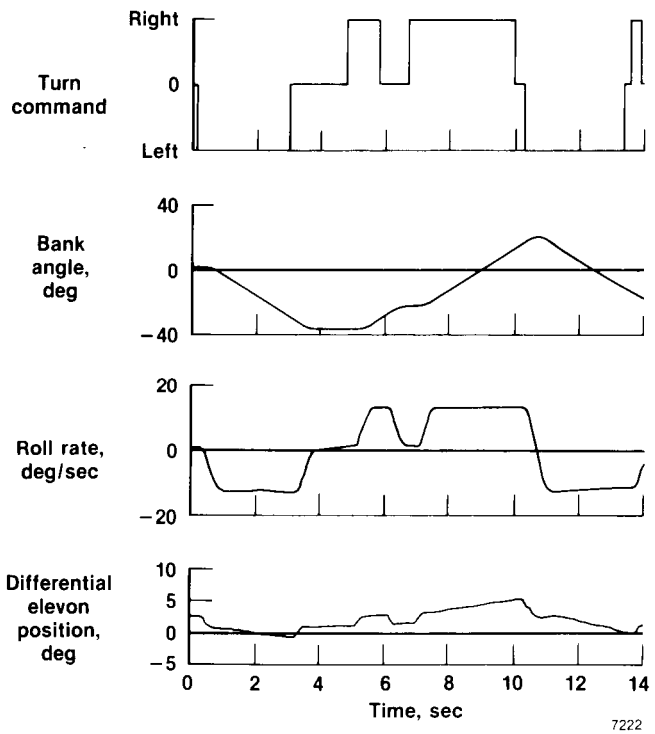


*(b) Roll-rate command, Mach number = 0.50, h = 5,500 ft, $\bar{q}$ = 300 lb/ft$^2$, $V_c$ = 296 knots.*

*Figure 44. Continued.*

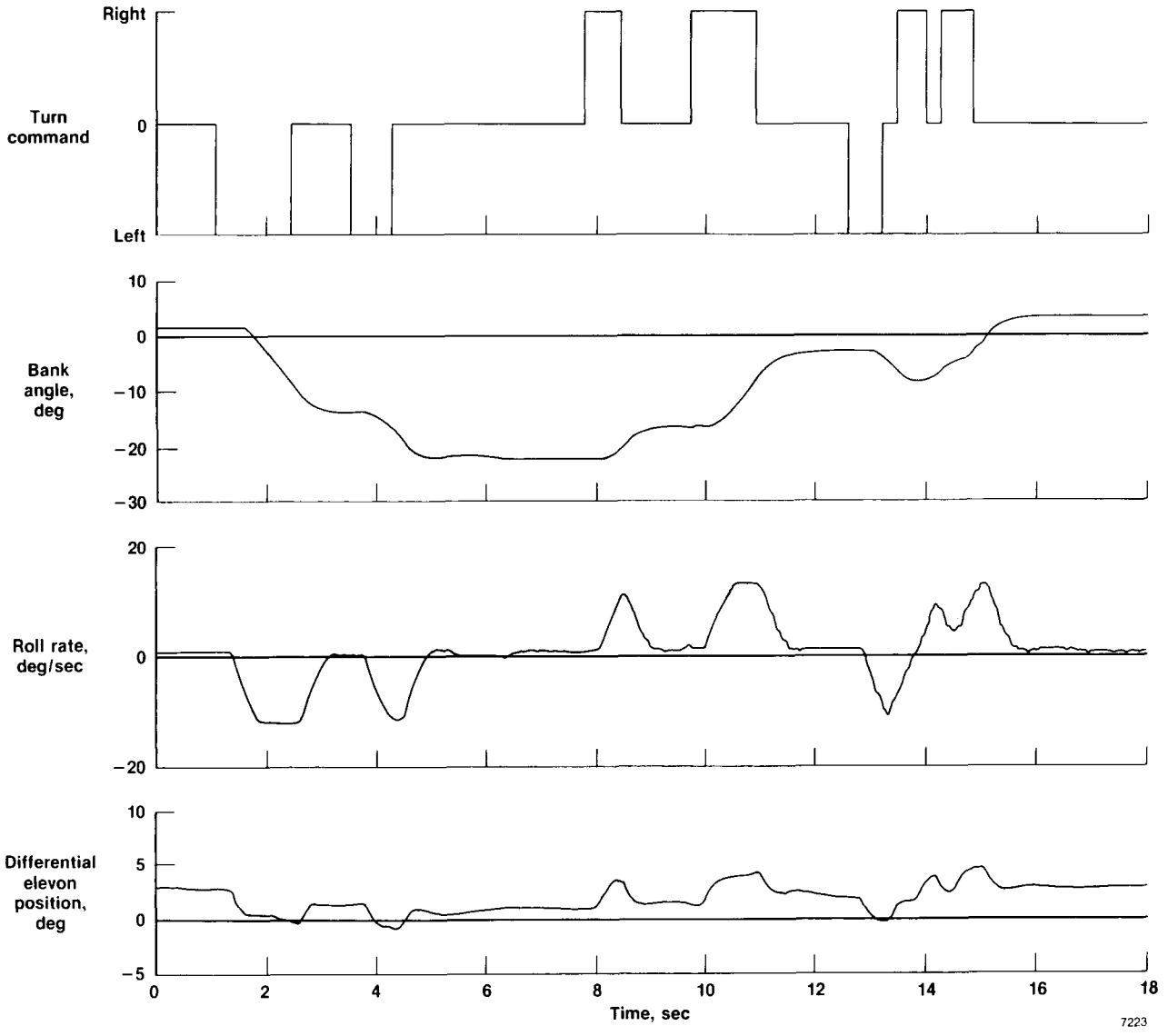


*(c) Roll-rate command, Mach number = 0.41, h = 5,200 ft, $\bar{q}$ = 202 lb/ft$^2$, $V_c$ = 246 knots.*

*Figure 44. Concluded.*

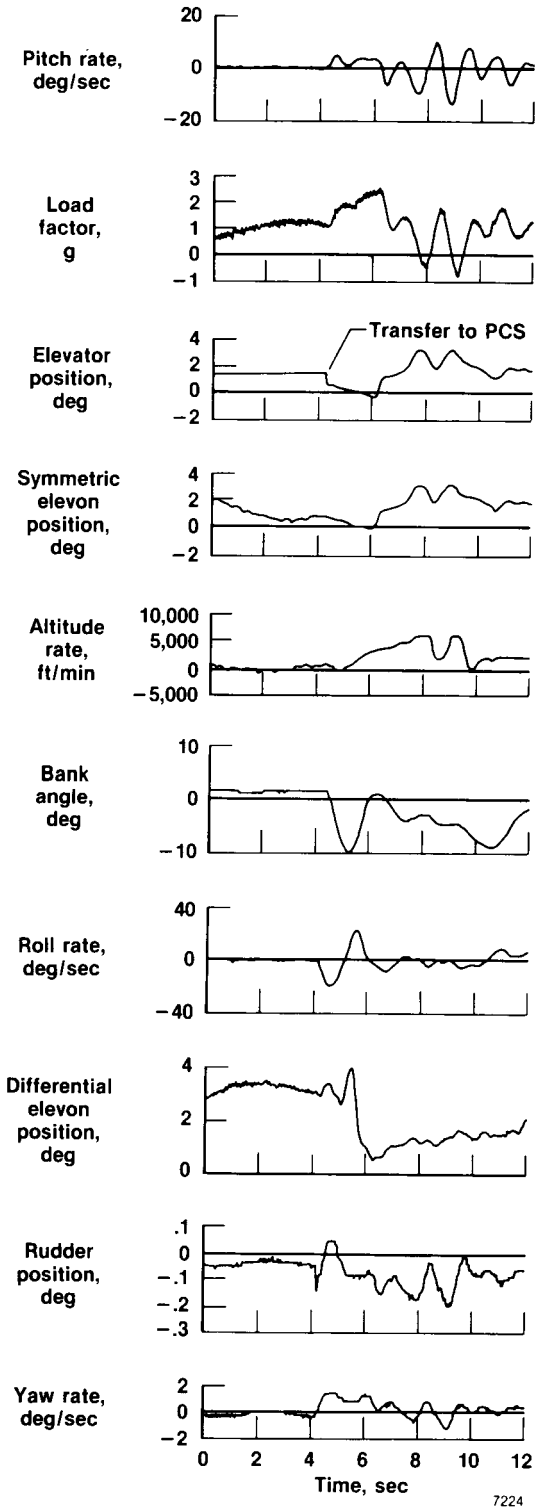


*(a) Mach number = 0.82, h = 25,800 ft, $\bar{q}$ = 350 lb/ft$^2$, $V_c$ = 337 knots.*

*Figure 45. HiMAT transfer from backup control to primary control.*

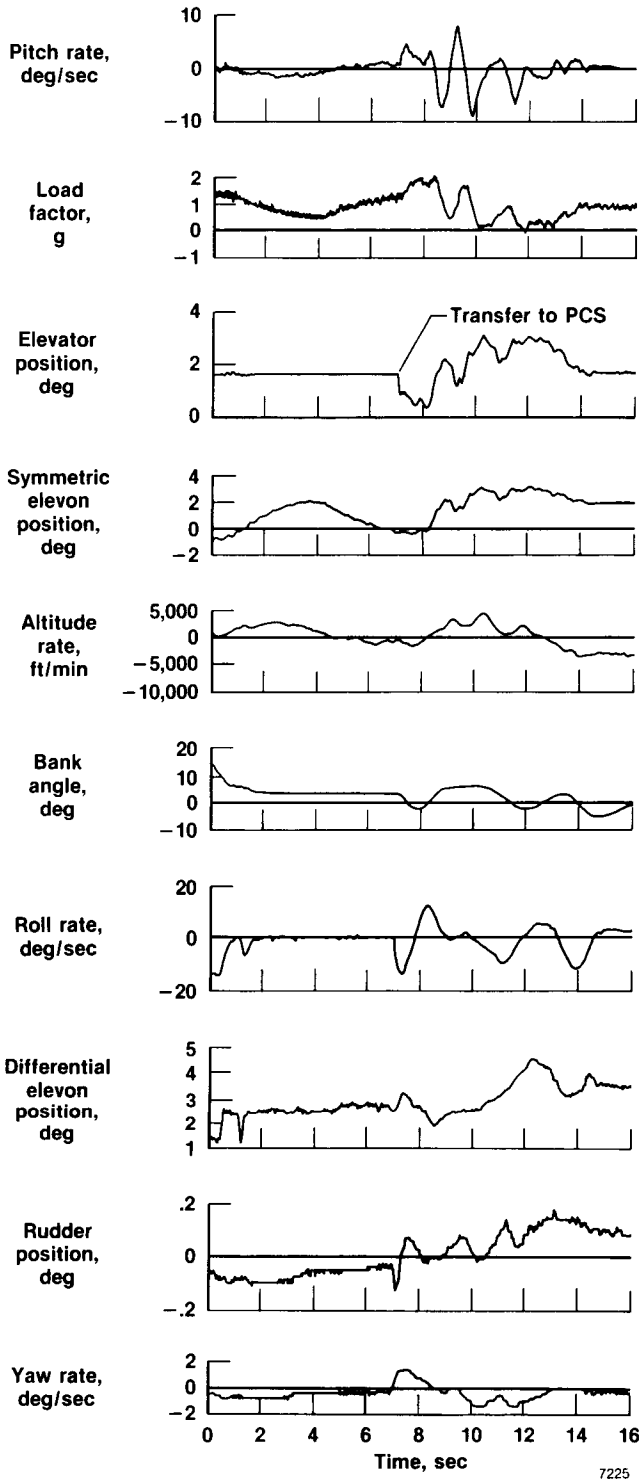


*(b) Mach number = 0.80, h = 26,900 ft,* $\bar{q}$ *= 325 lb/ft*$^2$*,* $V_c$ *= 325 knots.*

*Figure 45. Concluded.*

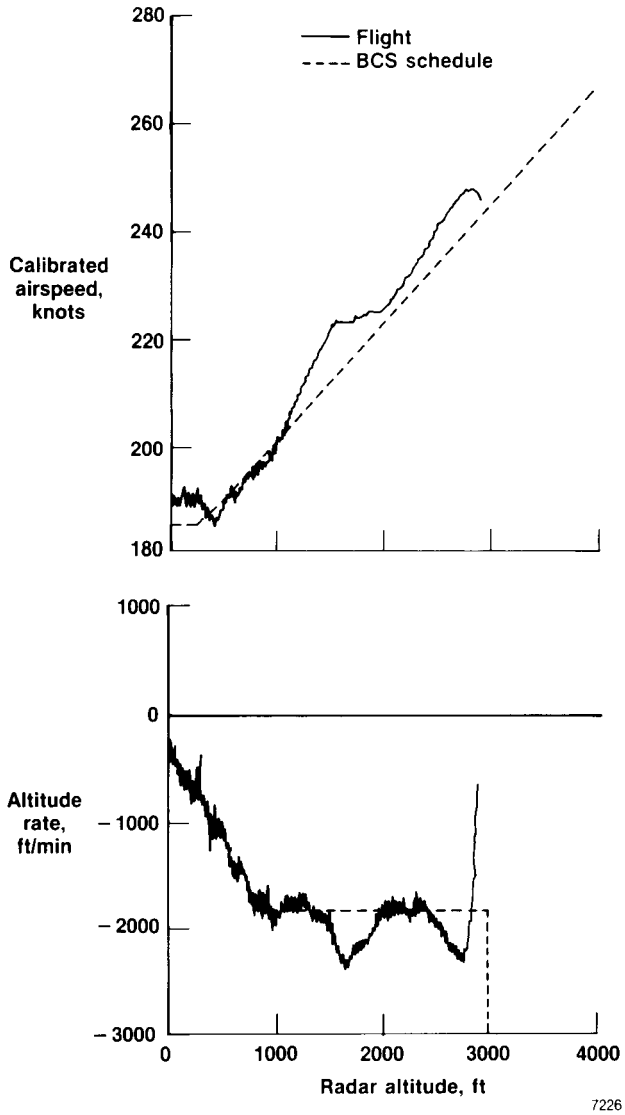


*Figure 46. HiMAT BCS-powered LAND mode landing; LAND mode selected at h = 2,950 ft.*

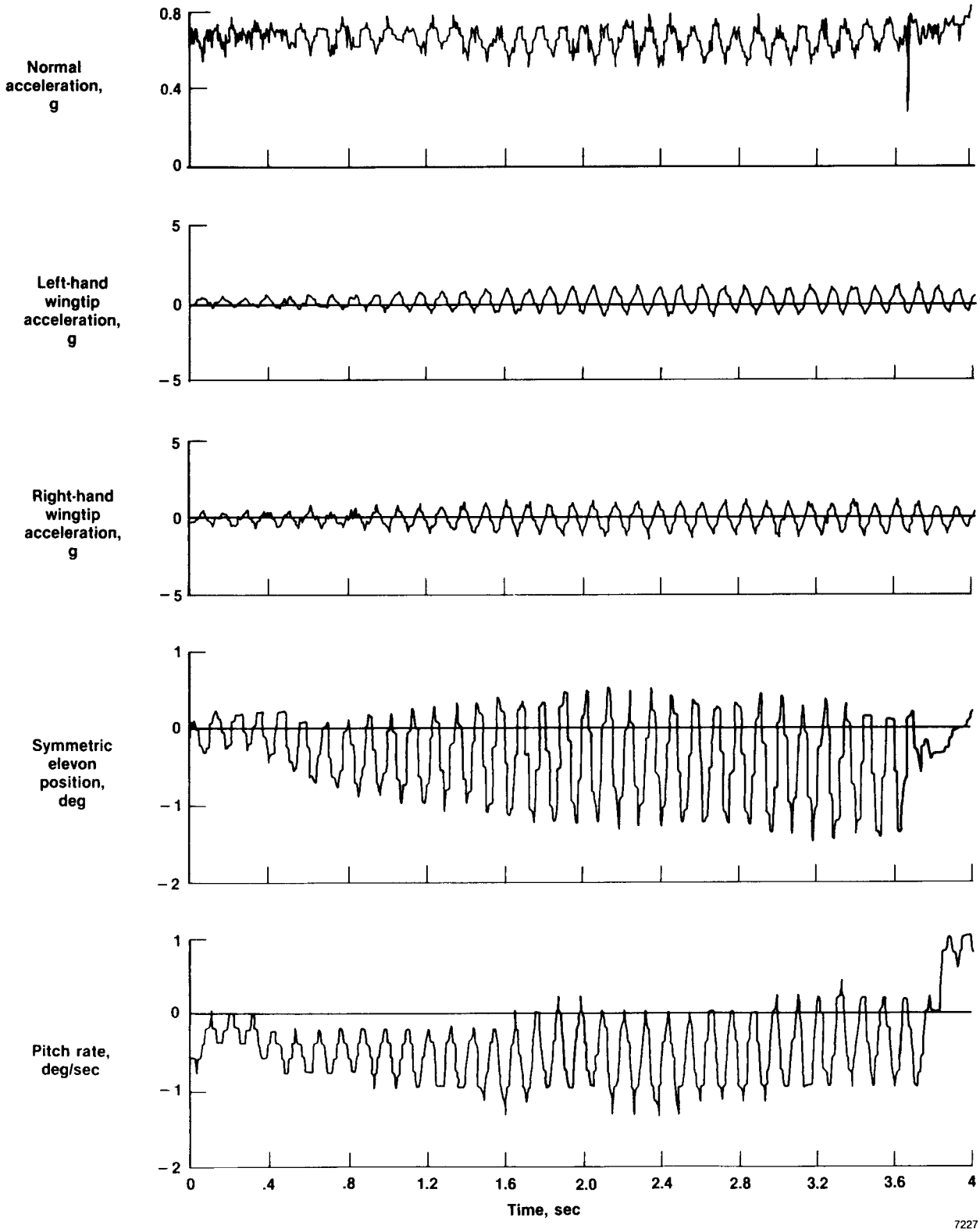


*Figure 47. HiMAT aeroservoelastic instability in backup control. h= 37,000 ft, $0.87 \leq M \leq 0.88$, $235 \leq \bar{q} \leq 245$ lb/ft$^2$.*

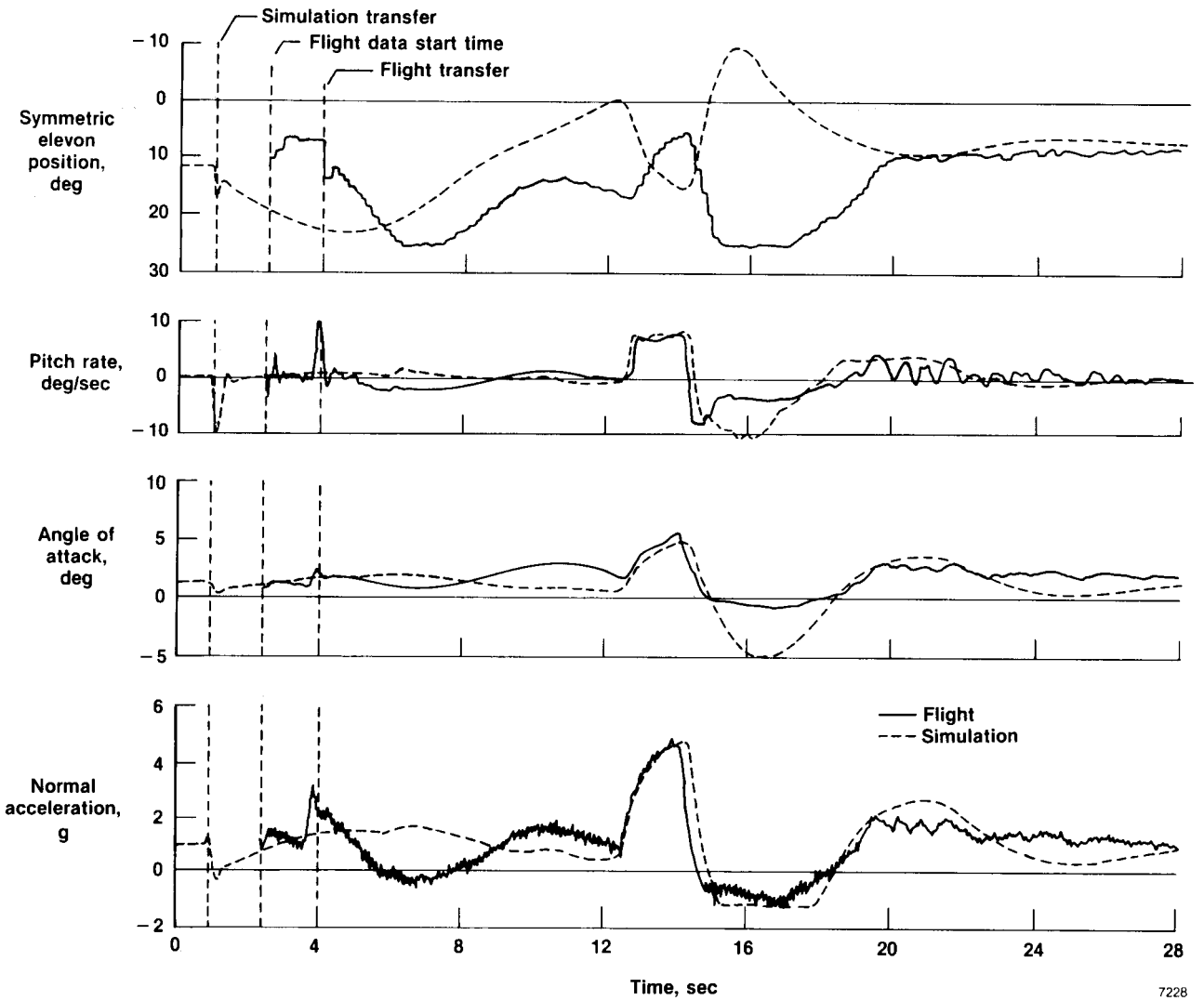


*Figure 48. HiMAT transfer to backup flight control at supersonic speed. $h$ = 23,980 ft, $M$ = 1.29, and center of gravity = 0 percent of $\bar{c}$.*

NASA
National Aeronautics and Space Administration

# Report Documentation Page

| 1. Report No. | 2. Government Accession No. | 3. Recipient's Catalog No. |
|---|---|---|
| NASA TP-2822 | | |

| 4. Title and Subtitle | 5. Report Date |
|---|---|
| Flight Control Systems Development and Flight Test Experience With the HiMAT Research Vehicles | June 1988 |
| | 6. Performing Organization Code |
| 7. Author(s) | 8. Performing Organization Report No. |
| Robert W. Kempel and Michael R. Earls | H-1428 |
| | 10. Work Unit No. |
| 9. Performing Organization Name and Address | 533-02-71 |
| NASA Ames Research Center<br>Dryden Flight Research Facility<br>P.O. Box 273, Edwards, CA 93523-5000 | 11. Contract or Grant No. |
| 12. Sponsoring Agency Name and Address | 13. Type of Report and Period Covered |
| National Aeronautics and Space Administration<br>Washington, DC 20546 | Technical Paper |
| | 14. Sponsoring Agency Code |

15. Supplementary Notes

16. Abstract

Two highly maneuverable aircraft technology (HiMAT) remotely piloted vehicles were flown a total of 26 flights. These subscale vehicles were of advanced aerodynamic configuration with advanced technology concepts such as composite and metallic structures, digital integrated propulsion control, and ground (primary) and airborne (backup) relaxed static stability, digital fly-by-wire control systems. Extensive systems development, checkout, and flight qualification were required to conduct the flight test program. The design maneuver goal was to achieve a sustained 8-g turn at Mach 0.9 at an altitude of 25,000 ft. This goal was achieved, along with the acquisition of high-quality flight data at subsonic and supersonic Mach numbers. Control systems were modified in a variety of ways using the flight-determined aerodynamic characteristics. The HiMAT program was successfully completed with approximately 11 hr of total flight time.

| 17. Key Words (Suggested by Author(s)) | 18. Distribution Statement |
|---|---|
| Digital flight controls<br>Remotely piloted vehicle<br>Flight test | Unclassified — Unlimited<br><br>Subject category 08 |

| 19. Security Classif. (of this report) | 20. Security Classif. (of this page) | 21. No. of pages | 22. Price |
|---|---|---|---|
| Unclassified | Unclassified | 86 | A05 |

NASA FORM 1626 OCT 86

*For sale by the National Technical Information Service, Springfield, VA 22161-2171.*

NASA-Langley, 1988